Instituto de Bioingeniería

Universidad Miguel Hernández

Temporal processing dynamics in neuronal populations

Memoria de Tesis Doctoral

Javier Alegre Cortés

Director de Tesis:

Dr. Eduardo Fernández Jover

Co-directora de Tesis:

Dra. Cristina Soto Sánchez

Elche, 2019

Programa de Doctorado en Bioingeniería

DOCTORAL THESIS BY COMPENDIUM OF PUBLICATIONS

To whom it may concern:

The doctoral thesis developed by me, Javier Alegre Cortés, with title: **"Temporal processing dynamics in neuronal populations"** is a compendium of publications and includes the following publications in which I am the first author:

Time–frequency analysis of neuronal populations with instantaneous resolution based on noise-assisted multivariate empirical mode decomposition
Javier Alegre-Cortés, Cristina Soto-Sánchez, AG Pizá, Ana Lia Albarracin, Fernando Daniel Farfan, Carmelo Jose Felice, Eduardo Fernandez
Journal of Neuroscience Methods, 2016 267:35-44 doi: 10.1016/j.jneumeth.2016.03.018

Multiscale dynamics of interstimulus interval integration in visual cortex
Javier Alegre-Cortés, Cristina Soto-Sánchez, Eduardo Fernandez
PLoS ONE 2018 13(12):e0208822 doi: 10.1371/journal.pone.0208822

Toward an Improvement of the Analysis of Neural Coding
Javier Alegre-Cortés, Cristina Soto-Sánchez, Ana L Albarracín, Fernando D Farfán, Mikel Val-Calvo, José M Ferrandez, Eduardo Fernandez
Frontiers in neuroinformatics 2018 11(77) doi: 10.3389/fninf.2017.00077

I declare that these publications were not used and will not be used in any other thesis.

INFORME DE LA COMISION ACADEMICA DEL PROGRAMA DE DOCTORADO EN BIOINGENIERIA

A quien corresponda:

Por la presente, la Comisión Académica del Programa de Doctorado en Bioingeniería:

Informa FAVORABLEMENTE el depósito de la Tesis presentada por D. Javier Alegre Cortés,

Realizada bajo la dirección del Dr. Eduardo Fernández Jover y la co-dirección de la Dra. Cristina Soto Sánchez

Titulada: **"Temporal processing dynamics in neuronal populations"**.

Presentada por compendio de publicaciones.

Elche de 2019

Dr. José Manuel Pérez

Coordinador del programa de Doctorado en Neurociencias

El Dr. Eduardo Fernández Jover, Catedrático de la Universidad Miguel Hernández, y la Dra. Cristina Soto Sánchez, Profesor contratado doctor de la Universidad Miguel Hernández,

Autorizan la presentación de la Tesis Doctoral titulada **"Temporal processing dynamics in neuronal populations"**, realizada por D. Javier Alegre Cortés (DNI 18455343M) bajo su inmediata dirección y supervisión en el Instituto de Bioingeniería, centro de la universidad Miguel Hernández, y que presenta para la obtención del grado de Doctor por la Universidad Miguel Hernández.

Y para que así conste, y a los efectos oportunos, expiden y firman el presente certificado en Elche, a de 2019.

Fdo.: Dr. Eduardo Fernández Jover

Fdo.: Dr. Cristina Soto Sánchez

AKNOWLEDGEMENTS

Tras estos 4 años termina una etapa única en mi vida y quiero agradecer a las personas que me han ayudado y han estado a mi lado este tiempo;

En primer lugar a mi director de tesis, Eduardo. Gracias por abrirme las puertas de tu laboratorio, confiar en mí y permitirme realizar una tesis con la que tanto he crecido, aprendido y disfrutado.

A Cristina, que me ha dirigido, acompañado y enseñado estos años. Gracias por enseñarme todo lo que me has enseñado, estar a mi lado en los mejores y peores momentos en el laboratorio y haber sido siempre un apoyo.

A todos mis compañeros presentes y antiguos del NBIO: Lawrence, Sonia, Jenny, María Dolores, Conchi, Juanma, Desi, Ari, Gema, Alfonso, Miguel…, y especialmente a Antonio, Mikel y Sebas, compañeros de fatigas y momentos de diversión que han hecho estos años mucho más fáciles. De todos vosotros he tenido la oportunidad de aprender.

A mis compañeros del máster con los que inicié mi etapa investigadora, sobre todo a Adri, Josemi y Aitana. También a todas las demás personas que he tenido la oportunidad de conocer en este mundo de la Neurociencia. En primer lugar a Miguel Maravall, mi primer mentor y la persona que me enseñó a ser el investigador que soy ahora. A Ramón Reig, por enseñarme tanto y darme apoyo cuando lo necesité. A Roberto, María, Jorge, Adam, Saurabh, Aroa, Michael, Diana, Kevin, Mercedes, Sandra, Amr, Pablo, Joan, Kat, Yuki… Gracias a todos por compartir buenos y malos momentos durante estos años.

A Elisa, con quien he luchado estos años por conseguir ese sueño de ser científicos. Siempre estuviste a mi lado y te deseo la máxima felicidad.

Por último, a las personas que siempre han sido parte de mi vida, a mis amigos, a mi hermano Andrés y, por encima de todo, a mis padres. Gracias por todo, sin vosotros, sin vuestro apoyo, ánimos y ayuda, yo no estaría aquí.

INDEX

Abstract/Resumen 13

Abstract 15

Resumen 16

1. Introduction 19

1.1 Cortical oscillations 21

1.1.1 Spontaneous oscillations 21

1.1.2 Role in information transfer 22

1.1.3 Nonlinear properties of biological oscillations 23

1.2 Visual Cortex 25

1.2.1 Deep layers in visual cortex 27

1.2.2 Oscillations during visual response 29

1.3 Time-Frequency analysis 31

1.3.1 Fast Fourier Transform 32

1.3.2 Short-Term Fourier Transform 33

1.3.3 Wavelet analysis 34

1.3.4 Empirical Mode Decomposition 35

1.3.5 MEMD 37

1.3.6 Noise assisted EMDs 38

1.3.7 The use of EMDs in neuroscience 40

1.3 The use of machine learning in neuroscience 40

1.4 Research lines 42

2. Objectives 43

3. Material and methods 47

3.1 Rat visual cortex recordings 49

3.1.1 Surgery 49

3.1.2 Acquisition system 49

3.1.3 Visual stimulation 50

3.2 Other recordings used in this thesis 50

3.3 NA-MEMD 50

3.4 Machine learning 50

3.5 Statistical analysis 51
4. Results 53
5. Discussion 57
5.1 NA-MEMD as a tool to study spike oscillations 59
5.2 Interstimulus interval at seconds scale is encoded in spikes oscillation of Deep layers in V1 59
5.3 NA-MEMD+ML for neural activity pattern analysis 61
5.4 The elephant in the room, why we didn´t apply ML to understand visual interstimulus timing. 61
5.5 Future lines of research 62
6. Conclusions/Conclusiones 65
7. Bibliography 69
8. Annex: Publications 81
PAPER I: Time–frequency analysis of neuronal populations with instantaneous resolution based on noise-assisted multivariate empirical mode decomposition 83
PAPER II: Multiscale dynamics of interstimulus interval integration in visual cortex 111
PAPER III: Toward an Improvement of the analysis of neural coding 127

Abstract/Resumen

Abstract

Time is crucial for our understanding of our environment and our behaviour. We require to process time to execute motor actions, predict future events from the past ones and anticipate events. Despite many efforts, the neural basis of temporal processing remains elusive. It is an open question to understand how the brain perceives time, given the absence of any "time receptor", as it is the case for vision, audition or any other perception. In this thesis I focused on the study of time representation in the seconds range during sensory stimulation by means of cortical spike oscillations.

First, I show a novel framework to analyse spike oscillatory activity, specifically considering preserving its nonlinear and nonstationary properties. To do so, I showed that a combination of NA-MEMD + Hilbert Transform overcomes traditional Time-Frequency techniques to analyse neuronal recordings. I demonstrated it by comparing the obtained spectral properties obtained with our framework with previously published results using vibrissal nerve recording during tactile stimulation. As a second example, I used spike oscillations from neuronal populations of deep layers of visual cortex of anesthetised rats during visual stimulation.

Once a proper framework to analyse spike oscillations was found, I studied how time interval at the seconds range during sensory stimulation in anesthetised rats was represented in deep layers of visual cortex. I demonstrated that when longer intervals than one second are used, the firing rate of deep layers of visual cortex in response to a moving grating is increased and the response becomes more stable. These results were more evident when three or five seconds interval were used and decreased when seven seconds intervals were used. In order to better understand the coding of interval at seconds scale in visual cortex, I studied the Time-Frequency dynamics of the evoked response with different intervals. Multiple differences at different times and frequencies were found when one second interval was compared both with three and five seconds intervals. Some of these differences were still present when seven seconds interval was used, suggesting an optimal interval window around three to five seconds. There were differences during the whole stimulation in the 6 Hz and the 10 Hz bands, as well as transient differences in higher frequencies. Considering these results, I proposed a phase space were interval time could be discriminated by means of the evoked trajectories during stimulation. Altogether, these results suggest a multiplexed processing of time interval using spike oscillations of neuronal populations from deep layers of visual cortex. They also suggest an optimal interval length of three to five seconds were the evoked response is maximal.

At last, I suggest a new framework to study the oscillatory dynamics of single trials in neuroscience. I demonstrated that a combination of NA-MEMD to extract Time-Frequency features combined with Machine Learning classification, both supervised and unsupervised, outperforms classical tools in the characterization of single-trial dynamics. Given the ongoing interest of the field in the study of the brain activity and behaviour in single trials, this new framework promises to become a useful new tool in our quest to understand how the brain works.

Resumen

El tiempo es crucial para entender nuestro entorno y nuestro comportamiento. Necesitamos procesar el tiempo para ejecutar acciones motoras, predecir eventos futuros a partir de los pasados, y anticipar nuevos eventos. Pese a todos los esfuerzos realizados, seguimos son conoces el sustrato neuronal para el procesamiento temporal. Cómo el cerebro percibe el tiempo es todavía una pregunta abierta, teniendo en cuenta que no existe ningún "receptor del tiempo", como sí es el caso de la visión, el oído o cualquier otra percepción. En esta tesis he estudiado la representación del tiempo en el rango de segundos durante la estimulación sensorial por medio de oscilaciones de potenciales de acción corticales.

En primer lugar, he mostrado un nuevo enfoque para el análisis de oscilaciones de potenciales de acción, teniendo especialmente en cuenta preservar sus propiedades no-lineales y no-estacionares. Para ello, he mostrado como una combinación de NA-MEMD junto con la Transformada de Hilbert supera a las técnicas tradicionales de Tiempo-Frecuencia para el análisis de registros neuronales. Para demostrarlo, he comparado las propiedades espectrales obtenidas mediante estos algoritmos con resultados publicados previamente usando registro en el nervio vibrisal durante una tarea de estimulación táctil. Como un segundo ejemplo, he utilizado oscilaciones de potenciales de acción de poblaciones neuronales de capas profundas de la corteza visual de ratas anestesiadas durante una tarea de estimulación visual.

Una vez encontrados una serie de algoritmos adecuados para el análisis de oscilaciones de potencial de acción, estudié como se representaba el intervalo temporal en la escala de segundos durante una tarea de estimulación visual en las capas profundas de la corteza visual de ratas anestesiadas. Demostré que cuando se usaban intervalos de mayor duración que un segundo, aumentaba la tasa de disparo de las capas profundas de la corteza visual en respuesta a la estimulación con un enrejado en movimiento, así como la respuesta se volvía más estable. Estos resultados eran más claros cuando se usaron intervalos de tres o cinco segundos y disminuyeron cuando se usó un intervalo de siete segundos. Con el objetivo de entender mejor la codificación del intervalo en la escala de segundos en corteza visual, estudié la dinámica Tiempo-Frecuencia de la respuesta evocada usando diferentes intervalos. Encontré múltiples diferencias a diferentes tiempos y en diferentes frecuencias cuando comparé la respuesta con un intervalo de un segundo con intervalos de tres y cinco segundos. Algunas de estas diferencias seguían existiendo cuando usé intervalos de siete segundos, sugiriendo una ventana óptima de duración del intervalo de entre tres y cinco segundos. Encontré diferencias a lo largo de toda la ventana de estimulación en las bandas de 6 y 10 Hz, así como diferencias transitorias en frecuencias más altas. Estos resultados sugieren un procesamiento multiplexado del intervalo temporal mediante oscilaciones de potenciales de acción de poblaciones neuronales en capas profundas de la corteza visual. También sugieren una ventana óptima de duración del intervalo, de entre tres y cinco segundo, en la que la respuesta evocada es máxima.

Por último, propuse un nuevo enfoque para el estudio de oscilaciones neuronales para pruebas experimentales individuales en neurociencia. Demostré que una combinación de NA-MEMD

para extraer características en Tiempo-Frecuencia, combinado con herramientas de aprendizaje automático, tanto supervisado como no supervisado, para su clasificación, superaba a las herramientas usadas tradicionales para el estudio de la dinámica de pruebas experimentales individuales. Considerando el creciente interés del campo en el estudio de la actividad cerebral y el comportamiento en pruebas experimentales individuales, este nuevo enfoque promete ser una herramienta de gran utilidad en nuestra lucha por entender cómo funciona el cerebro.

1. Introduction

1.1 Cortical oscillations

Our brain is the combination of billions of neurons, each of them receiving and up to 60.000 connections from other neurons [1]. This extremely complex network produces collective patterns of activity; including oscillatory behaviours. Brain oscillations are known since 1929 [2],when Berger described the alpha rhythm (8-12 Hz) in the EEG of human patients. Four years later, Bishop suggested that these oscillations might been related by changes in the excitability of the neurons [3] Since then, neuroscientists have incessantly studied how the brain creates and uses this, and others, oscillations [4,5] [Random reviews]. By means of these studies, they aim to put some light into how neuronal populations, both in small networks of few tens of neurons or at whole-brain scale, do work cooperatively in a time organized manner to produce behaviour.

1.1.1 Spontaneous oscillations

Perhaps the most studied brain oscillation is the Slow Wave Oscillation (SWO) [6,7]. This oscillation is a collective phenomenon of +/-1 Hz frequency that is originated in the cortex during sleep [8,9],anaesthesia or rest, and then propagates to all the brain (Fig.1).

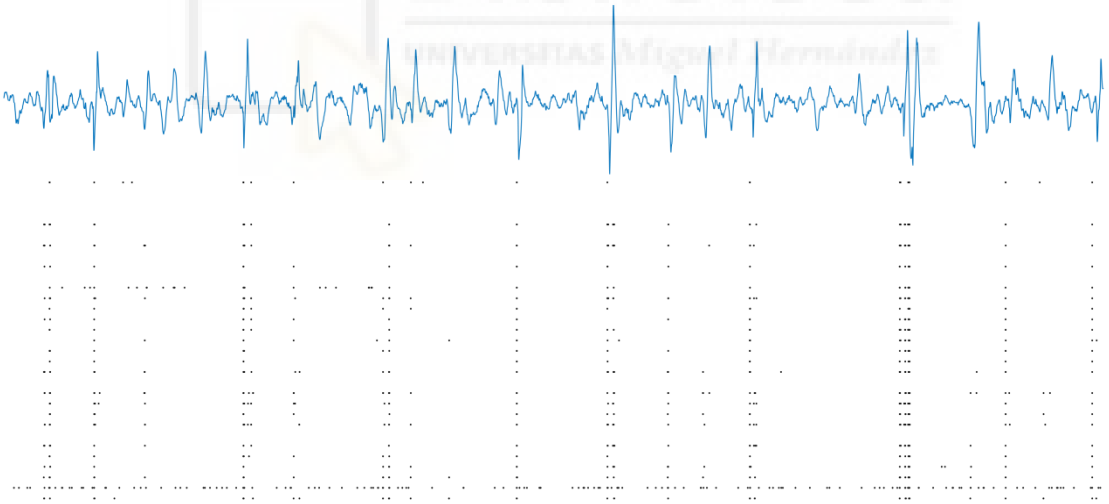

Figure 1. Slow wave oscillation. Example of SWO oscillation recorded in V1. Notice how the spikes of the neurons are phase aligned to the Up states recorded in the Local Field Potential in blue. Neurons are represented in rows and spikes for each neuron as black spots in its corresponding row, creating a raster plot.

It can be described as a bi-stable state with two possible configurations, “Down” states where the network is mostly hyperpolarized and silent and “Up” states, where neurons are activated co-ordinately and the waves propagates to the surrounding neurons, creating a

travelling wave. This wave is not only detectable as a network phenomenon but at the level of individual neurons in the cortex [9,10] and subcortical nuclei [11–13].

The cortical origin of this oscillation was first demonstrated “ex vivo” [8], demonstrating that global oscillatory event emerged in brain slices and had a cortical origin and was later confirmed by Timofeev [14], who isolated cortical regions in a living animal and showed that oscillations were still present in the isolated region. Moreover, other studies [11,15]have demonstrated that subcortical regions such as the thalamus have a key role on the modulation of the SWO.

In addition, recent studies have demonstrated that this spontaneous SWO is not restricted to anaesthesia or sleep regimens, but can sometimes be recorded in awake animals during period of rest and inactivity [16,17].

In summary, we can affirm that the brain presents oscillatory phenomena during resting/sleep that are whole-brain coordinated and modulated, suggesting that oscillations are a key resource that neuronal populations use for information transfer and decoding.

1.1.2 Role in information transfer

Our brain show multiple oscillators at different frequencies ranging from 0.05 to 500 Hz [5], that are typically associated with different brain states and functions. Once we focus on information transfer across neuronal populations, recent theories have highlighted the relevance of the temporal pattern of the spike trains, suggesting that complex dynamics, still time ordered, are created during cortical activity as structured packets of activity [18] are sent back and forth among different populations. This phenomenon, on which multiple oscillations at different frequencies are present in the activity of neuronal populations is called Multiplexed theory [19] and was described for the first time in the visual cortex.

Despite Multiplexed theory is still a novel explanation that has to be studied, something that was not possible until the appearance of novel techniques that allow us to record from multiple neurons at different spatial locations simultaneously [20–23], the role of oscillations in information processing has been widely studied during the last decades.

Gamma oscillation

One of the widest studied oscillations during perception is the Gamma oscillation (30-100 Hz) [24], which is putatively used by the brain to synchronize different brain regions that are going to be involved in a given task. The first studies were done 3 decades ago by Singer and others [25–27] as a component present in visual response and has been later found in multiple sensory [28–30] and non-sensory [31,32] regions of the brain. The main hypothesis is that Gamma oscillation acts as a coincidence detector, so that if a given neuron receives simultaneous information from different presynaptic neurons during the positive phase of

the gamma oscillation it will lead to stronger or earlier responses. Therefore gamma oscillation opens a possibility to produce a code that relies not in the firing rate but in the precise spike timing of the presynaptic populations[33]. Furthermore, despite it has been mostly studied during stimulus perception, it is known to play a role in higher cognitive phenomena such as attention [34].

Alpha oscillation

A different brain oscillation that has received an enormous scientific interest is the alpha oscillation (7-13 Hz), the first oscillation ever recorded [2] almost one century ago. This oscillation has been traditionally studied in the visual system since Berger's discovery relative to the alpha power modulation in the visual system depending on whether the subject had its eyes open or closed. In this scenario, alpha oscillation is supposed to be an active inhibitory mechanism that modulates stimulus relevance by adjusting gamma oscillation amplitude during the response to visual stimulation.

Delta-Theta oscillation

At last, slower oscillation in the delta-theta regime (2-8 Hz) are suggested to control time prediction during sensory stimulation in order to prepare the brain to process a given stimulus. When a given stimulus is delivered in a predictive manner, delta-theta activity can be recorder before the stimulation occurs, suggesting a mechanisms to predict "when" a given stimulus is expected [35]. Therefore, when combined with other oscillations, it provides a mechanism to balance the behavioural relevance of a stimulus (attention) and the probability of a previously known stimulus to happen (expectation) [4].

In conclusion, our brain does use multiple oscillatory mechanisms to modulate the flow of information that provide information about the properties and timing of stimulus as well as high cognitive activities. Thus, when studying a novel phenomenon in the brain, it is not surprising to address whether the neuronal activity of interest presents any kind of oscillatory modulation during the given task.

1.1.3 Nonlinear properties of biological oscillations

Neuronal oscillations are nonlinear [36–39]. This means that they cannot be characterized using a sinusoidal template, nor with any other approach that relies on a fixed shaped wave. Recorded waveforms in the brain display a variety of shapes [39], as different waves are the results of the combination of multiple neurons interacting among each others [40], complex Excitatory/Inhibitory balances and neurons firing at different timescales simultaneously [19,41]. This apparently innocuous statement turns to become critical given that the vast majority of the spectral analysis done in neuroscience has de underlying assumption that the studied oscillation are sinusoidal [39,42]. When neuronal oscillations are studied based on fixed templates the result is compromised and artefactual. Therefore, it becomes

controversial to extract biological meaning from a spectral analysis whose assumption have not been fulfilled by the data [43].

In figure 2 we can see a representative example: The shape of the theta oscillation in the hippocampus changes as a function of recording depth, since the whole brain regions is oscillating synchronously, but different cell types are present at different depths (from [39]).

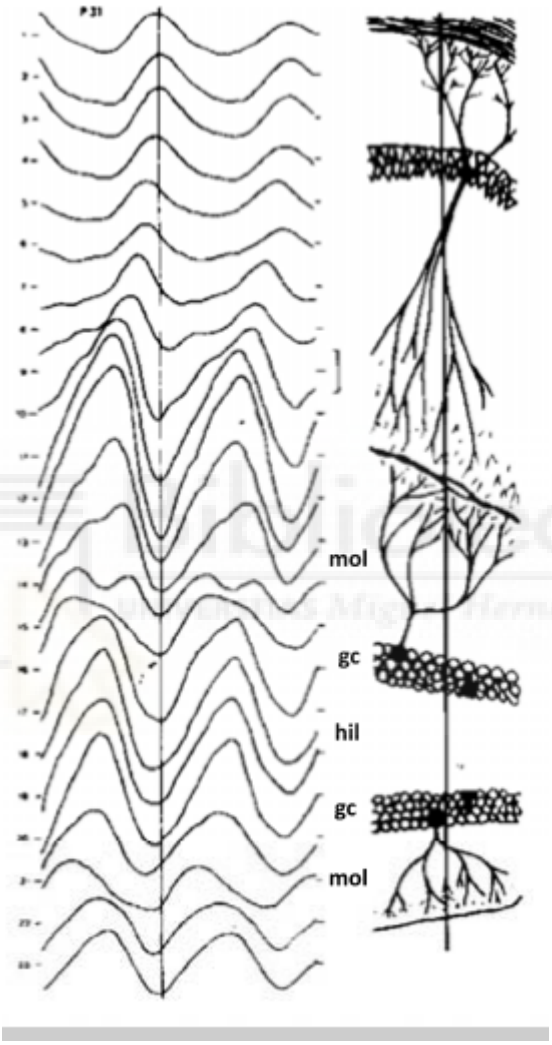

Figure 2. Wave shape is not constant. Changes in the shape of theta oscillation as a result of depth in the hippocampus, from [39].

A more technical visualization of the nonlinearities present in neuronal oscillations is presented in figure Figure 3. Different individual cycles of the wave have different Instantaneous Frequency; therefore, its shape is not sinusoidal, as it requires a unique frequency in the entire wave. In addition, different cycles have different distribution of IF along time; this means that there is not a unique waveform, but minor changes across cycles. Therefore, a correct decomposition of this wave requires a template-free approach that does not depend on any fixed shape to transform the signal into the frequency domain.

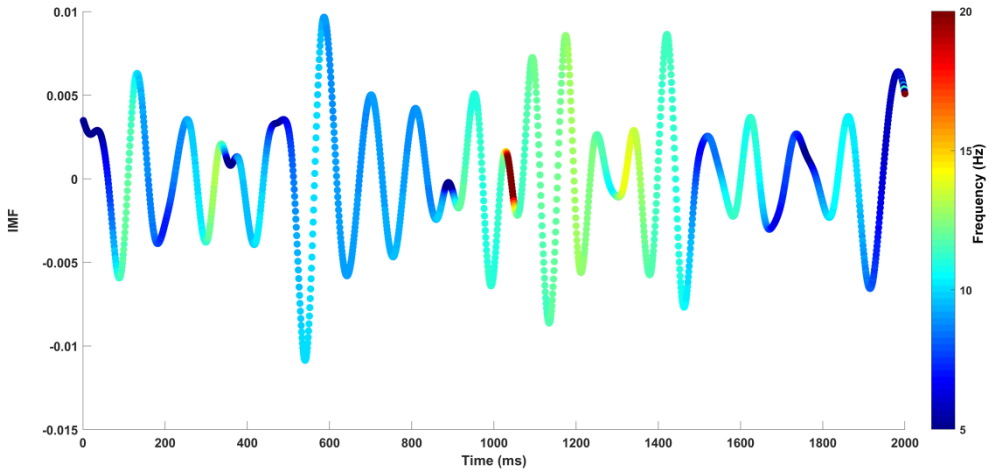

Figure 3. Nonlinear properties of spike oscillations. Instantaneous frequency of an example spike oscillations in visual cortex. There exist changes of instantaneous frequency within the same cycle, thus being a nonlinear oscillation.

1.2 Visual Cortex

We use our sight as our primary source of information of the world. To do so, we have complex eyes, big regions of the brain devoted to vision and multiple pathways across the CNS devoted to the extraction of different visual features from our environment. Given the importance of vision, neuroscientists have devoted countless efforts to understand how the visual cortex works.

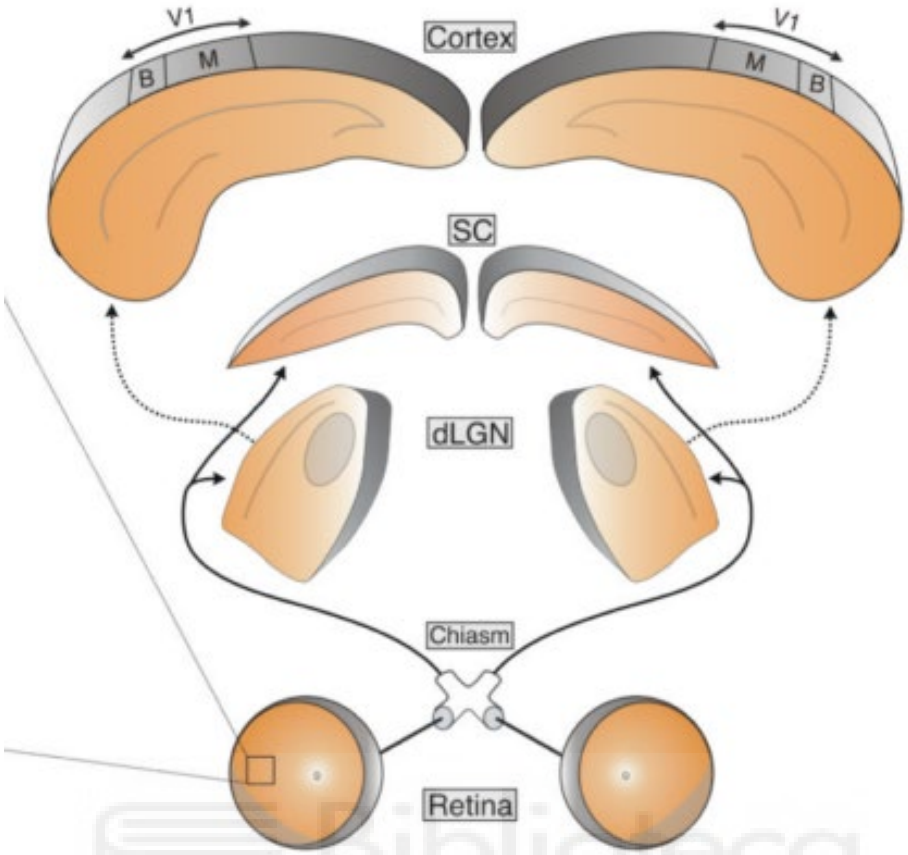

Figure 4. Schematically representation of mouse visual system, from [44].

An scheme of the rodent visual system is present in Figure 4, extracted from [44]. In brief, the environment is at first perceived in the retina. Considering the main pathway of visual information, the retina projects its axon to the Thalamus, and more precisely the dorsal Lateral Geniculate Nucleus (dLGN) that will in turn project to the Visual Cortex. It is worth to note that minor parallel pathways exist during visual processing, as explained in Lennie's review [45].

Our understanding of how the visual cortex works started with the work of the Nobel Laureates David Hubel and Torsten Wiesel [46–48]. They discovered the columnar organization of the visual cortex as a tool used by the brain to perform efficient computations. Cortical columns in mammal visual cortex work as feature extractors of the perceived image that are subsequently sent to higher visual areas. This regions will lately provide feedback information to V1 [49,50], consistent with a communication based on packets of information that are sent across multiple brain regions [18].

1.2.1 Deep layers in visual cortex

Mammal visual cortex is structured in a 6-layered structure [48]. While different columns are supposed to be feature extractors from the image perceived in the retina [51–54], layered structure is created by different microcircuits with different intrinsic properties and levels of connectivity within and outside the column. In this section, we will focus on the deep layers of the cortical column, which are Layer V, mostly, and Layer VI, which is by far the least understood layer of the cortex (Figure 5).

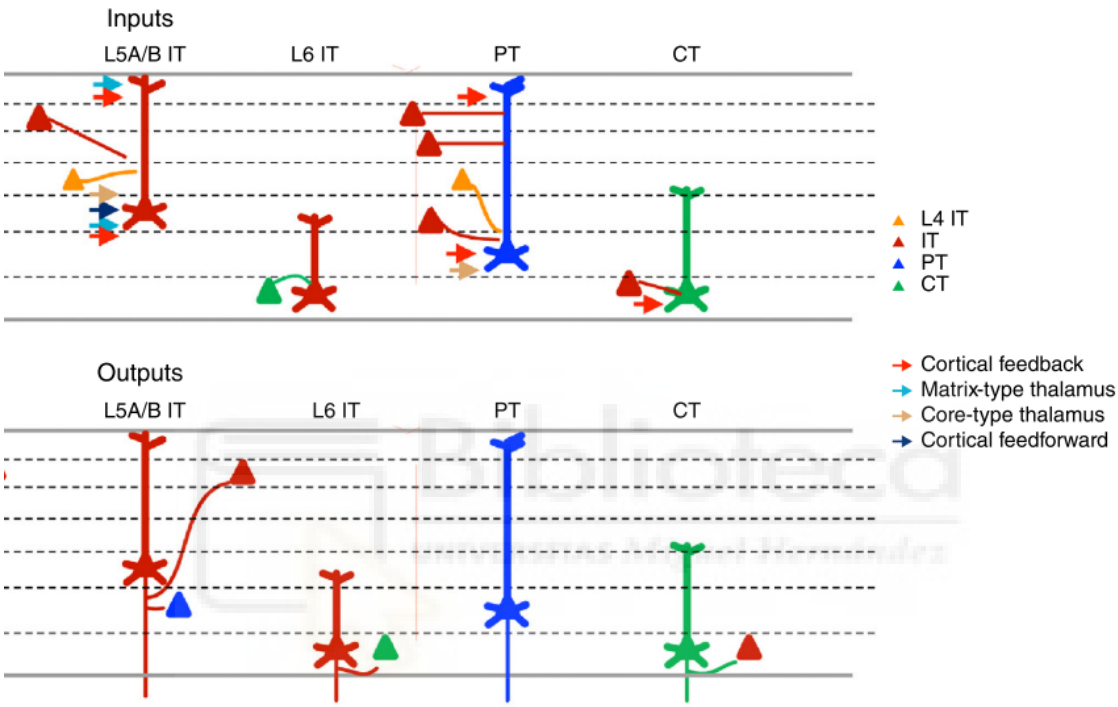

Figure 5. Scheme of the inputs and outputs of cortical deep layers, modified from [55]. Each layer has a specific distribution of inputs, outputs and cell types that determine the computations on which it is involved.

Layer V

Layer V receives projections from Layers I to V of the cortex [55–57], both from the same column as well as other cortical areas, as well as projections from the thalamus, as it has been recently discovered [58]. Layer V is considered the most active layer of the cortex [59–62], and it's known to present oscillatory activity because of the strong recurrent activity of tufted Layer V pyramidal neurons [56]. As a representative example, layer 5b is known to be the origin of the previously explained SWO [8] (Figure 6).

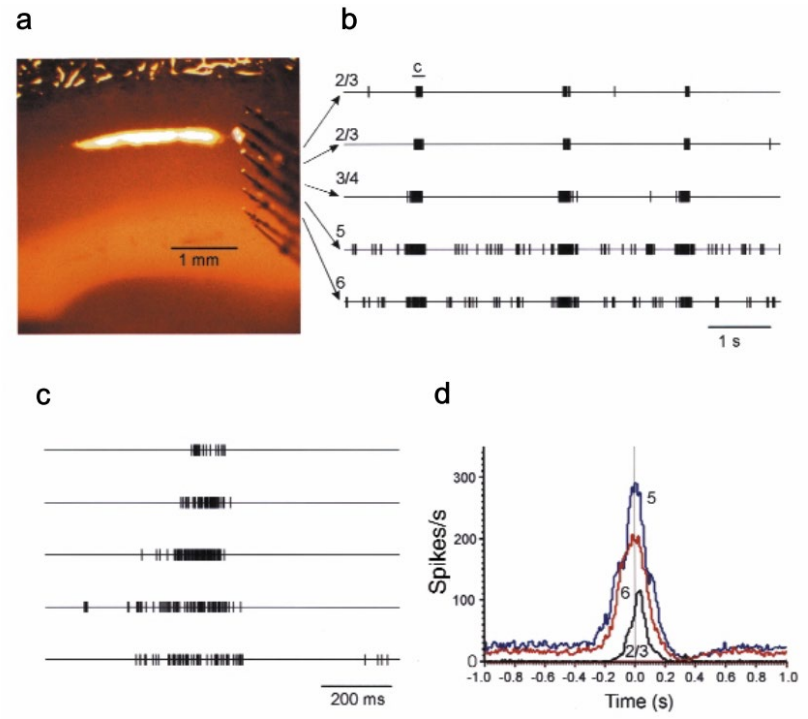

Figure 6. Slow wave oscillation originates in layer V. Slow wave oscillation, the most representative oscillation during sleep/anaesthesia is originated in the deep layers of the cortex, from [8].

There are two main types of Excitatory neurons in Layer V, smaller intratelencephalic (IT)[63] and the giant tuft pyramidal neurons (PT)[56], which mostly projects to subcortical regions, as well as create a dense recurrent network among themselves. IT neurons receive inputs from other IT neurons in layers 2/3, the thalamus and other Layer V excitatory cells [55,64,65], and project to Layer 2/3 IT neurons and Layer V IT and PT neurons, both for the same column and other cortical regions, as well as to the striatum [55]. Talking about its electrophysiological properties, they are hyperpolarized and fire scarcely; nevertheless, Layer V IT neurons are the ones more active of this neuron type [61,66]. The other main type of excitatory neuron is the Tuft Pyramidal Neuron, which conforms the PT. These cells receive inputs from the whole column [55,56] and project to ITs in layers 2/3 (weakly) and V, other Tufted pyramidal neurons and to layer VI neurons, as well as to many subcortical regions (brainstem, tectum, spinal cord, thalamus, basal ganglia…) in what is named the Pyramidal Tract. These cells are depolarized and present bursting (oscillatory) "dense" activity [55,59], thanks to its dense recurrent connectivity [56].

Given the presented connectivity, layer V results the main source of long-range inputs and outputs of the column, hence it has a major role on information transfer among cortical regions as well as to other brain nuclei.

Layer VI

The deepest layer of the cortical column is still an unsolved enigma. Despite its particular connectivity and firing properties, its functional role remains elusive.

Layer VI receives projections directly from the thalamus [58,67] as well as the rest of the cortical column, mostly the deep layers. As in layer V, it has both IT and ET excitatory neurons [64]. Layer VI ET neurons are also known as corticothalamic neurons (CT), they receive inputs from Layers IV and V, the thalamus and multiple long range connections from other cortical regions [68]; they project to different regions of the thalamus, together with sparse projections to layers IV and V [68], present a sparse firing and are the only known type of ET that lacks of any kind of long range corcticocortical projections. There also exist a second type of ET neurons with similar electrical properties that conveys the only cortical projections to the Claustrum [69].Layer VI IT receive most of its inputs from deep layers of the cortex (Layer V and VI) [70]. They show scarce projections to L IV [71] as well as long and short range horizontal connections to other IT neurons in the same layer.

1.2.2 Oscillations during visual response

It is known since decades ago that mammal visual cortex response to visual stimulation has certain oscillatory properties [25,26,72].

Spike oscillations during the response to visual stimulation were discovered by Gray and Singer in 1989 [25] (Figure 7); they demonstrated that neurons in cat V1 fired aligned to a 40 Hz oscillation in a stimulus dependent manner, whereas the thalamus didn´t. By doing such discovery, they found that sensory cortex can phase align its activity during perception as a tool to perform the required computations, hence making evident that not only the amount of spikes but the time of such event was relevant for the neuronal coding, as it has been widely studied afterwards, both in the visual system [19,41] and as a general framework to understand brain computations [18].

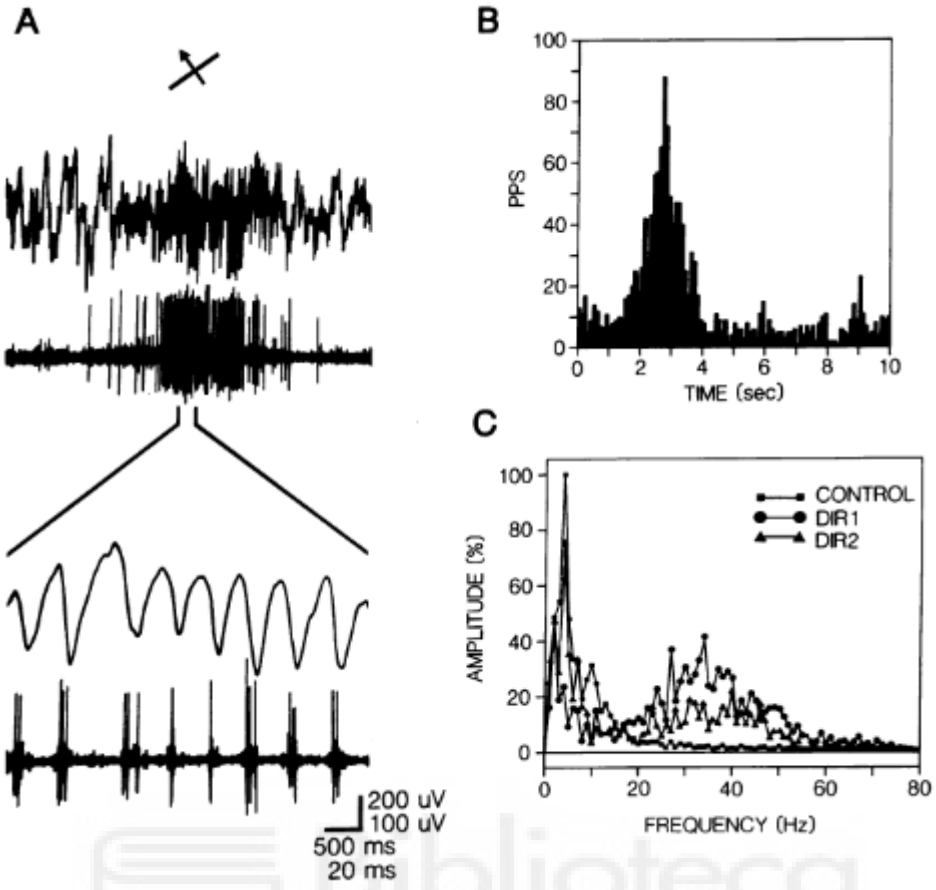

Figure 7. Stimulus specific oscillations during visual response. LFP and spiking response recorded in cat visual area 17 in response to an optimally oriented light bar. There exists an increase of power at 35-45 Hz. From [25]

In a new paper published in the same year, Singer lab demonstrated that the phase alignment of the visual response in the visual cortex was used to synchronize the response of different columns that were responding selectively to a given stimulus, presumably integrating different features of the stimulus [26,72]. Therefore, it was demonstrated an active role of spike oscillations in visual processing. Once the ongoing mechanisms was suggested, posterior studies demonstrated that spike oscillations in the Gamma ranged were involved in stimulus selection [73], therefore not being just an epiphenomenon of visual cortex computation. In addition, this oscillation is used during visual coding not only to phase align neuronal population in different columns of visual cortex, but to synchronize different regions of the brain involved in higher processing of the visual stimulus [33] that will in turn provide feedback to primary visual cortex [49]. Therefore, gamma oscillation during visual response are used to synchronized multiple populations and brain regions, that communicate at different time scales, sending “packets” of information among each other [18,19].

Visual cortex neural oscillations have been also described in tasks beyond passive perception. Shuler lab demonstrated that reward timing modulated the activity of visual cortex [74]; they show how training induced changes in V1 activity that were correlated with

reward expectation and consisted on neuronal oscillations in the theta frequency band [75,76]. These works provided two interesting points for discussion: On the one hand, the role of neural oscillations in visual cortex was not limited to visual perception but was related to different higher order processing tasks. This supports the suggested role of neural oscillations to coordinate the activation of different cortical regions that are required to work together for a certain task [35]. On the other hand, they provided an insight of the capacity of visual cortex to modulate its activity in a time dependent manner at the seconds scale.

In this thesis, we asked whether primary visual cortex encodes interstimulus interval in the range of seconds in the oscillatory dynamics of the evoked response. To address this question we first extended the use of NA-MEMD (see later) to study the oscillatory properties of spike trains **Paper I**. Then, we recorded neuronal populations from rat visual cortex during visual stimulation while modifying the interstimulus interval in the seconds range and studied the changes that it produced on the evoked population response. By means of this approach, we demonstrate in **Paper II** that visual cortex encodes interstimulus interval in the seconds scale using the oscillatory properties of the evoked response.

1.3 Time-Frequency analysis

In this chapter, I will discuss the standard methods for Frequency and Time-Frequency analysis that are most commonly used in neuroscience, as well as introduce the Empirical Mode Decomposition (EMD) and derived algorithms, which have provided the computational basis for the study of the oscillatory properties of neuronal populations presented in this thesis. I will discuss the limitations of each method and how they constrain the study of biological signals. In addition, I will provide the basis to support the work developed in this thesis of searching for new algorithms that made more feasible the Time-Frequency analysis of neuronal signals, especially spike trains of multiple neurons.

To do so, I will use a known oscillatory signal as ground truth, shown in Figure 8, consisting on a corrupted linear chirp; a sine wave that is uniformly accelerating and that has been corrupted adding White Noise (WN). I will compare the results of the decomposition of this known signal with the different techniques that are traditionally used in neuroscience to focus on its flaws and the need of introducing new Time-Frequency techniques in the field.

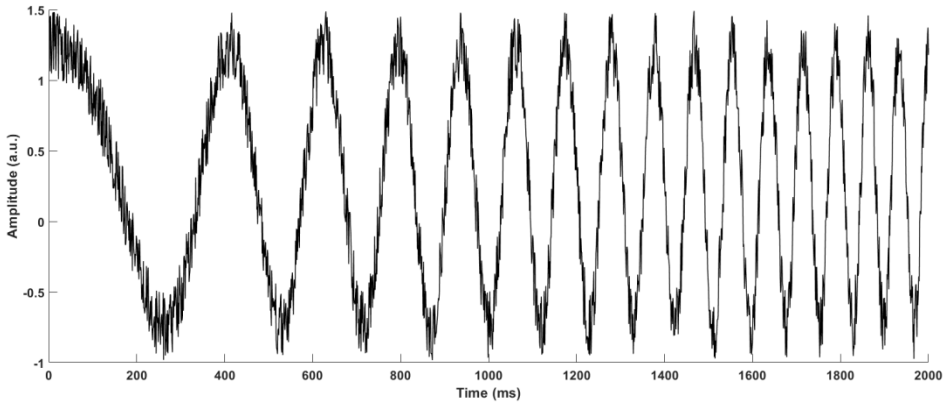

Figure 8. Ground truth signal. Corrupted linear chirp used in all demonstrations.

1.3.1 Fast Fourier Transform

Fourier Series is a mathematical approach to decompose a given vector as the sum of sine waves, based on the following approximation:

$$f(x) = \frac{1}{2} a_0 + \sum_{n=1}^{\infty} a_n \cos(n x) + \sum_{n=1}^{\infty} b_n \sin(n x),$$

The objective of these series, published by Fourier in 1822 in his *Mémoire sur la propagation de la chaleur dans les corps solides*, is to decompose a given signal into an infinite sum of oscillatory functions, under certain assumptions. These assumptions are that the signal is composed by a finite number of sine waves and that it is stationary.

The application of the ideas behind Fourier series became popular after the Discovery of the Fast Fourier Transform (FFT), which was introduced by Cooley and Tukey in 1965 [77] and became widely used once it was simplified by Winograd [78].

Once we focus on the assumptions of the FFT, there exist two main problems when we apply it to neuronal signals. One is that these signals are not always, or are oddly, sinusoidal. When FFT is computed in a non-sinusoidal oscillatory signal, the resolution on the frequency domain gets compromised [36]. The other problem is that FFT shifts the signal from the temporal to the frequency domains, thus it provides a representation of the existing frequencies in the signal, assuming that is stationary, which means that these frequencies are present all the time, something that does not always occur in biological signals.

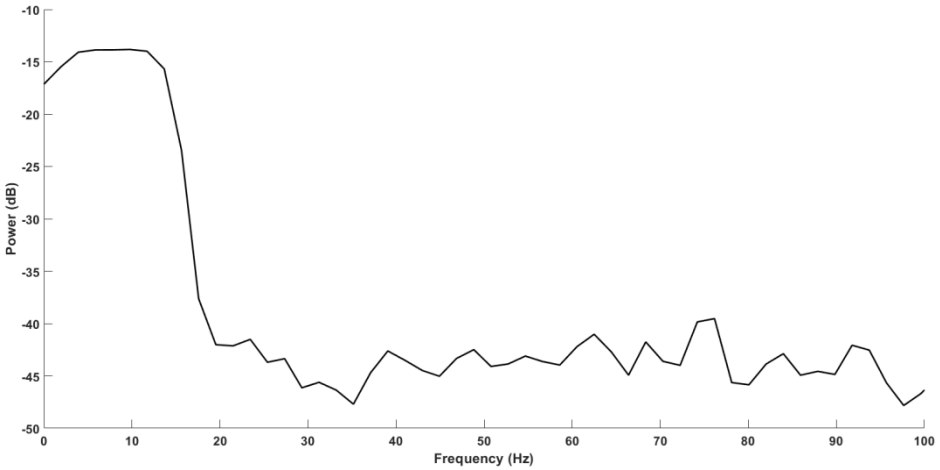

Figure 9. Fourier power spectrum from the ground truth signal.

When the FFT of the ground truth signal is computed, Figure 9, the fact that the frequency is linearly increasing and therefore there is not overlap of multiple frequencies is lost. The outcome of FFT thus allows understanding that multiple oscillators are present from 0 to ≈ 15 Hz, but gives not temporal information, as expected. In addition, the resolution in the frequency domain is quite poor, as the ground truth signal finishes abruptly in 15 Hz but the FFT predicts a soft decay that covers several Hz in the frequency axis.

1.3.2 Short-Term Fourier Transform

Short-Time Fourier Transform (STFT) is an extension of the Fourier Transform that aims to preserve the temporal information existing in the signal [79]. In summary, it divides a longer signal in multiple fragments and computes the Fourier Transform of each of them.

The critical point in the computation of the STFT is the size of the window that is going to be used to divide the original signal. This non-trivial decision while determine the definitive output, as big windows are better to obtain a correct description of the changes in time of slow frequencies to the price of a poorer temporal resolution in high frequencies. On the other hand small windows will favour the analysis of high frequencies at the cost of losing temporal and frequency resolution in slow frequencies. This trade-off between frequency and temporal resolution is known as Heisenberg Uncertainty Principle. In addition, the assumption that the signal is composed by an infinite series of sine waves is still presents, with its subsequent problems when used in nonlinear signals.

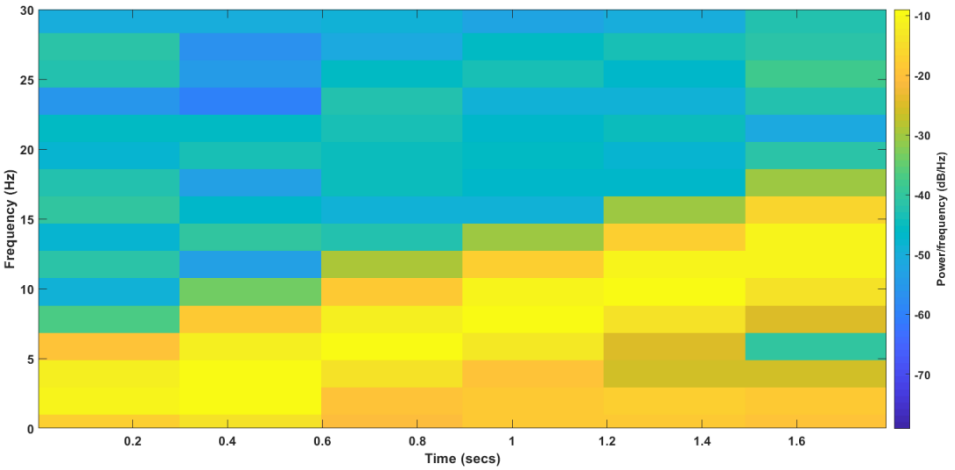

Figure 10. Spectrogram from ground truth signal.

The computation of the STFT to the ground truth signal, using an spectrogram [79], Figure 10, provides a time-frequency spectrum on which it is possible to appreciate that the signal is conveyed between 0 and 15 Hz, as well as an increase through time of the signal frequency. Nevertheless, the frequency resolution is very poor (≈ 5Hz resolution) and the temporal resolution is also bad; since big windows had to be used to obtain the best resolution possible at low frequencies.

1.3.3 Wavelet analysis

Wavelets analysis is an alternative Time-Frequency analysis that have been widely used in neuroscience during the last decades [79–81] [+refs]. The main advantage is that neuroscientists can use wavelets of any arbitrary shape to decompose the signal into a set of components, in a similar approach to the one of STFT but with a template that is, or tries to be, much similar to the neuronal signal that is being studied. In order to achieve this, many families of wavelets have evolved to mimic a variety of wave shapes, either biological or of any source [refs].

The other major improvement that was introduced into Time-Frequency analysis when Wavelets were invented is its approach against the Heisenberg Uncertainty Principle. The concept of Heisenberg Uncertainty Principle in Time-Frequency analysis refers to the compromise between the resolution in the temporal and frequency domains of the decomposition. In order to be able to depict a slow oscillation, the selected window has to have a time length enough as to cover a full cycle of such waves; hence, the temporal resolution of the higher frequencies inside this window will be very poor, as they are treated as stationary following FFT assumptions. The approach used by wavelet analysis is to divide the frequency axis in a subset of bands, then to start with a window of the same length of the signal. This window is used to compute the spectral properties of the band of the slowest

existing frequency. Afterwards, the signal is split in two halves and the coefficients of the second band are computed. This process is repeated along all the subset of bands in the frequency axis, so that the resolution between frequency and temporal resolution is optimal in every frequency band.

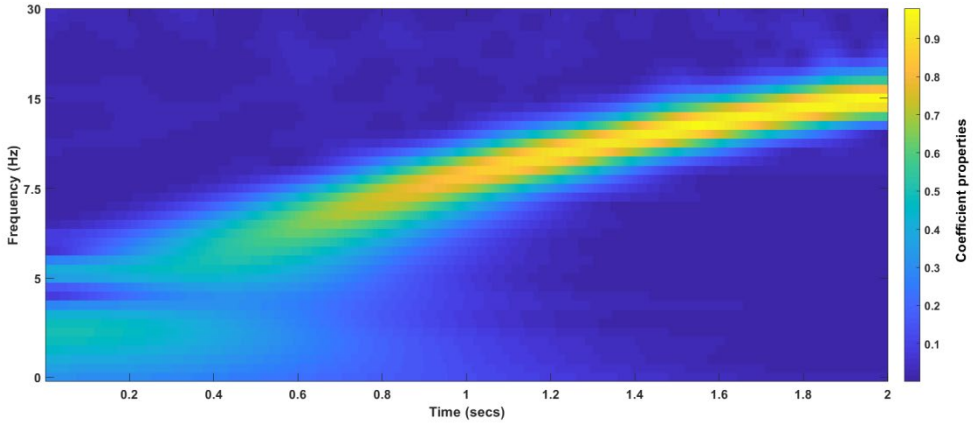

Figure 11. Wavelet decomposition of the ground truth signal

When we compute the continuous wavelet transform of the ground truth, Figure 11, signal we can easily see that the obtained T-F spectrum is improved in comparison to the STFT. Temporal and frequency resolution are greatly improved. Nevertheless, they are still blurred, especially for low frequencies; we see how the resolution in the frequency axis is still imperfect and the decomposition in the 0-5 Hz range is very noisy and lacks of temporal resolution.

Thus, we conclude that the use of wavelets implied a major improvement in the T-F analysis of nonlinear signals, but that this technique is still not precise enough as to depict the subtleties of complex oscillators. Hence, new techniques, which for the first time didn't depend on fixed templates, were developed.

1.3.4 Empirical Mode Decomposition

The Empirical Mode Decomposition (EMD) was created by Huang and presented for the first time in his seminal paper from 1998 [82] entitled "The empirical mode decomposition and the Hilbert spectrum for nonlinear and non-stationary time series analysis". EMD supposed the first method that was specifically designed to analyse nonlinear and nonstationary signal with no regards to the cycle by cycle shape of the signal of interest.

In brief, EMD consists on the interpolation via a cubic spline and posterior subtraction of the local maxima and minima present in the signal until a certain criteria is satisfied [83]. By means of this data-driven approach, a subset of function called Intrinsic Mode Functions (IMFs) is created. Once the original signal is decomposed in a subset of IMFs, which carry

the oscillatory components at different frequency bands, Hilbert transform (HT) is applied. The Hilbert transform is a point by point convolution that allows computing the instantaneous frequency (IT) and amplitude of the signal, hence retaining the original temporal resolution of the signal.

Algorithm 1. The standard EMD algorithm[82].

1. Find the locations of all the extrema of $x'(k)$.

2. Interpolate (using cubic spline interpolation) between all the minima (respectively maxima) to obtain the lower signal envelope, $e_{min}(k)$ (respectively $e_{max}(k)$).

3. Compute the local mean $m(k) = [e_{min}(k) + emax(k)]/2$.

4. Subtract the mean from the signal to obtain the 'oscillatory mode' $s(k) = x'(k) - m(k)$.

5. If $s(k)$ obeys the stopping criteria, then we define $d(k) = s(k)$ as an IMF, otherwise set $x'(k) = s(k)$ and repeat the process from step 1.

Thanks to this novel approach, the EMD implied several drastic improvements in the field if T-F analysis [43]:

First, it does not use any kind of predefined template to decompose the signal, unlike Fourier and wavelet approaches; therefore, it does not depend on any wave shape assumption that can compromise the reliability of the decomposition if not satisfied.

Second, the amplitude and IF of the IMFs is calculated in a point by point convolution which does not compromise the time resolution of the signal. This means that the use of EMD+HT does not suffer from the uncertainty principle that affects to Fourier or wavelets decomposition. This principle implies that if you increase the resolution in the frequency domain it will be to the prize of compromising the temporal resolution and vice versa. The temporal resolution of your signal is determined by the size of the window you use, and this compromises both the resolution of the obtained spectrum and the analysis of nonstationary signals. Thanks to the accurate data-driven band-passing of the signal that is produced when the EMD is computed, HT can be applied to each of them without the risk of high frequencies being overrepresented, thus maintaining the original resolution of the data.

Third, the use of a data-driven band-passing of the signal allows the researcher to study the multiple oscillatory components of the signal of interest without introducing his/her own biases via the selection of specific frequency bands. By means of using EMD, the original signal is band-passed based on the existing oscillators of the signal. If we consider that neuronal signal oscillate at multiple time scales simultaneously [5,18,19,40,84], this improvement from previous T-F tools turns to be extremely important.

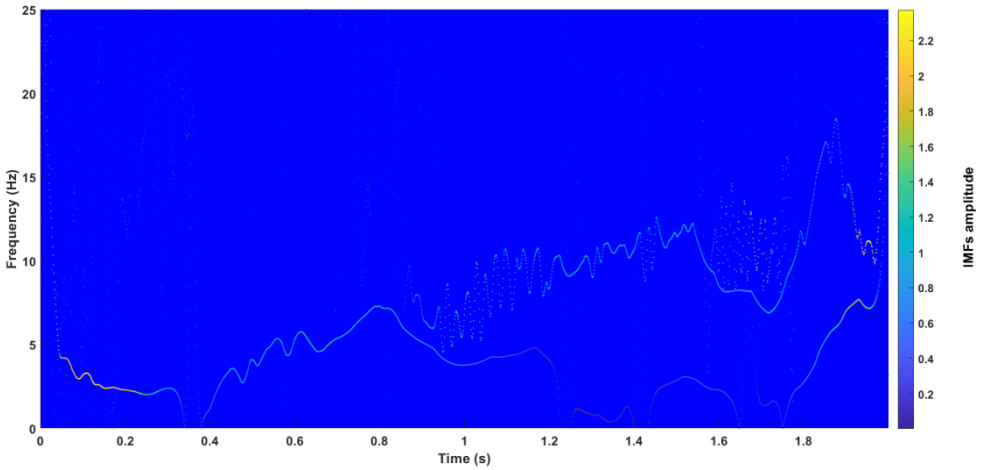

Figure 12. IMFs obtained from EMD decomposition of the ground truth signal.

When we apply the EMD to the ground truth signal, Figure 12, it is seen that the obtained spectrum is remarkably different, due to the reasons explained above. The so called Huang-Hilbert Spectrum (HHS) results from the representation of the frequency and amplitude of all the obtained IMFs. It preserves the temporal resolution of the signal and is able to capture the corruption of the signal that was produced by the addition of white noise. The fact that these properties are present in the HHS converts it into a major improvement when it is compared with previous T-F analysis tools.

Nevertheless, there are some issues in the use of EMD that have to be addressed. The first and more obvious is that there is a loss of resolution in the boundaries of the signal; this issue is frequently solved by attaching white noise vectors to the borders of the signal of interest and then removing them after the computation of EMD. The second problem is called “mode mixing”[82,85,86], it consist on punctual overlaps in the frequency domain among different IMFs (see seconds 1.6 to 1.8 in Fig. X). When this occurs, the assumption that each IMFs carries the information at a certain frequency bandwidth is violated, and hence compromises the accurate decomposition of the signal. To solve this problem, there were suggested different types of algorithms (see *Noise assisted EMDs*).

1.3.5 MEMD

The data driven approach of the EMD provides an extreme flexibility to decompose an oscillatory signal despite the changes in the cycle-by-cycle shape and the intermittency of the different frequency bands. The prize it has to pay is the variable dimensionality of its output, due to the iterative processed used to compute the IMFs leads to a variable number of them. Therefore, it is hard to compare the spectra of multidimensional signals (e.g. EEG [87]) as each of them may be represented by a different number of IMFs.

This problem was solved by Rehman and Mandic in 2010, who developed the multivariate extension of the EMD, called Multivariate Empirical Mode Decomposition or MEMD [88]. The idea is to apply the EMD to all the dimensions of the signal simultaneously to ensure that the same number of IMFs will be produced from each channel. The difficulty to achieve this consisted on the fuzzy definition of local extrema in multidimensional signals. To do so, MEMD computes multiple uniformly distributed projections in the n- dimensional space are calculated using a V-point Hammersley sequence [89] ; these projections extrema are interpolated with a cubic spline and averaged to compute the local mean, as in the original EMD [82].

Algorithm 2. Multivariate extension of EMD[88].

1. Choose a suitable point set for sampling on an (n −1) sphere.
2. Calculate a projection, denoted by $p^{\theta k}(t)\}_{t=1}^{T}$, of the input signal $\{v(t)\}_{t=1}^{T}$ along the direction vector $x^{\theta k}$, for all k (the whole set of vectors), giving $p^{\theta k}(t)\}_{t=1}^{T}$ as the set of projections.
3. Find the time instants $\{t_i^{\theta k}\}$ corresponding to the maxima of the set of projected signals $p^{\theta k}(t)\}_{t=1}^{T}$.
4. Interpolate $[t_i^{\theta k}, v(t_i^{\theta k})]$ to obtain multivariate envelope curves $e^{\theta k}(t)\}_{k=1}^{K}$.
5. For a set of K direction vectors, the mean m(t) of the envelope curves is calculated as $m(t) = \frac{1}{K}\sum_{k=1}^{K} e^{\theta k}(t)$.
6. Extract the 'detail' d(t) using d(t) = x(t) - m(t). If the 'detail' d(t) fulfils the stoppage criterion for a multivariate IMF, apply the above procedure to x(t) – d(t), otherwise apply it to d(t).

Thanks to the MEMD it became possible to analyse multidimensional signals using EMD algorithms. Then, the next step was to solve the mode mixing problem; to do so, novel algorithms were designed that profited from the statistical properties of white noise to assist the decomposition of the signal.

1.3.6 Noise assisted EMDs

Several works in the early 2000s [90,91] demonstrated that when applied to pure white noise, the EMD acted as an adaptive dyadic filter bank, as white noise is present in all frequencies at any time, it avoid the presence of intermittences in the signal, as it is projected on top of a uniform noise background. Therefore, the presence of a uniformly distributed signal across all frequencies, together with the decrease of intermittency of the signal lead to a major decrease of the mode mixing. This approaches were noise is used to enhance the analysis of a given signal are called Noise Assisted Data Analysis algorithms

(NADA). Two main NADA EMDs derived algorithms will be discussed here, EEMD[86] and NA-MEMD[92], being the later the algorithm used for T-F analysis in this work.

The Ensemble Empirical Mode Decomposition (EEMD) is a noise assisted extension of the original EMD [86]. In brief, the idea is to add white noise to the signal before computing the EMD. Since the addition of white noise can substantially corrupt the original signal, this process is repeated many times and averaged. Therefore, only the original signal will remain after the calculation of the mean of all repetitions and the noise will be cancelled out. Despite the improvement of the EEMD when compared with EMD, in terms of an improvement in the mode mixing, it still has some crucial flaws, as it is restricted to univariate signal an extremely computationally expensive, given that the EMD has to be computed many times to produce the ensembles that will be averaged.

The Noise-Assisted Multivariate Empirical Mode Decomposition (NA-MEMD) is as, as self-explained in its name, a NADA version of the MEMD [92]. The idea is to add white noise in independent dimensions of the signal, so that they when decomposed via MEMD they will act as dyadic filter bank from where the channels that carry the real signal will benefit. It has two major improvements when compared with the EEMD: First, the noise is never mixed with the original signal hence contamination is not possible; second, as an extension of the MEMD, it can be used in multivariate signals.

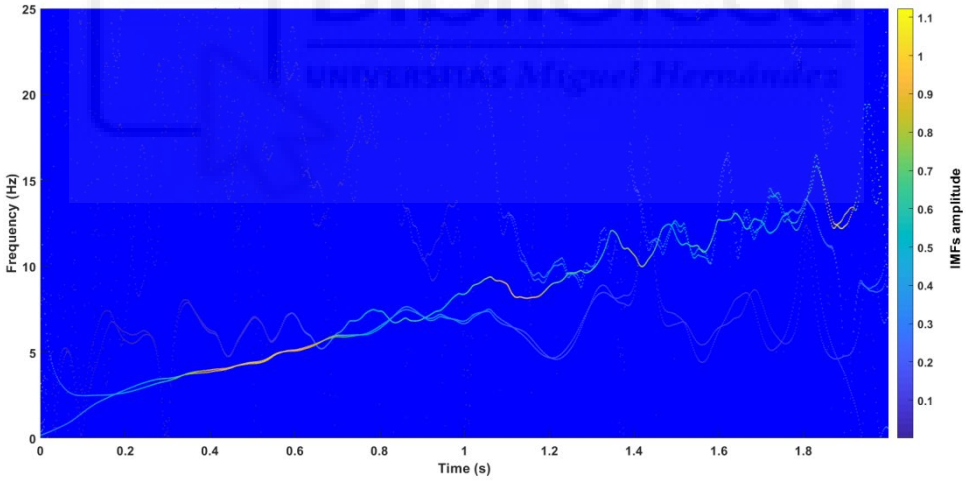

Figure 13. IMFs obtained from NA-MEMD decomposition of the ground truth signal.

In order to compute the NA-MEMD of the ground-truth signal, Figure 13, we created a 3-dimensional vector including 2 vectors composed of white noise; then, we computed the NA-MEMD of this matrix and obtained the IMFs resulting from the decomposition of the ground-truth signal, discarding those obtained from the decomposition of the WN once it had fulfilled its utility as filter bank. We can see that there exists and improvement in performance when compared with the classical EMD decomposition: The resolution of the decomposition has improved, especially in the borders of the signal and mode mixing has been strongly reduced.

1.3.7 The use of EMDs in neuroscience

Since its origin in 1998, EMD algorithm and its derivatives have been gradually introduced to the toolbox of neuroscience research. Nevertheless, the number of research groups that have moved to this type of analysis is still scarce due to the novelty and complexity of the analysis of IMFs.

To the best of our knowledge, the use of EMD in neuroscience had been restricted to the study of the oscillatory activity of big cortical regions (EEG, LFP) until the publication of paper 1 presented in this thesis [36]. It was originally introduced for the study of neural signals by Liang in 2005 [93] for the study of local field potentials from macaque V4. Later, other EMD derived algorithms were introduced into neuroscience to analyse LFPs, such as MEMD[94,95] as well as to EEG studies [96–98]. In all these works, it became obvious the advance of using nonlinear and nonstationary tools to study the T-F properties of neuronal oscillations, meaning a major improvement in comparison to previous tools.

The great results presented in these papers promise an extremely exciting future where major advances in the study of the oscillatory properties of neural systems.

At this point, we have presented and extensive demonstration of the different results obtained when using different T-F algorithms to study the oscillatory properties of a known signal which has the particular properties of being nonlinear and corrupted by noise, something we expect from neuronal signals. We have shown how EMDs implied a major improvement in T-F analysis in comparison to previous existing tools, which were dependent on templates and the uncertainty principle. In particular, we have shown how NA-MEMD is the most powerful existing tool when one plans to study the oscillatory properties of nonlinear nonstationary signals. Based on these evidences, NA-MEMD is the elected tool to study the oscillatory properties of neuronal populations of visual cortex in response to visual stimulation, **Papers I & II**.

1.3 The use of machine learning in neuroscience

We will finish this chapter with a brief introduction to the multiple uses of machine learning in neuroscience. ML is a subfield of statistics and computer science, which takes advantage of the power of computers to perform iterative computations to identify the existing patterns on the data to make future models and predictions. The increase in the use of such techniques during the last years is well-known, given the growing number of papers that rely upon machine learning tools (Figure 14).

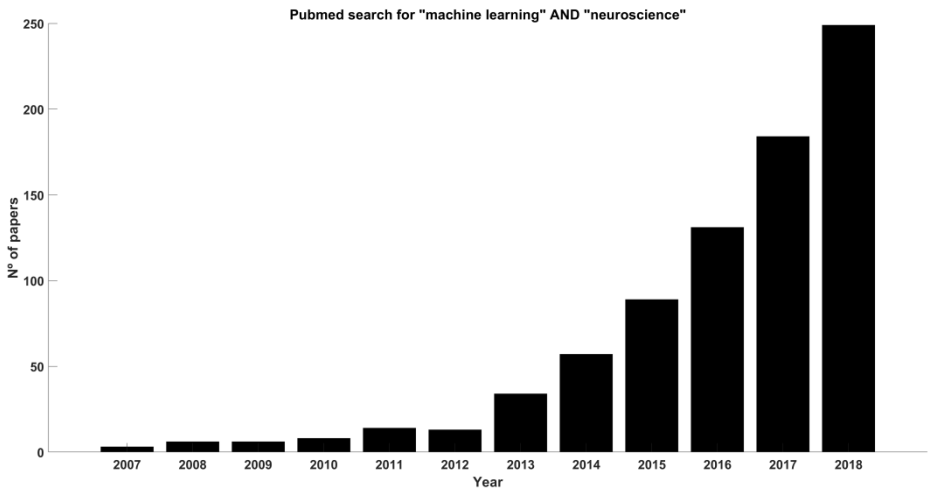

Figure 14. Evolution of the number of papers using the terms Machine Learning and Neuroscience. The use of Machine Learning tools in Neuroscience has grown exponentially during the last decade.

The increasing volume and complexity of the generated data in neuroscience exceeds the capacity of classical analysis, and they are becoming more and more difficult to analyse. Therefore, the emergence of artificial computation and machine learning techniques is becoming crucial for the interpretation and analysis of these complex data. Some examples are the interaction between networks and behaviour [99], stimulus coding [100,101], population dynamics in neural networks [102], classification of behavioural states [103,104], modelling of sensory responses [105,106] and spike sorting procedures [107–109].

In this thesis, we present a novel approach to the use of machine learning tools for the analysis of T-F properties on neuronal signals. We demonstrate in **Paper III** how the combined use of EMDs family of algorithms plus machine learning, both supervised and unsupervised, algorithms is a promising framework for the study of biological oscillations that overcomes many of the previously existing problems in this field of research. The reason for the improvement in the classification was the use of NA-MEMD algorithm to transform the data into the T-F domain. By means of this approach, there was no information loss because of any required assumption of the algorithm and the classification in this new space was optimal both using supervised and unsupervised techniques. In the other hand, when classical linear techniques were used (Fourier, wavelets), the required information blurred the signals and the consequent loss of information impaired an effective classification.

1.4 Research lines

This thesis will combine two main research lines: The first is the search of new computational tools for the study of neural oscillations in general and spike oscillations in particular, considering their nonlinear properties. The other main research line in this thesis is the study of interval time coding in the primary visual cortex.

Regarding the former objective, the search of new tools to analysis neural, mainly spikes, oscillations, I studied the use of Noise-Assisted Multivariate Empirical Mode Decomposition for the analysis of the oscillation of neuronal populations. The main advantages of this algorithm compared to previously used techniques is the capacity to deal with the nonlinear and nonstationary properties of neural oscillations. To the best of our knowledge, this thesis was the first scientific study on which any EMD algorithm was used to study oscillatory spiking dynamics. The results of this research line are published in the **paper "Time–frequency analysis of neuronal populations with instantaneous resolution based on noise-assisted multivariate empirical mode decomposition"**. In a later stage of this thesis, we extended this research line, studying whether a combination of NA-MEMD plus machine learning classification could be an effective tool to cluster and study neural oscillations. The results of this second part of this research line are published in the paper **"Toward an improvement of neural coding"**.

Regarding the later line of research, consisting on the study of interval time coding in the primary visual cortex, we studied if interstimulus interval in the seconds range was encoded in spiking oscillations of the deep layers of visual cortex. I studied if the response to a known grating visual stimulation was modulated by the temporal length of the interstimulus interval in the seconds range. In particular, this research line focused on the study of global oscillation in the population response to the visual stimulation that might be informative of the interval of stimulation. The results of this research line are published in the paper **"Multiscale dynamics of interstimulus interval integration in visual cortex"**.

2. Objectives

The aim of this Thesis is to find novel computational tools suitable for the analysis of neural oscillations specifically addressing their nonlinear and nonstationary properties and to use them to study how the deep layers of visual cortex encode interval time at seconds scale.

Specifically, the main objectives are:

1. Design a new framework for the study of neuronal oscillations, studying the most suitable algorithms for the analysis of neuronal oscillations in general, and spike oscillations in particular.

2. Apply the novel analysis to the study of the evoked spiking oscillatory activity of deep layers of visual cortex to understand how interval length at seconds scale is represented during sensory stimulation.

3. Propose a new perspective on the study of neuronal oscillations combining the use of algorithms suitable for the analysis of nonlinear and nonstationary signals and machine learning tools.

3. Material and methods

In this chapter, we will summarize the experimental procedures carried out during this Thesis.

3.1 Rat visual cortex recordings

3.1.1 Surgery

Visual cortex multi-unit recordings were obtained from male Long Evans adult rats weighing 450–500 g. Animals were pre-treated with dexamethasone (1 mg kg−1i.p) 24 h and 20 min prior to surgery in order to avoid brain oedema caused by the electrode insertion and analgesia was induced by buprenorphine (0.025 mg kg−1s.c), and surgical anaesthesia and sedation were induced by ketamine HCl (40 mg kg−1i.p). The anaesthesia was maintained with a mix of oxygen and 2% of isoflurane during the surgery and afterwards reduced to 1.5% during the electrophysiological recordings. The blinking and toe pinch reflexes, body temperature, heart rate and 0_2 concentration were continuously checked along the experiment to guarantee a proper level of anaesthesia for the animal. A craniotomy was drilled on top of the visual cortex and the electrode array was inserted 2 mm lateral to the midline and from 0.5 mm anterior to lambda. Then, a Utah array was inserted in the deep layers of the visual cortex (>600 μm) with a Blackrock pneumatically-actuated inserter device specifically designed for implanting the Utah array through the duramatter with a minimal tissue offense (Blackrock Microsystems, Salt Lake City, USA). The customized microelectrode Utah array consisted of 6 × 6 tungsten microneedles, covering a brain surface of 2 mm × 2 mm millimetres (400 μm spacing). After the insertion, the ipsilateral eyelid to the craniotomy site was closed with cyanoacrylate and atropine sulphate 1% was used to dilate the pupil of the contralateral eye.

3.1.2 Acquisition system

In vivo neural activity from visual cortex was recorded simultaneously from 16 individual electrodes with the Utah array. The Utah array was connected to a MPA32I amplifier (Multichannel Systems, MCS) and the extracellular recordings were digitized with a MCS analog-to-digital board. The data were sampled at a frequency of 20 kHz and slow waves were digitally filtered out(100–3000 Hz, 2nd order Butterworth type IIR digital filter) from the raw data. Neural spike events were extracted with a free tool application for offline spike sorting analysis (Neural Sorter, http://sourceforge.net/projects/neuralsorter/) and the resulting multiunit information obtained from each electrode was stored for further analysis.

3.1.3 Visual stimulation

Visual stimulation consisted on a vertical drifting square-wave grating (90◦, light and dark bars, 100% contrast, 6 Hz, 0.6cycles/degree) of 500 ms duration interspersed with a dark (uniform) stimulus of equal duration. The stimulus was displayed on a LCD monitor (refresh rate 60 Hz) and a luminance of ≈100 cd/m2 placed 25 cm in front of the right eye, approximately at 30◦ from the midline and covering a visual field spanning ≈10. The stimulus was generated using the vision egg library and a python script. The room was kept in darkness throughout the visual stimulation.

3.2 Other recordings used in this thesis

Recordings obtained from collaboration with other labs or members from our lab were used during this thesis. The methods used to obtain vibrissal nerve recordings are presented here [110], while methods used to obtain the neuronal culture recordings are presented here [111].

3.3 NA-MEMD

We used an extension of the EMD algorithm to study the T-F properties of the neural response. The Multivariate Empirical Mode Decomposition (MEMD), which is a multivariate extension of EMD algorithm, where analysis of simultaneous dimensions is performed simultaneously to obtain a meaningful decomposition of the whole multidimensional signal in a subset of vectors called Intrinsic Mode Functions (IMFs). Furthermore, we added White Gaussian Noise (WGN) to the MEMD, which increases its performance via reducing mode mixing produced by signal intermittency. This procedure acts as a filter bank that enhances time-frequency resolution.

3.4 Machine learning

We used different machine learning algorithms to classify neural activity patterns from its Time-Frequency domain. Supervised classification was performed using MLPs, a fully connected multi-layered neuronal network. When unsupervised classification was performed, t-SNE + k-means or PCA + DBSCAN approaches were used.

3.5 Statistical analysis

All experimental comparisons were tested using Wilcoxon rank-sum test. P values for multiple comparisons were corrected ad hoc using Storey method.

4. Results

The main goals of this thesis consist on the search of novel computational frameworks for the study of neuronal oscillations, as well as the use of such tools to study interval integration in neuronal populations of deep layers of visual cortex.

We have demonstrated that NA-MEMD is an effective tool to analyse population recordings. This algorithm is capable of dealing with the nonlinear and nonstationary properties of neuronal signals, thus overcoming the limitations of classical T-F tools (Fourier, wavelets…) **[Paper I in this thesis]**. To do so we used two different types of neuronal recordings. First, we compared the efficiency to distinguish different textures in contact with a whisker by means of recording in the trigeminal nerve, this data was contributed by our collaborators from Felipe lab. We showed that a transformation of this data to the T-F domain using the NA-MEMD algorithm outperformed previous results on this dataset. We also demonstrated that nonlinearities were present on the data and they were adequately captured by the NA-MEMD. In addition, we recorded neuronal populations from rat visual cortex during visual stimulation with a moving grating. We compared the projection into the T-F space of the evoked spiking activity using traditional techniques (spectrogram) and NA-MEMD and showed how the signal was again nonlinear and intermittent, compromising the accuracy of traditional linear techniques. Therefore, we demonstrated that NA-MEMD is a proper tool for the study of spiking oscillatory activity.

Once we found an adequate tool for the study of spike oscillations, we used it to study whether interval time at seconds scale is represented in the deep layers of visual cortex by spiking oscillatory activity **[Paper II in this thesis]**. To do so, we recorded neuronal populations from the deep layers of visual cortex in anaesthetised rats while being visually stimulated with an unchanged moving grating and different intervals between repetitions of 1, 3, 5 or 7 seconds. As a first approach to study the effect of ISI at seconds range during visual stimulation, we showed that the firing rate was increased for 3 or 5 seconds intervals when compared with 1 second, as well that the C.V. was decreased for longer than 1 second intervals. Both results together suggest a more robust and reliable evoked response when longer intervals were used.

In order to better describe the changes in the evoked spiking response, we studied its oscillatory properties using NA-MEMD as described in Paper I of this thesis. We computed the HHS of the mean population spiking activity in response to the same grating stimulus while stimulating with different intervals in seconds range and compared the obtained spectra. Major differences at multiple frequencies and times were seen when 1 second was compared with longer times, especially with 3 and 5 seconds. Two frequencies bands were significantly different during almost the whole stimulation window. The band centred around 6Hz, was interesting because it coincided with the grating frequency and was increased only when 3 or 5 seconds intervals, but not 7, were used. It was also worth to note the relevance of the frequency band around 10 Hz, which was significantly relevant when all longer ISIs were compared with 1 seconds. The effect of ISI time length in higher frequency oscillations of spikes (33 to 150 Hz bandwidth) was more intermittent.

Statistically significant different remained present with different temporal profiles, mostly for 3 and 5 seconds ISIs. A brief significant window occurred 200 ms after stimulus onset when all intervals longer than 1 second were used; in addition, a second discrimination window in the second half of the response was visible only when 3 or 5 seconds intervals were used.

Considering these results, we proposed a phase space on which ISI could be discriminated, in which visual cortex neuronal populations would be able to discriminate among ISIs depending on the elicited dynamics, using three relevant parameters of the response: firing rate, low frequency (6 Hz) and high frequency (18 Hz) dynamics. In this space, population dynamics were confined to an attractor until stimulation, when different trajectories emerge depending on the used ISI during stimulation. When we computed the Euclidean distance to the centroid of this attractor we could demonstrate that 1 second ISI didn´t evoked a trajectory that left the attractor, 3 and 5 seconds ISI produced big trajectories that didn't return to the original subspace until stimulation was finished, and 7s ISI produced a trajectory that left transitory the initial subspace and returned 200-300 afterwards. These results support the idea of a multiscale response, in which neuronal populations encode ISI information using multiple frequencies and firing rates in their spiking dynamics.

Following our interest on studying the strengths in the use of NA-MEMD as a tool to study neuronal oscillations, we decided to combine it with supervised ML classification to classify single-trial stimulation based on its oscillatory activity **[Paper III in this thesis]**. We hypothesized that the use of NA-MEMD would prevent from any information loss in the transformation of the data to the T-F domain from where to extract the desired parameters to classify the neuronal activity. Therefore, as all the information would be available for the classification, it would not be required to rely on complex deep ML tools, but to use more straightforward, shallow algorithms.

To address our hypothesis, we used NA-MEMD + ML tools to classify single trials of trigeminal nerve recordings during tactile stimulation with different textures. We demonstrated than once the T-F features were obtained by means of NA-MEMD plus Hilbert Transform, 100% correct classification could be obtained both with supervised (MLP) and unsupervised (t-SNE + k-means clustering) techniques. This result outperformed the existing bibliography on the classification of the same dataset, which used standard T-F tools and was limited to 70% correct classification.

In a second experiment, we recorded populations from a neuronal culture seeded over a multielectrode array and classified the individual trials while stimulating on one from two possible electrodes. We demonstrated again that the use of NA-MEMD and Hilbert Transform together with either supervised (MLP) or unsupervised (PCA + DBSCAN clustering) outperformed traditional T-F tools that were not able to be used to classify the evoked neuronal patterns over chance level.

5. Discussion

In this chapter, we will discuss the results obtained in the present Thesis.

5.1 NA-MEMD as a tool to study spike oscillations

In Paper I I studied the computational strength of NA-MEMD algorithm to provide an accurate T-F decomposition of spike oscillations. The difficulty of this task is due to the nonlinear and nonstationary properties of spike dynamics [37,38,112]. These makes traditional T-F techniques unviable tool for a correct understanding of the oscillatory properties of spikes, since they require certain assumptions, like fixed wave-shape and stationarity, that are not fulfilled. To overcome this problem, EMD algorithms have been used in neuroscience during the last years, although its implementation in the field is still scarce and mostly focused on global oscillations as EEG or LFP [87,94–96], rather than discrete neurons or populations. We extended this study to the study of spikes oscillations, therefore providing the first demonstration of the viability of NA-MEMD as an efficient tool to directly study neuronal activity.

I was able to demonstrate the necessity to use instantaneous frequency to correctly study the existing nonlinearities in spike oscillations. To do so, I made clear the presence of intrawave modulation within each cycle during spike trains and other neural recordings. It is obvious that any analysis based on fixed templates will not be able to catch these intrawave modulations and therefore will blur the obtained results.

This result also implies than a re-analysis of pre-existing recordings may provide novel insights about how the brain works without the need to design new experiments, as new knowledge can emerge once the linearity and stationarity assumptions that have historically dominated T-F analysis are overcame. Paper III in this thesis presents a clear example. The possible impact of re-analysing decades of neuronal recordings in neuroscience is unknown, but it may become a major step forward in our understanding of the nervous system.

5.2 Interstimulus interval at seconds scale is encoded in spikes oscillation of Deep layers in V1

One of the main objectives of this thesis was to study the changes in visual response of rats in response to changes in the ISI at seconds scale. This question is of great interest to understand how the brain works, as the understanding of time processing has been elusive despite the decades of research on this topic that have been devoted to answer this question since the first related experiment [113].

I have demonstrated that the ISI in the seconds range is encoded in the population response during a visual stimulation task. These changes were present at the level of firing rate and the oscillatory dynamics of the response. I did also demonstrate that changes in the ISI had an effect on multiple frequencies simultaneously; therefore we support a multiplexed mechanism for time encoding in visual cortex, on which multiple oscillators are involved [19]. It is also worth to notice that the oscillations present in the visual response were intermittent and nonlinear, supporting the use of NA-MEMD to analyse them. I did also show that these changes were restricted to a certain time window of 3-5 seconds and were reduced for longer intervals (7 seconds). Therefore, this work suggests that visual cortex can encode visual information through time up to several seconds.

In an effort to better describe our results, I created a low dimensional phase space on which I could project the evoked trajectories produced by visual stimulation, using a subset of features that we had demonstrated to be relevant in ISI encoding. These selected features were the firing rate and the amplitude at 6Hz and 18Hz. In this phase space, the averaged population activity was confined into a small attractor during spontaneous activity until the stimulus started. Once the stimulus was triggered, the evoked response was represented as a given trajectory as the evolution of the selected features during time. These trajectories were remarkably different depending on the used ISI. The evoked trajectories were projected more distantly and during more time from the attractor when 3 or 5 seconds ISI were used, while there were almost no changes when 1s ISI was used. The trajectory corresponding to 7 seconds ISI was clearly leaving the attractor, but not as distantly as when 3 or 5 seconds ISI were used, and returned to the original point earlier. Therefore, it turned clear that we could create a boundary in this phase space which would be useful to separate the ISIs with a bigger effect on the visual response (3 or 5 seconds) from the others (1 or 7 seconds). The fact that multiple oscillators were relevant to generate this phase space once again reinforces the idea of multiplexed time processing in visual cortex.

In conclusion, I have demonstrated that visual cortex can encode temporal information in seconds scale, a computational property that was not expected to be found in a primary sensory cortex. I have also studied the dynamics of ISI encoding in visual cortex, we showed that certain interval time windows (3-5 seconds) evoke a response in neuronal populations of visual cortex with an increased firing rate when compared to classical (1 second) intervals. Moreover, spiking activity was organized in multiplexed nonlinear oscillators depending on the ISI. A combination of firing rate and amplitude of oscillation at certain frequency created a phase space in which the visual response to the same grating stimulus could be separated unambiguously depending of the ISI used during stimulation.

5.3 NA-MEMD+ML for neural activity pattern analysis

Despite the major advances in neuroscience that have been produced thanks to the introduction of ML tools into the neuroscientist toolbox [100–103,109,114,115], it is surprising that T-F analysis has not evolved proportionally. I hypothesized that problems in ML classification/modelling of neuronal activity in the T-F domain are caused, not because of a bad implementation or lack of power of the ML algorithms, but from the stationary and linear assumptions of the tools that are classically used to project the data into the T-F domain (Fourier series, wavelets…); these assumptions produce an information loss that blurs any posterior analysis. In this context, we suggested that a faithful transformation of the data to the T-F domain would produce major improvements in the classification/modelling of neuronal oscillatory events.

In this thesis, I addressed such question, demonstrating that a combination of NA-MEMD + ML algorithms greatly outperforms to classical spectral tools. The improvement in the classification of the neuronal events is thanks to the increase in the faithfulness of the transformation to the T-F space thanks to the capacity of NA-MEMD to accurately describe the nonlinearities and nonstationarities present in the neuronal data.

I suggest that this new approach to T-F classification/modelling of neuronal data may lead to a new step in our understanding of the brain and the use of neuronal signal for BMIs. I base this statement on our results, which have shown that NA-MEMD+ML classification not only outperformed classical analysis but also became more reliable in a single-trial analysis framework.

5.4 The elephant in the room, why we didn´t apply ML to understand visual interstimulus timing.

The problem I faced is known as the curse of dimensionality, the amount of data you require to model/classify a given problem grows exponentially with the number of dimensions in the data, and visual cortex dynamics are high-dimensional [Stringer papers 2018].

There were two main sources of variability, trial-by trial variability and neurons heterogeneous responses:

The evoked response in visual cortex neurons to a given visual stimulus is highly variable from one trial to the following [116–118]. It is of special interest that the main source of this variability is not the perception of the environment by itself, but is self-generated in the cortex, given that trial-to-trial variability in V1 is much higher than in the lateral geniculate

nucleus of the thalamus [116]. This variability is correlated among the neurons of the populations [37], so it cannot be easily subtracted by averaging their evoked activity. The source of this shared trial-to-trial variability is not stochastic but due to different synaptic activation dynamics during cortical sensory activation [117,119]. This variability is supposed to be caused by parallel computations to perception that are carried on in the visual cortex together with vision; in example, recent works from Carandini and Harris' lab [20] have demonstrated that activity in visual cortex is strongly driven by motor activity, both during darkness periods and stimulation. These hidden variables during the recordings increase the variability and thus the difficulty of studying the different intervals used by means of Machine Learning tools, extremely data avid.

The other source of variability is the heterogeneity of responses in visual cortex. Rodent visual cortex has a salt-and-pepper distribution of neurons with highly specific receptive fields that create multiple sub-networks intermixed in space [44,120]. Therefore, when you record a population of random neurons in visual cortex, you find a great variability of RFs profiles that increase the variability and dimensionality of the recorded population.

Taking together the heterogeneity of visual tuning and the major modulation of visual responses by the ongoing state of the cortex, it turns out that the number of dimensions that are required to accurately describe all the variability existent in visual cortex may range from 50 to 100 dimensions [20,121]. Given a general rule of thumb that states a minimum of 20 data points per dimension for a reliable classification, it might be required experiments with ~2000 trials when ML tools want to be used to study visual cortex population dynamics. Even if dimensionality can be reduced via feature extraction from the recorded population, these numbers give an idea of the enormous variability and therefore data that must be collected, both in terms of neurons and trials, to perform a robust trial-by-trial study of interval timing in visual cortex.

Nevertheless, I am positive about the future. Recent improvements in massive neuronal recordings and behaviour tracking create a fascinating landscape on which we cannot but expect exciting result from the combination of such techniques with NA-MEMD and ML tools to understand the role of oscillations in visual cortex during timing tasks in particular, and behaviour in general.

5.5 Future lines of research

Once we have demonstrated that interstimulus intervals, at the level of seconds scale, modulates the activity of neuronal populations of deep layers of visual cortex, our next step is to study how this code is distributed through the population.

Our aim is to study the specific weight of individual neurons in the representation of interstimulus interval, looking for answer to questions as if the changes at the population

level are caused by a minority of neurons persistently through all the trials or if it's distributed through all the neurons. We do also want to address whether there exists a subpopulation of neurons which play a role in interval but not visual perception coding. To do so, we plan to perform new experiments on which not only the interval but also the physical properties of the grating are changed. These experiments will let us understand the specific weight of individual neurons on the coding of grating perception together with time interval.

The research on time perception in sensory systems will benefit from the understanding of the intersection between sensory and time coding in visual cortex. Once we understand if the coding of time is distributed across the whole circuit or constrained to certain neurons that perform a particular subpopulation will be pivotal to design new interventional experiments to understand how does our brain perceive time.

6. Conclusions/Conclusiones

1. NA-MEMD is an effective tool for the analysis of spike oscillations.
2. Neuronal populations of deep layers of visual cortex encode interstimulus interval in the seconds range.
3. This coding of interstimulus interval involves oscillatory dynamics at the population level.
4. An optimal interval window of 3-5 seconds exists on which visual evoked response has a higher firing rate and is less variable.
5. NA-MEMD + supervised/unsupervised classification techniques outperform previously used techniques for the study of single-trial oscillatory neuronal dynamics.

1. La NA-MEMD es una herramienta efectiva para el análisis de oscilaciones de potenciales de acción.
2. Poblaciones neuronales de las capas profundas de la corteza visual codifican el intervalo inter-estímulo en el rango de segundos.
3. Este código para el intervalo inter-estímulo implica oscilaciones al nivel de la población neuronal.
4. Existe una ventana óptima de 3-5 segundos de intervalo en la que la respuesta evocada por estimulación visual tiene una mayor tasa de disparo y es más estable.
5. La combinación de NA-MEMD más técnicas de clasificación supervisada mejoras los resultados obtenidos previamente con otras técnicas para el estudio de la dinámica de oscilaciones neuronales en pruebas únicas.

7. Bibliography

1. Defelipe J, Fariñas I. The pyramidal neuron of the cerebral cortex: morphological and chemical characteristics of the synaptic inputs. Prog Neurobiol. 1992;39: 563–607.
2. Berger H. Uber das Elektrenkephalogramm des Menschen. J Psycho Neurol. 1929;40: 160–179.
3. Bishop GH. Cyclic changes in excitability of the optic pathway of the rabit. 1933;
4. Schroeder CE, Lakatos P. Low-frequency neuronal oscillations as instruments of sensory selection. Trends Neurosci. 2009;32: 9–18. doi:10.1016/j.tins.2008.09.012
5. Buzsáki G, Draguhn A. Neuronal Oscillations in Cortical Networks. 2014;1926: 1926–1930. doi:10.1126/science.1099745
6. Steriade M, Nuñez A, Amzica F. A novel slow (< 1 Hz) oscillation of neocortical neurons in vivo: depolarizing and hyperpolarizing components. J Neurosci. 1993;13: 3252–3265. doi:3252-3265
7. Steriade M, Nunez a, Amzica F. Intracellular analysis of relations between the slow (< 1 Hz) neocortical oscillation and other sleep rhythms of the electroencephalogram. J Neurosci. 1993;13: 3266–3283. doi:10.1073/pnas.90.5.2078
8. Sanchez-Vives M V, McCormick DA. Cellular and network mechanisms of rhythmic recurrent activity in neocortex. Nat Neurosci. 2000;3: 1027–34. doi:10.1038/79848
9. Compte A, Reig R, Descalzo VF, Harvey MA, Puccini GD, Sanchez-Vives M V. Spontaneous high-frequency (10-80 Hz) oscillations during up states in the cerebral cortex in vitro. J Neurosci. 2008;28: 13828–44. doi:10.1523/JNEUROSCI.2684-08.2008
10. Sanchez-Vives M, Mattia M, Compte A, Perez-Zabalza M, Winograd M, Descalzo VF, et al. Inhibitory Modulation of Cortical Up States. J Neurophysiol. 2010;104: 1314–1324. doi:10.1152/jn.00178.2010
11. Timofeev I, Steriade M. Low-frequency rhythms in the thalamus of intact-cortex and decorticated cats. J Neurophysiol. 1996;76: 4152–4168. doi:10.1152/jn.1996.76.6.4152
12. Stern E a, Kincaid a E, Wilson CJ. Spontaneous subthreshold membrane potential fluctuations and action potential variability of rat corticostriatal and striatal neurons in vivo. J Neurophysiol. 1997;77: 1697–1715.
13. Wilson CJ, Kawaguchi Y. The origins of two-state spontaneous membrane potential fluctuations of neostriatal spiny neurons. J Neurosci. 1996;16: 2397–410. doi:10.1016/0006-8993(81)90211-0
14. Timofeev I. Origin of Slow Cortical Oscillations in Deafferented Cortical Slabs. Cereb Cortex. 2000;10: 1185–1199. doi:10.1093/cercor/10.12.1185
15. Gent TC, Bandarabadi M, Herrera CG, Adamantidis AR. Thalamic dual control of sleep and wakefulness. Nat Neurosci. Springer US; 2018; doi:10.1038/s41593-018-0164-7
16. Petersen CCH. Whole-Cell Recording of Neuronal Membrane Potential during Behavior. Neuron. Elsevier Inc.; 2017;95: 1266–1281. doi:10.1016/j.neuron.2017.06.049
17. Sippy T, Lapray D, Petersen CCH, Sippy T, Lapray D, Crochet S, et al. Cell-Type-Specific Sensorimotor Processing in Striatal Projection Neurons during Goal-Directed Report

Cell-Type-Specific Sensorimotor Processing in Striatal Projection Neurons during Goal-Directed Behavior. Neuron. 2015;88: 1–8. doi:10.1016/j.neuron.2015.08.039
18. Luczak A, McNaughton BL, Harris KD. Packet-based communication in the cortex. Nat Rev Neurosci. Nature Publishing Group; 2015;16: 745–755. doi:10.1038/nrn4026
19. Victor JD. How the brain uses time to represent and process visual information. Brain Res. 2000;886: 33–46. doi:10.1016/S0006-8993(00)02751-7
20. Stringer C, Pachitariu M, Steinmetz N, Reddy CB, Carandini M, Harris KD. Spontaneous behaviors drive multidimensional, brain-wide population activity. bioRxiv. 2018; 306019.
21. Okun M, Steinmetz N, Cossell L, Iacaruso MF, Ko H, Barthó P, et al. Diverse coupling of neurons to populations in sensory cortex. Nature. 2015; doi:10.1038/nature14273
22. Safaai H, von Heimendahl M, Sorando JM, Diamond ME, Maravall M. Coordinated population activity underlying texture discrimination in rat barrel cortex. J Neurosci. 2013;33: 5843–55. doi:10.1523/JNEUROSCI.3486-12.2013
23. Klaus A, Martins GJ, Paixao VB, Zhou P, Paninski L, Costa RM. The Spatiotemporal Organization of the Striatum Encodes Action Space. Neuron. Elsevier Inc.; 2017;95: 1171–1180.e7. doi:10.1016/j.neuron.2017.08.015
24. Fries P, Nikolić D, Singer W. The gamma cycle. Trends Neurosci. 2007;30: 309–316. doi:10.1016/j.tins.2007.05.005
25. Gray CM, Singer W. Stimulus-specific neuronal oscillations in orientation columns of cat visual cortex. Proc Natl Acad Sci U S A. 1989;86: 1698–1702. doi:10.1073/pnas.86.5.1698
26. Engel AK, König P, Gray CM, Singer W. Stimulus-dependent neuronal oscillations in cat visual cortex: inter-columnar interactions as determined by cross-correlation analysis. Eur J Neurosci. 1990;2: 588–606.
27. Fries P, Roelfsema PR, Engel AK, König P, Singer W. Synchronization of oscillatory responses in visual cortex correlates with perception in interocular rivalry. Proc Natl Acad Sci U S A. 1997;94: 12699–12704. doi:10.1073/pnas.94.23.12699
28. Fontolan L, Morillon B, Liegeois-Chauvel C, Giraud AL. The contribution of frequency-specific activity to hierarchical information processing in the human auditory cortex. Nat Commun. Nature Publishing Group; 2014;5: 1–10. doi:10.1038/ncomms5694
29. Hamada Y, Miyashita E, Tanaka H. Gamma-band oscillations in the “barrel cortex” precede rat’s explratory whisking. Science. 1999;88: 667–671.
30. Brosch M, Budinger E, Scheich H. Stimulus-related gamma oscillations in primate auditory cortex. J Neurophysiol. 2002;87: 2715–2725. doi:10.1152/jn.00583.2001
31. Murthy VN, Fetz EE. Coherent 25- to 35-Hz oscillations in the sensorimotor cortex of awake behaving monkeys. Proc Natl Acad Sci. 1992;89: 5670–5674. doi:10.1073/pnas.89.12.5670
32. Penttonen M, Kamondi A, Acsády L, Buzsáki G. Gamma frequency oscillation in the hippocampus of the rat: Intracellular analysis in vivo. Eur J Neurosci. 1998;10: 718–728. doi:10.1046/j.1460-9568.1998.00096.x
33. Womelsdorf T, Schoffelen J-M, Oostenveld R, Singer W, Desimone R, Engel AK, et al. Modulation of neuronal interactions through neuronal synchronization. Science.

2007;316: 1609–1612. doi:10.1126/science.1139597
34. Fries P, Reynolds JH, Rorie AE, Desimone R. Modulation of oscillatory neuronal synchronization by selective visual attention. Science. 2001;291: 1560–1563. doi:10.1126/science.1055465
35. Arnal LH, Giraud A-L. Cortical oscillations and sensory predictions. Trends Cogn Sci. Elsevier Ltd; 2012;16: 390–398. doi:10.1016/j.tics.2012.05.003
36. Alegre-Cortés J, Soto-Sanchez C, Piza AG, Albarracin AL, Farfan FD, Felice CJ, et al. Time-frequency analysis of neuronal populations with instantaneous resolution based on noise-assisted multivariate empirical mode decomposition. J Neurosci Methods. 2016;267: 35–44. doi:10.1016/j.jneumeth.2016.03.018
37. Averbeck BB, Latham PE, Pouget A. Neural correlations, population coding and computation. Nat Rev Neurosci. 2006;7: 358–66. doi:10.1038/nrn1888
38. Shamir M, Sompolinsky H. Nonlinear Population Codes. Neural Comput 16,. 2004;1136: 1105–1136.
39. Cole SR, Voytek B. Brain Oscillations and the Importance of Waveform Shape. Trends Cogn Sci. Elsevier Ltd; 2017;21: 137–149. doi:10.1016/j.tics.2016.12.008
40. Buzsáki G, Anastassiou C a, Koch C. The origin of extracellular fields and currents--EEG, ECoG, LFP and spikes. Nat Rev Neurosci. 2012;13: 407–20. doi:10.1038/nrn3241
41. Victor JD, Purpura KP. Nature and precision of temporal coding in visual cortex: a metric-space analysis. J Neurophysiol. 1996;76: 1310–26.
42. Amzica F, Steriade M. Electrophysiological correlates of sleep delta waves. Electroencephalogr Clin Neurophysiol. 1998;107: 69–83. doi:10.1016/S0013-4694(98)00051-0
43. Mandic DP, Ur Rehman N, Wu Z, Huang NE. Empirical mode decomposition-based time-frequency analysis of multivariate signals: The power of adaptive data analysis. IEEE Signal Process Mag. 2013;30: 74–86. doi:10.1109/MSP.2013.2267931
44. Huberman AD, Niell CM. What can mice tell us about how vision works? Trends Neurosci. 2012;29: 997–1003. doi:10.1016/j.biotechadv.2011.08.021.Secreted
45. Lennie P. Parallel Visual Pathways a Review.Pdf. 1974;
46. Hubel DH, Wiesel TN. Laminar and columnar distribution of geniculo???cortical fibers in the macaque monkey. J Comp Neurol. 1972;146: 421–450. doi:10.1002/cne.901460402
47. Hubel DH, Wiesel TN. Receptive Fields and Functional Architecture. J Physiol. 1968;195: 215–243.
48. Hubel DH, Wiesel TN. Receptive fields, binocular interaction and functional architecture in the cat's visual cortex. J Physiol. 1962;160: 106–154.2. doi:10.1523/JNEUROSCI.1991-09.2009
49. Roelfsema PR, de Lange FP. Early Visual Cortex as a Multiscale Cognitive Blackboard. Annu Rev Vis Sci. 2016;2: 131–151. doi:10.1146/annurev-vision-111815-114443
50. Roelfsema PR. Cortical Algorithms for Perceptual Grouping. Annu Rev Neurosci. 2006;29: 203–227. doi:10.1146/annurev.neuro.29.051605.112939
51. Drager UC. Receptive fields of single cells and topography in mouse visual cortex. J Comp Neurol. 1975;160: 269–290. doi:10.1002/cne.901600302

52. Niell CM, Stryker MP. Highly Selective Receptive Fields in Mouse Visual Cortex. 2011;28: 7520–7536. doi:10.1523/JNEUROSCI.0623-08.2008.Highly
53. Lund RD, Girman S V, Sauve Y, Sergej V, Receptive RDL, Sauvé Y. Receptive field properties of single neurons in rat primary visual cortex. J Neurophysiol. 1999;82: 301–11.
54. Métin C, Godement P, Imbert M. The primary visual cortex in the mouse: receptive field properties and functional organization C. 1986; 272–279.
55. Harris KD, Shepherd GMG. The neocortical circuit: themes and variations. Nat Neurosci. 2015;18: 170–181. doi:10.1038/nn.3917
56. Markram H. A network of tufted layer 5 pyramidal neurons. Cereb Cortex. 1997;7: 523–533. doi:10.1093/cercor/7.6.523
57. Gal E, London M, Globerson A, Ramaswamy S, Reimann MW, Muller E, et al. Rich cell-type-specific network topology in neocortical microcircuitry. Nat Neurosci. 2017; 1–10. doi:10.1038/nn.4576
58. Constantinople CM, Bruno RM. Deep Cortical Layers Are Activated Directly by Thalamus. Science (80-). 2013;1591: 1591–1594. doi:10.1126/science.1236425
59. Crochet S, Petersen CCH. Cortical Dynamics by Layers. Neuron. 2009;64: 298–300. doi:10.1016/j.neuron.2009.10.024
60. Swadlow HA. Efferent neurons and suspected interneurons in motor cortex of the awake rabbit: axonal properties, sensory receptive fields, and subthreshold synaptic inputs. J Neurophysiol. 1994;71: 437–53. doi:10.1523/JNEUROSCI
61. Medini P. Layer- and Cell-Type-Specific Subthreshold and Suprathreshold Effects of Long-Term Monocular Deprivation in Rat Visual Cortex. J Neurosci. 2011;31: 17134–17148. doi:10.1523/JNEUROSCI.2951-11.2011
62. Sakata S, Harris KD. Laminar Structure of Spontaneous and Sensory-Evoked Population Activity in Auditory Cortex. Neuron. Elsevier Ltd; 2009;64: 404–418. doi:10.1016/j.neuron.2009.09.020
63. Hooks BM, Hires SA, Zhang YX, Huber D, Petreanu L, Svoboda K, et al. Laminar analysis of excitatory local circuits in vibrissal motor and sensory cortical areas. PLoS Biol. 2011;9. doi:10.1371/journal.pbio.1000572
64. Baker A, Kalmbach B, Morishima M, Kim J, Juavinett A, Li N, et al. Specialized Subpopulations of Deep-Layer Pyramidal Neurons in the Neocortex: Bridging Cellular Properties to Functional Consequences. J Neurosci. 2018; 0150-18. doi:10.1523/JNEUROSCI.0150-18.2018
65. Adesnik H, Scanziani M. Lateral competition for cortical space by layer-specific horizontal circuits. 2010;464: 1155–1160. doi:10.1038/nature08935.Lateral
66. Lefort S, Tomm C, Floyd Sarria JC, Petersen CCH. The Excitatory Neuronal Network of the C2 Barrel Column in Mouse Primary Somatosensory Cortex. Neuron. Elsevier Inc.; 2009;61: 301–316. doi:10.1016/j.neuron.2008.12.020
67. Gilbert CD. Microcircuitry of the Visual Cortex. Annu Rev Neurosci. 1983;6: 217–247. doi:10.1146/annurev.ne.06.030183.001245
68. Thomson A. Neocortical layer 6, a review. Front Neuroanat. 2010;4: 1–14. doi:10.3389/fnana.2010.00013

69. LeVay S, Sherk H. The visual claustrum of the cat. J Neurosci. 1981;1: 956–980.
70. Vélez-Fort M, Rousseau C V., Niedworok CJ, Wickersham IR, Rancz EA, Brown APY, et al. The stimulus selectivity and connectivity of layer six principal cells reveals cortical microcircuits underlying visual processing. Neuron. 2014;83: 1431–1443. doi:10.1016/j.neuron.2014.08.001
71. Lee CC. Modulator property of the intrinsic cortical projection from layer 6 to layer 4. Front Syst Neurosci. 2009;3: 1–5. doi:10.3389/neuro.06.003.2009
72. Gray CM, König P, Engel AK, Singer W. Oscillatory responses in cat visual cortex exhibit inter-columnar synchronization which reflects global stimulus properties. Nature 1989; 338:334–337.
73. Fries P, Schröder J-H, Roelfsema PR, Singer W, Engel AK. Oscillatory neuronal synchronization in primary visual cortex as a correlate of stimulus selection. J Neurosci. 2002;22: 3739–3754. doi:20026318
74. Shuler, Marshall; Bear M. Reward Timing in the Primary Visual Cortex. Science (80-). 2006; 1606–1610.
75. Levy JM, Zold CL, Namboodiri VMK, Hussain Shuler MG. The Timing of Reward-Seeking Action Tracks Visually-Cued Theta Oscillations in Primary Visual Cortex. J Neurosci. 2017; 0923-17. doi:10.1523/JNEUROSCI.0923-17.2017
76. Zold CL, Hussain Shuler MG. Theta Oscillations in Visual Cortex Emerge with Experience to Convey Expected Reward Time and Experienced Reward Rate. J Neurosci. 2015;35: 9603–9614. doi:10.1523/JNEUROSCI.0296-15.2015
77. Cooley JW, Tukey JW. An Algorithm for the Machine Calculation of Complex Fourier Series. Math Comput. 1965;19: 297. doi:10.2307/2003354
78. Winograd S. On Computing the Discrete Fourier Transform. Math Comput. 1978;32: 175–199.
79. Zhan Y, Halliday D, Jiang P, Liu X, Feng J. Detecting time-dependent coherence between non-stationary electrophysiological signals-A combined statistical and time-frequency approach. J Neurosci Methods. 2006;156: 322–332. doi:10.1016/j.jneumeth.2006.02.013
80. Samar VJ, Swartz K. Wavelet Analysis of Neuroelectric Waveforms : A Conceptual Tutorial. Brain Lang. 1999;60: 7–60.
81. Quiroga RQ, Nadasdy Z, Ben-Shaul Y. Unsupervised Spike Detection and Sorting with Wavelets and Superparamagnetic Clustering. Neural Comput. 2004;16: 1661–1687. doi:10.1162/089976604774201631
82. Huang NE, Shen Z, Long S, Wu M, Shih H, Zheng Q, et al. The empirical mode decomposition and the Hilbert spectrum for nonlinear and non-stationary time series analysis. Proc R Soc London Ser A Math Phys Eng Sci. 1998;454: 903–995. doi:10.1098/rspa.1998.0193
83. Rilling G, Flandrin P, Gon P, Lyon D. On Empirical Mode Decomposition and Its Algorithms. IEEEEURASIP Work Nonlinear Signal Image Process NSIP. 2003;3: 8–11.
84. Panzeri S, Brunel N, Logothetis NK, Kayser C. Sensory neural codes using multiplexed temporal scales. Trends Neurosci. Elsevier Ltd; 2010;33: 111–20. doi:10.1016/j.tins.2009.12.001

85. Fosso OB, Molinas M. Method for Mode Mixing Separation in Empirical Mode Decomposition. 2017; 1–7. Available: http://arxiv.org/abs/1709.05547
86. Wu, Zhaohua and Huang NE. Ensemble Empirical Mode Decomposition : A Noise Assisted Data Analysis Method. Adv Adapt Data Anal. 2009;1: 1–41. doi:10.1142/S1793536909000047
87. Liang H, Bressler SL, Buffalo E a., Desimone R, Fries P. Empirical mode decomposition of field potentials from macaque V4 in visual spatial attention. Biol Cybern. 2005;92: 380–392. doi:10.1007/s00422-005-0566-y
88. Rehman N, Mandic DP. Multivariate empirical mode decomposition. Proc R Soc A Math Phys Eng Sci. 2010;466: 1291–1302. doi:10.1098/rspa.2009.0502
89. Niederreiter H. Random number generation and Quasi-Monte Carlo methods. 1992.
90. Flandrin P, Rilling G, Goncalves P. Empirical mode decomposition as a filter bank. IEEE Signal Process Lett. 2004;11: 112–114. doi:10.1109/LSP.2003.821662
91. Wu Z a, Huang NE. A study of the characteristics of white noise using the empirical mode decomposition method. 2004; 1597–1611.
92. Ur Rehman N, Mandic DP. Filter bank property of multivariate empirical mode decomposition. IEEE Trans Signal Process. 2011;59: 2421–2426. doi:10.1109/TSP.2011.2106779
93. Liang H, Bressler SL, Desimone R, Fries P. Empirical mode decomposition: A method for analyzing neural data. Neurocomputing. 2005;65–66: 801–807. doi:10.1016/j.neucom.2004.10.077
94. Hu M, Liang H. Intrinsic mode entropy based on multivariate empirical mode decomposition and its application to neural data analysis. Cogn Neurodyn. 2011;5: 277–284. doi:10.1007/s11571-011-9159-8
95. Hu M, Liang H. Noise-assisted instantaneous coherence analysis of brain connectivity. Comput Intell Neurosci. 2012;2012: 275073. doi:10.1155/2012/275073
96. Naik G, Selvan S, Nguyen H. Single-Channel EMG Classification With Ensemble-Empirical-Mode-Decomposition-Based ICA for Diagnosing Neuromuscular Disorders. IEEE Trans Neural Syst Rehabil Eng. 2015;4320: 1–1. doi:10.1109/TNSRE.2015.2454503
97. Al-Subari KSA, Al-Baddai SMH, Tomé AM, Goldhacker M, Faltermeier R, Lang EW. EMDLAB : a toolbox for analysis of single-trial EEG dynamics using empirical mode decompostion. J Neurosci Methods. Elsevier B.V.; 2015;253: 1–14. doi:10.1016/j.jneumeth.2015.06.020
98. Huang JR, Fan SZ, Abbod MF, Jen KK, Wu JF, Shieh JS. Application of multivariate empirical mode decomposition and sample entropy in EEG signals via artificial neural networks for interpreting depth of anesthesia. Entropy. 2013;15: 3325–3339. doi:10.3390/e15093325
99. Bathellier B, Ushakova L, Rumpel S. Discrete neocortical dynamics predict behavioral categorization of sounds. Neuron. Elsevier Inc.; 2012;76: 435–49. doi:10.1016/j.neuron.2012.07.008
100. Nikolić D, Häusler S, Singer W, Maass W. Distributed fading memory for stimulus properties in the primary visual cortex. PLoS Biol. 2009;7: e1000260.

doi:10.1371/journal.pbio.1000260
101. Klampfl S, David S V, Yin P, Shamma S a, Maass W. A quantitative analysis of information about past and present stimuli encoded by spikes of A1 neurons. J Neurophysiol. 2012;108: 1366–80. doi:10.1152/jn.00935.2011
102. Buonomano D V, Merzenich MM. Temporal Information Transformed into a Spatial Code by a Neural Network with Realistic Properties. Science. 1995;267: 1028–1030.
103. Kabra M, Robie AA, Rivera-Alba M, Branson S, Branson K. JAABA: interactive machine learning for automatic annotation of animal behavior. Nat Methods. 2012;10: 64–67. doi:10.1038/nmeth.2281
104. Mathis A, Mamidanna P, Abe T, Cury KM, Murthy VN, Mathis MW, et al. Markerless tracking of user-defined features with deep learning. arXiv. 2018; 1–14.
105. Lozano A, Soto-Sanchez C, Garrigos J, Martinez JJ, Ferrandez JM, Fernandez E. A 3D convolutional neural network to model retinal ganglion cell's responses to light patterns in mice. Int J Neural Syst. 2018; S0129065718500430. doi:10.1142/S0129065718500430
106. Zhao CW, Daley MJ, Pruszynski JA, O DDM, Ruff NL, Dyck RH. Neural network models of the tactile system develop first-order units with spatially complex receptive fields. Biorxiv. 2017;9: 5–9. doi:10.1101/164954
107. Bongard M, Micol D, Fernández E. NEV2lkit: A new open source tool for handling neuronal event files from multi-electrode recordings. Int J Neural Syst. 2014;24: 1450009. doi:10.1142/S0129065714500099
108. Lee J, Goetz G, Carlson D, Hagen E, Batty E. YASS : Yet Another Spike Sorter. 2017; 1–24.
109. Dimitriadis G, Neto J, Kampff A. T-SNE visualization of large-scale neural recordings. bioRxiv. : 1–22.
110. Albarracín AL, Farfán FD, Felice CJ, Décima EE. Texture discrimination and multi-unit recording in the rat vibrissal nerve. BMC Neurosci. 2006;7: 42. doi:10.1186/1471-2202-7-42
111. Alegre-Cortés J, Soto-Sánchez C, Albarracín AL, Farfán FD, Val-Calvo M, Ferrandez JM, et al. Toward an Improvement of the Analysis of Neural Coding. Front Neuroinform. 2018;11: 1–6. doi:10.3389/fninf.2017.00077
112. Laurent G. Dynamical representation of odors by oscillating and evolving neural assemblies. Trends Neurosci. 1996;19: 489–496. doi:10.1016/s0166-2236(96)10054-0
113. Segundo JP, Moore GP, Stensaas LJ, Bullock TH. Sensitivity of neurons in Aplysia to temporal patterns of arriving impulses. J Exp Biol. 1963;40: 643–667.
114. Bathellier B, Ushakova L, Rumpel S. Discrete neocortical dynamics predict behavioral categorization of sounds. Neuron. Elsevier Inc.; 2012;76: 435–49. doi:10.1016/j.neuron.2012.07.008
115. Carlson DE, Vogelstein JT, Wu Q, Lian W, Zhou M, Stoetzner CR, et al. Multichannel Electrophysiological Spike Sorting via Joint Dictionary Learning & Mixture Modeling. 2013;61: 1–14. Available: http://arxiv.org/abs/1304.0542
116. Scholvinck ML, Saleem AB, Benucci A, Harris KD, Carandini M. Cortical State

Determines Global Variability and Correlations in Visual Cortex. J Neurosci. 2015;35: 170–178. doi:10.1523/JNEUROSCI.4994-13.2015

117. Carandini M. Amplification of trial-to-trial response variability by neurons in visual cortex. PLoS Biol. 2004;2: E264. doi:10.1371/journal.pbio.0020264
118. Arieli A, Sterkin A, Grinvald A, Aertsen A. Dynamics of Ongoing Activity: Explanation of the Large Variability in Evoked Cortical Responses. Science. 1996;273: 1868–1871. doi:10.1126/science.273.5283.1868
119. Mainen ZF, Sejnowski TJ, Series N, Jun N. Reliability of Spike Timing in Neocortical Neurons Reliability of Spike Timing in Neocortical Neurons. Science. 2007;268: 1503–1506.
120. Ohki K, Reid RC. Specificity and randomness in the visual cortex. Curr Opin Neurobiol. 2007;17: 401–407. doi:10.1016/j.conb.2007.07.007
121. Stringer C, Pachitariu M, Steinmetz N, Carandini M, Harris KD. High-dimensional geometry of population responses in visual cortex. bioRxiv. 2018; 374090. doi:10.1101/374090
122. Bathellier B, Buhl DL, Accolla R, Carleton A. Dynamic ensemble odor coding in the mammalian olfactory bulb: sensory information at different timescales. Neuron. 2008;57: 586–98. doi:10.1016/j.neuron.2008.02.011
123. Theunissen F, Miller JP. Temporal encoding in nervous systems: A rigorous definition. J Comput Neurosci. 1995;2: 149–162. doi:10.1007/BF00961885
124. Buonomano D V, Maass W. State-dependent computations: spatiotemporal processing in cortical networks. Nat Rev Neurosci. 2009;10: 113–25. doi:10.1038/nrn2558
125. Naik G, Selvan S, Nguyen H. Single-Channel EMG Classification With Ensemble-Empirical-Mode-Decomposition-Based ICA for Diagnosing Neuromuscular Disorders. IEEE Trans Neural Syst Rehabil Eng. 2015;4320: 1–1. doi:10.1109/TNSRE.2015.2454503
126. Dürig F, Albarracín AL, Farfán FD, Felice CJ. Design and construction of a photoresistive sensor for monitoring the rat vibrissal displacement. J Neurosci Methods. 2009;180: 71–76. doi:10.1016/j.jneumeth.2009.02.020
127. Pardey J, Roberts S, Tarassenko L. A review of parametric modelling techniques for EEG analysis. Med Eng Phys. 1996;18: 2–11. doi:10.1016/1350-4533(95)00024-0
128. Bhattacharyya A. On a measure of divergence between two multinominal populations. Nature. 1946;157: 869–869. doi:10.1038/157869b0
129. Hu M, Liang H. Search for information-bearing components in neural data. PLoS One. 2014;9: e99793. doi:10.1371/journal.pone.0099793
130. N CK. Signal Denoising Using EMD and Hilbert Transform and Performance Evaluation with K-S Test. 2013;2: 190–192.
131. Phinyomark A, Limsakul C, Phukpattaranont P. A Novel Feature Extraction for Robust EMG Pattern Recognition. J Comput. 2009;1: 71–80. Available: http://arxiv.org/abs/0912.3973
132. Luczak A, Barthó P, Marguet SL, Buzsáki G, Harris KD. Sequential structure of neocortical spontaneous activity in vivo. Proc Natl Acad Sci U S A. 2007;104: 347–352.

doi:10.1073/pnas.0605643104
133. Petersen CCH, Hahn TTG, Mehta M, Grinvald A, Sakmann B. Interaction of sensory responses with spontaneous depolarization in layer 2/3 barrel cortex. Proc Natl Acad Sci U S A. 2003;100: 13638–13643. doi:10.1073/pnas.2235811100
134. Haider B, Duque A, Hasenstaub AR, Yu Y, McCormick D a. Enhancement of visual responsiveness by spontaneous local network activity in vivo. J Neurophysiol. 2007;97: 4186–4202. doi:10.1152/jn.01114.2006
135. Okun M, Yger P, Marguet S, Gerard-mercier F, Katzner S, Busse L, et al. Population rate dynamics and multineuron firing patterns in sensory cortex. 2013;32: 17108–17119. doi:10.1523/JNEUROSCI.1831-12.2012.Population
136. Druckmann S, Chklovskii DB. Neuronal circuits underlying persistent representations despite time varying activity. Curr Biol. Elsevier Ltd; 2012;22: 2095–103. doi:10.1016/j.cub.2012.08.058

8. Annex: Publications

PAPER I: Time–frequency analysis of neuronal populations with instantaneous resolution based on noise-assisted multivariate empirical mode decomposition

Javier Alegre-Cortés, Cristina Soto-Sánchez, AG Pizá, Ana Lia Albarracin, Fernando Daniel Farfan, Carmelo Jose Felice, Eduardo Fernandez

Journal of Neuroscience Methods, 2016 267:35-44

doi: 10.1016/j.jneumeth.2016.03.018

Time-Frequency analysis of neuronal populations with instantaneous resolution based on Noise-Assisted Multivariate Empirical Mode Decomposition

Alegre-Cortés J[1], Soto-Sánchez C[1,2], Pizá ÁG[3,4], Albarracín AL[3,4], Farfán FD[3,4], Felice CJ[3,4] and Fernández E[1,2]

[1] Bioengineering Institute, Miguel Hernández University (UMH), Alicante, Spain
[2] Biomedical Research Networking center in Bioengineering, Biomaterials and Nanomedicine (CIBER-BBN), Zaragoza, Spain
[3] Laboratorio de Medios e Interfases (LAMEIN), Departamento de Bioingeniería, Facultad de Ciencias Exactas y Tecnología, Universidad Nacional de Tucumán, Tucumán, Argentina.
[4] Instituto Superior de Investigaciones Biológicas (INSIBIO), Consejo Nacional de Investigaciones Científicas y Técnicas (CONICET), Tucumán, Argentina.

***Address all correspondence to:**

Dr. Eduardo Fernández
Universidad Miguel Hernández
Instituto de Bioingeniería
Elche 03202, SPAIN
Tel.: +34 96522 2001
Email: e.fernandez@umh.es

ABSTRACT

***Background**:* Linear analysis has classically provided powerful tools for understanding the behavior of neural populations, but the neuron responses to real-world stimulation are nonlinear under some conditions, and many neuronal components demonstrate strong nonlinear behavior. In spite of this, temporal and frequency dynamics of neural populations to sensory stimulation have been usually analyzed with linear approaches.

***New method**:* In this paper, we propose the use of Noise-Assisted Multivariate Empirical Mode Decomposition (NA-MEMD), a data-driven template-free algorithm, plus the Hilbert Transform as a suitable tool for analyzing population oscillatory dynamics in a multi-dimensional space with instantaneous frequency (IF) resolution.

***Results**:* The proposed approach was able to extract oscillatory information of neurophysiological data of deep vibrissal nerve and visual cortex multiunit recordings that were not evidenced using linear approaches with fixed bases such as the Fourier analysis.

***Comparison with existing methods**:* Texture discrimination analysis performance was increased when Noise-Assisted Multivariate Empirical Mode plus Hilbert Transform was implemented, compared to linear techniques. Cortical oscillatory population activity was analyzed with precise Time-Frequency resolution. Similarly, NA-MEMD provided increased Time-Frequency resolution of cortical oscillatory population activity.

***Conclusions**:* Noise-Assisted Multivariate Empirical Mode Decomposition plus Hilbert Transform is an improved method to analyze neuronal population oscillatory dynamics overcoming linear and stationary assumptions of classical methods.

Keywords: NA-MEMD, nonlinear analysis, non-stationary analysis, neuronal population.

1 INTRODUCTION

Biological signal analysis has been historically limited due to nonlinearity and non-stationarity of the data. In particular, the nervous system detects and processes world information continuously through highly complex dynamics from peripheral nerves to the cortex [22,37,122] at very different time scales [101,123,124]. A common example is the production of action potentials by a neuron, where the output signal has no simple linear relationship to the input. However, the development of general methods for analyzing nonlinear systems and interpreting the results has been delayed due to the theoretical and computational complexities involved.

In this paper we propose the use of Noise-Assisted Multivariate Empirical Mode Decomposition (NA-MEMD) [43] together with Hilbert Transform (Huang et al. 1998) as a tool for the study of neuronal population dynamics with high temporal resolution. Multivariate Empirical Mode Decomposition (MEMD) [88] was proposed as a n-dimensional extension of empirical mode decomposition (EMD) (Huang et al. 1998). This is an empirical adaptive method which iteratively subtracts the mean vector obtained from binding the local maxima and minima with a cubic spline until a certain criterion is satisfied. The result of this algorithm is a variable number of Intrinsic Mode Functions (IMFs) that contains the existent data oscillations in decreasing frequency order. The extension to n-dimensions of this method described in Rehman and Mandic 2010, is based on real-valued projections along multiple directions on hyperspheres, in order to calculate the envelopes and the local mean of multivariate data. Furthermore, the addition of new dimensions containing white Gaussian noise (NA-MEMD) (Rehman and Mandic 2011) acts as a filter bank that helps to resolve the mode mixing and mode misalignment problem present in MEMD algorithms. In addition, the additional number of extrema provided by noise channels confers an increase in accuracy when intermittent signals are decomposed, which is crucial when leading with neuronal population dynamics.

EMD family of algorithms has recently been applied to discriminate between whole LFPs of macaque V4 while performing a visual illusion task without specifically considering neuronal dynamics via EMD [87,93] and MEMD [94,95]. In addition, EMDs have been used successfully to analyze EEG and EMG recordings [97,98,125] in the last years. Bearing this in mind, we aim to explore the potential usefulness of this methodology for describing and understanding local neuronal population recordings with precise instantaneous temporal resolution.

In this paper we describe the implementation of the technique and then apply it on to real data. In particular, we show how neural activity oscillatory activity changes in two different experimental paradigms: evoked activity recorded from the deep vibrissal nerve of anesthetized rats and spike trains of simultaneously recorded neurons from deep layers of rat visual cortex. Our results suggest that NA-MEMD plus Hilbert transform analysis is a improved tool to study local neuronal activity with instantaneous time and frequency resolution, consistently with recent works (Hu and Liang 2014) where NA-MEMD

decomposition plus Wasserstein distance based analysis of LFP recordings increased whole recordings discrimination accuracy.

2 METHODS

2.1 Experimental methods

2.1.1 Electrophysiological recordings

Deep vibrissal nerve recordings were obtained from five male Wistar adult rats weighing 300–350 g. Surgical anesthesia was induced by urethane (1.5 g/kg) and temperature was maintained at 37° by a servo-controlled heating pad. Surgery and experimental protocol have been previously described in detail by Albarracín et al., 2006. The procedures are briefly described below. Vibrissa movements were induced by electrical stimulation of facial motor nerve (VII). Square-wave pulses (30 μs, 7 V supramaximal, 5 Hz) simulated vibrissal whisking at its natural frequency (Fig. 1A). Nerve activity was recorded and digitized at 20 kHz (sampling rate) during a 100 ms window following onset of each cycle of whisker movement with a Digidata 1322A (Axon Instruments). Fifty whisker movement cycles were obtained for each whisker-surface contact, and an additional 50 cycles were recorded while whisker moved unobstructed in air (control).

Four slip-resistance levels were presented for each surface by mounting the surface at different distances from the whisker base (Fig. 1A, Albarracín et al. 2006, for details). The swept surfaces tested in this paper were surfaces with different textures: wood, metal, acrylic and sandpaper P1000. Movements of the Gamma whisker were recorded simultaneously with nerve activity using a custom-made photoresistive sensor [126]. The frequency response of the sensor was maximal in the range 0–100 Hz, enabling direct identification of the protraction and retraction phases of the movement cycle.

Visual cortex multi-unit recordings were obtained from 5 male Long Evans adult rats weighing 450-500 gr. Analgesia was induced by buprenorphine (0.025mg kg-1 s.c), and surgical anesthesia and sedation were induced by ketamine HCl (40 mg kg-1 i.p). The anesthesia was maintained with a mix of oxygen and 2% of isoflurane during the surgery and afterwards reduced to 1.5% during the electrophysiological recordings. The blinking and the toe pinch reflexes were continuously checked along the experiment to guarantee a proper level of anesthesia for the animal. The body temperature was maintained with a thermal pad and the heart rate and O2 concentration in blood were monitored throughout the experiment. Animals were pre-treated with dexamethasone (1 mg kg^{-1} i.p) 24 hours and 20 minutes prior to surgery in order to avoid brain edema caused by the electrode insertion. A craniotomy was drilled on top of the visual cortex and the electrode array was inserted 2 mm lateral to the midline and from 0.5 mm anterior to lambda. Then, a Utah array was inserted in the deep layers of the visual cortex (>600 μm) with a Blackrock pneumatically-actuated inserter device specifically designed for implanting the Utah

array through the duramatter with a minimal tissue offense (Blackrock Microsystems, Salt Lake City, USA). The customized microelectrode Utah array consisted of 6 x 6 tungsten microneedles, covering a brain surface of 2 mm x 2 mm millimeters (400 µm spacing). After the insertion, the ipsilateral eyelid to the craniotomy site was closed with cyanoacrylate and atropine sulphate 1% was used to -dilate the pupil of the contraleral eye.

In vivo neural activity from visual cortex was recorded simultaneously from 16 individual electrodes with the Utah array (Fig 2A). The Utah array was connected to a MPA32I amplifier (Multichannel Systems, MCS) and the extracellular recordings were digitized with a MCS analog-to-digital board. The data were sampled at a frequency of 20 kHz and slow waves were digitally filtered out (100-3000 Hz, 2^{nd} order Butterworth type IIR digital filter) from the raw data (Fig 2B). Neural spike events were extracted with a free-tool application for offline spike sorting analysis (Neural Sorter, http://sourceforge.net/projects/neuralsorter/) and the resulting multiunit information obtained from each electrode was stored for further analysis.

Visual stimulation consisted on a vertical drifting square-wave grating (90°, light and dark bars, 100% contrast, 6 Hz, 0.6 cycles/degree) of 500 ms duration interspersed with a dark (uniform) stimulus of equal duration. The stimulus was displayed on a LCD monitor (refresh rate 60 Hz) and a luminance of ≈100 cd/m^2, placed 25 cm in front of the right eye, approximately at 30° from the midline and covering a visual field spanning ≈100° (Fig. 2A). The stimulus was generated using the vision egg library and a python script. The room was kept in darkness throughout the visual stimulation.

2.1.2 Ethical approval

All the procedures carried out at the Institute for Biological Research (INSIBIO)/Instituto Superior de Investigaciones Biológicas, were in accordance with the recommendations of the Guide for the Care and Use of Laboratory Animals (National Research Council, NRC).

All the experimental procedures carried out at the Miguel Hernandez University were conformed to the directive 2010/63/EU of the European Parliament and of the Council, and the RD 53/2013 Spanish regulation on the protection of animals use for scientific purposes and approved by the Miguel Hernandez University Committee for Animal use in Laboratory.

2.2 Data analysis

Neural activity analysis was performed in Matlab (MathWorks). In the case of the rat visual cortex multiunit recordings, single or multiunit spiking activity was isolated

from the background. We observed multiunit activity in the majority of the electrodes through the whole recording sessions, and only those electrodes with neural activity higher than 0.5 spikes/s were considered in the analysis.

We constructed time-dependent population activity vectors from rat visual cortex multiunit recordings by temporally locking the activity of each electrode with 1 ms resolution from one second before to one second after each stimulus presentation. The deep vibrissal nerve recordings remained at recording resolution (20 kHz).

2.2.1 NA-MEMD

EMDs are data-driven algorithms suitable for nonlinear and non-stationary analysis [43]; therefore, they have become a promising tool in the analysis of neural data [87]. 'Classical' EMD analysis (Huang et al. 1998) decomposes a given signal in a set of oscillatory modes called IMFs. Each IMF contains the oscillations present in the original data at a certain temporal scale and therefore is independent of templates. Thus this procedure provides a much more elaborate means of applying nonlinear analysis to neuronal population recordings than standard procedures.

The MEMD [88] is a multivariate extension of EMD algorithm, where analysis of simultaneous dimensions is performed simultaneously to obtain a meaningful decomposition of the whole multidimensional signal, This method overcomes the problems resulting from univariate EMD analysis application to each dimension independently: different number of IMFs and unscaled alignments. It obtains generalized oscillations, known as rotational modes, via estimation of the local n-dimensional mean. To this end, multiple uniformly distributed projections in the n-dimensional space are calculated using a V-point Hammersley sequence [89]; these projections extrema are interpolated with a cubic spline and averaged to compute the local mean. As in the original EMD algorithm (Huang et al. 1998), this mean vector is subtracted from the original n-dimensional data and the process is repeated iteratively to obtain the subsequent IMFs until a certain stopping criteria is achieved, such as symmetry of the upper and lower envelopes or that the number of extrema and the number of zero-crossings differ at most by 1. The final IMF does not contain any oscillation other than the trend of the data.

Whereas complete MEMD algorithm is described elsewhere [88], Algorithm 1, as given in this paper, briefly describes for those unfamiliar with the technique, the basis of the method:

Algorithm 1. Multivariate extension of EMD.

1. Choose a suitable pointset for sampling on an (n −1) sphere.
2. Calculate a projection, denoted by $p^{\theta k}(t)\}_{t=1}^{T}$, of the input signal $\{\boldsymbol{v}(t)\}_{t=1}^{T}$ along the direction vector $\boldsymbol{x}^{\theta k}$, for all k (the whole set of vectors), giving $p^{\theta k}(t)\}_{t=1}^{T}$ as the set of projections.

3. Find the time instants $\{t_i^{\theta k}\}$ corresponding to the maxima of the set of projected signals $p^{\theta k}(t)\}_{t=1}^{T}$
4. Interpolate $[t_i^{\theta k}, \boldsymbol{v}(t_i^{\theta k})]$ to obtain multivariate envelope curves $\boldsymbol{e}^{\theta k}(t)\}_{k=1}^{K}$
5. For a set of K direction vectors, the mean $\boldsymbol{m}$(t) of the envelope curves is calculated as $\boldsymbol{m}(t) = \frac{1}{K}\sum_{k=1}^{K} e^{\theta k}(t)$
6. Extract the 'detail' d(t) using d(t) = x(t) - m(t). If the 'detail' d(t) fulfills the stoppage criterion for a multivariate IMF, apply the above procedure to x(t) – d(t), otherwise apply it to d(t).

White Gaussian Noise (WGN) addition to EMD analysis (EEMD, NA-MEMD) increases its performance via reducing mode mixing produced by signal intermittency (Zhaohua and Huang 2009) acting as a quasi-dyadic filter bank that enhances time-frequency resolution (Flandrin et al. 2004; Rehman and Mandic 2011). This increased performance is especially present in intermittent data, where aliasing among IMFs is more prone to happen; therefore the dyadic filter bank property of WGN decomposition helps to mitigate this effect. Given known the intermittency of neural signals, WGN is added in additional dimensions:

$$d = n + k,$$

Where *d* is the final number of dimensions, *n* the dimensions of the original data (electrodes, trials…) and *k* the number of additional dimensions including WGN (Rehman and Mandic 2011).

In order to apply NA-MEMD analysis to our data, we adapted MEMD Matlab package (http://www.commsp.ee.ic.ac.uk/~mandic/research/emd.htm). We used the low-discrepancy Hammersley sequence to generate a set of V = 300 direction vectors for computing signal projections and 3 WGN channels. Standard stopping criterion was described elsewhere [83].

We applied NA-MEMD in different ways accordingly to each dataset. When applied to deep vibrissal nerve recordings, we extended the analysis to all repetitions (*n* = 50), obtaining *d* = 53. When studying visual cortex results, we aimed to depict features present in the whole recorded population; therefore, we averaged the activity of all electrodes and trials (*n* = 1) and added 3 additional dimensions with WGN, *d* = 4. We kept applying NA-MEMD over EEMD (Zhaohua and Huang 2009) on visual cortex recordings collapsed to a single dimension to avoid mixing the added noise with the real signal, as it may increase residual error and produce different number of IMFs in each ensemble, therefore compromising IMFs alignment and subsequent analysis (see Figs. 5 & 8 in Mandic et al. 2013).

2.2.2 Hilbert Transform

We measured present frequencies in our data as the instantaneous frequency (IF) using Hilbert Transform (Huang et al. 1998). For a given time series x(t), its Hilbert Transform H(x)(t) is defined as:

$$H(x)(t) = \frac{1}{\pi} C \int_{-\infty}^{\infty} \frac{x(t')}{t-t'} dt',$$

Where C indicates the Cauchy principal value. Hilbert Transform results in a complex sequence with a real part which is the original data and an imaginary part which is a version of the original data with a 90º phase shift; this *analytic signal* is useful to calculate instantaneous amplitude and frequency; instantaneous amplitude is the amplitude of H(x)(t), IF is the time rate of change of the instantaneous phase angle.

2.2.3 Spectrogram via short-time Fourier transform (STFT)

STFT analyzes the signal x(t) through a short-time window $\omega(t) = x(t) \times \omega(t - \tau)$, and then a Fourier transform is performed on this product using complex exponential basis functions. The square modulus of STFT is referred to as the spectrogram (Zhan et al., 2006). In order to observe overall changes in the power spectral density (PSD), we computed it using a parametric autoregressive (AR) modeling [110,127] in both raw and decomposed signals.

2.2.4 Information measure with Bhattacharyya distance

The Bhattacharyya distance (Bd) is a measure of divergence between two distributions (Bhattacharyya, 1946). We measured this value to discriminate between possible pairs of experiments.

3 RESULTS

3.1 Deep vibrissal nerve recordings

The afferent discharge recorded is the average electrical activity of myelinated axons with different firing patterns (Albarracín et al., 2006; Farfán et al., 2013). This leads to a complex response to the stimulus where the individual response of each fiber is mixed in a summed response. Fig. 3A shows four afferent recordings (top) in different sweep situations and 6 IMFs obtained applying NA-MEMD analysis to each of the surfaces recordings individually. We decided to inspect all IMFs rather than statistically validate those carrying more information (Huang et al. 2013; Hu and Liang 2014) in order to understand the discrimination dynamics across time at all frequencies.

In order to observe overall changes in the power spectral density (PSD), we computed it using a parametric AR modeling [110,127] in both raw and decomposed signals. The PSD of raw signals revealed differences of amplitude (power of PSDs) and in its maximum-energy frequency components (Fig. 3B, top panel). In this analysis, both the electrical stimuli as well as EMG artifacts were dropped of PSD estimations to avoid spurious components. The Fm (mean frequency) values [131] of 50 PSD of each experimental situation were represented with its mean values bounded by its corresponding standard deviations (Fig. 3C, left). Significant differences among sweep

situations on metal, acrylic and sandpaper were observed, although not between sweeps on wood vs. metal (Kruskal Wallis test, p value < 0.05).

The PSD obtained from IMFs revealed spectral changes at different bandwidths (Fig. 3B). For instance, IMF 3 concentrated its energy content in the bandwidth of 1.25 to 2.5 kHz (for all sweep situations), while IMF 4 into 0.5 to 1.25 kHz approximately. Thus, the power remained increasingly bound in specific bands. The Fm values from each IMF and simulated whisking situation are represented in Fig. 3C (middle).

The spectral content of IMF 5 showed similarities with the spectral content of raw signals, regarding to the sweep situation on metal, acrylic and sandpaper, and a linear increase in Fm (Fig. 3C, right), however, results variance was notably reduced. For this IMF, the sweep on wood vs sweep on metal is significantly different ($p<0.01$, ANOVA test). The Fm values of IMF 6 showed a linear increase for sweep situations on wood, metal and acrylic. The sweep situation on sandpaper produces a spectral content characterized by Fm values of lower magnitude and dispersion compared to the PSD of the raw data (Fig. 3C, right).

Time-Frequency (T-F) discrimination analysis, as proposed by Pizá et al., 2014, was implemented in order to compare the NA-MEMD plus Hilbert transform as a method to extract time-frequency features of afferent recordings. Fig. 4A shows the methodology used to obtain a discriminability measure based on spectrograms. Each whisking situation was represented as a time series average and its corresponding standard deviation (mean ± std), in order to compare the temporal profile of different whisking situations.

Alternatively, the NA-MEMD was applied to raw signals and then the IF of selected IMFs was computed via Hilbert Transform (see methods). Therefore, we obtained T-F profiles for each whisking condition and IMF (one example condition shown in Fig. 4B). We could observe how time-frequency features of NA-MEMD plus Hilbert Transform analysis had lower dispersion than those obtained from the spectrograms (Supplementary Fig. 1).

Bd was used to compare T-F dynamics for three comparisons at three slip resistance levels, as we did not find substantial differences between slip resistances 2 & 3. Results are shown in Fig. 4C. Bd values increased in a range from 0-0.3 for comparisons based on spectrograms to 0-1.5 Bd values from Hilbert Transform of IMFs 5 & 6. Furthermore, the instantaneous T-F resolution of this procedure showed an enriched temporal dynamic of Bds. T-F analysis based on spectrogram reveals differences between wood and acrylic into the 16 to 24 ms time interval for all slip resistance levels (Fig 4C, top – left). In the same time interval, the Hilbert Transform of IMF 5 showed a peak of discrimination at 18 ms for slip resistance 4 , and at 22 ms for slip resistance 2 (Fig. 4C, middle – left). This situation was even clearer when IMF 6 Hilbert Transform was analyzed. In addition, a different peak in the discrimination analysis (Bd> 0.5) arose at 30 ms, for slip resistance 1 (Fig. 4C, bottom – left).

When this comparative analysis was extended to the discriminations between wood and metal, maximum Bd was found in retraction phase (20 – 45 ms approx.), at slip resistance 1 (Fig. 4C, top – middle) in the Hilbert Transform of IMF 6 (200 to 500 Hz) (Fig. 4C, bottom – middle), something completely absent in the spectrogram derived T-F profile.

Finally, spectrogram method revealed that acrylic vs sandpaper comparison had its greatest discriminability value in the protraction phase (16 to 25 ms approx.) (Fig. 4C, top – right). Hilbert Transform of IMF 5 displayed peaks in the Bd in the same window, although the measured value was higher and the increased temporal resolution demonstrated that maximum Bd was displaced for different resistances (maximum Bd with resistance 4), something previously blurred by the linear approach limitations; On the other hand, Hilbert Transform of IMF 6 had a maximum at a different resistance (resistance 2) as well as a different temporal profile.

These results clearly showed the advantages of NA-MEMD plus Hilbert Transform over T-F analysis based on spectrograms, as it was used to compute higher Bds in all situations with increased time resolution. Furthermore it was possible to differentiate the time of maximum Bd for different texture pairs.

3.2 Visual cortex recordings

Neurons of mammals neocortex oscillate spontaneously (Buzsáki and Draguhn 2004; Petersen et al. 2003; Luczak et al. 2007), both in awake and anesthetized states [132,134] although alternate with some periods of desynchronized activity [135]. In this conceptual framework, we have to take into account that the visual cortex neuronal populations recorded during visual stimulation may have different coupling among neurons. Thus, whereas some neurons fire independently others fire simultaneously in population oscillations [21] resulting in a strong variability in the population responses [117].

To analyze these data we averaged the spiking activity of the whole recorded population during visual stimulation and decomposed it with NA-MEMD. Fig. 5A shows the mean population response to a single trial (left) and two IMFs, one carrying information about the distribution of single spikes (IMF3, center) and the other about the low frequency oscillation (IMF7, right). IF (Fig. 5B) of the data shown in Fig. 5A is computed via Hilbert Transform and shows how IF vector of the original data (left) is artefactual, while center and right graphs show the IFs of the IMFs shown above and how they are restricted to a certain frequency range. It is especially notorious how NA-MEMD plus Hilbert Transform allowed to analyze intrawave oscillations (Figs. 5A& 5B, right), something which is not feasible by using linear techniques. Figs. 5C & 5D show the same scheme explained in the top part of Figs. 5A & 5B extended to the whole experiment averaged in a single vector. This was performed averaging the activity of all electrodes and trials. Note how IMF 3, containing high frequency components of the response is not stimulus-dependent, while IMF 7, containing low frequency oscillations (±10 Hz, see

right graph of Fig. 5D) is amplitude-modulated (AM) during the stimulation window (grey window). These results are consistent with the interpretation that the distribution of spikes is highly variable in response to each stimulation (IMF 3). This methodology also allows to discover oscillations in a different time-scale (IMF 7), which could be related to the stimulus [136].

In order to compare this analysis with traditional linear approach, we constructed averaged spiking activity power spectrums using spectrogram and NA-MEMD plus Hilbert Transform analysis independently (Fig. 6). Hilbert spectrum time resolution was increased, as it was obtained from a point-by-point convolution instead of windows superposition spectrogram analysis. Moreover, when Fig. 6C and Fig. 6D are compared, we can notice an increase in frequency resolution in Hilbert spectrum, whereas spectrogram frequency axis is blurred and lacks of the resolution achieved in Hilbert spectrum. When an accurate representation of nonlinear features is analyzed, we can observe how a power peak with a linear increase in frequency appears between 250 and 350 ms after stimulation onset and 35 and 45 Hz in Fig. 6D, computed with NA-MEMD plus Hilbert Transform, but is absent in Fig. 6C spectrogram, which was unable to depict this frequency increase along time due to its template restrictions.

In conclusion, NA-MEMD plus Hilbert Transform provided an enriched spectrum when compared with traditional techniques (spectrogram), with increased T-F resolution and a template-free representation of nonlinear response components, thanks to its template-free, local application. Thus, a T-F analysis of dynamical properties of multielectrode visual cortex recordings with IF resolution is feasible with NA-MEMD plus Hilbert transform.

4 DISCUSSION

The present results were obtained using NA-MEMD plus Hilbert Transform, an approach that enabled the study of population dynamics with instantaneous resolution. The absence of any fixed basis in the decomposition increased the accuracy of the analysis and avoided the T-F blurring of linear approaches. When linear or stationary assumptions are used, intrawave modulations result in spurious harmonics residing in higher frequencies that obscure the biological interpretation of the results. As neuronal dynamics are classically nonlinear (Laurent 1996; Shamir 2004; Averbeck et al. 2006), we suggest that nonlinear techniques are required for a more confident and meaningful analysis of neuronal data.

The EMD family of algorithms has been used in the recent years in neuroscience to overcome these difficulties (Liang et al. 2005b; Hu and Liang 2011, 2012, 2014, Naik et al. 2015). In the present study we have demonstrated that NA-MEMD, a noise-assisted data-driven Time-Frequency analysis algorithm, is a suitable tool to study local neuronal populations. Our results show that this approach may be useful to dramatically increase the time resolution of Time-Frequency analysis of neuronal population recordings.

Instantaneous frequency resolution is essential for a meaningful interpretation of nonlinear and non-stationary processes (Durstewitz and Deco 2008). Thus, by using the procedure described in the present study we have been able to show how afferent population activity presents intrawave frequency modulations (see Supplementary Fig. 2). Previous attempts were unavailable to achieve such temporal resolution in T-F analysis (Albarracín et al., 2006; Farfán et al., 2013), and blurred the information obtained. Thus, linear Fm analysis of the deep vibrissal nerve recordings used in those studies were not able to accurately explain the nerve responses to vibrissal stimulation, something fulfilled when using NA-MEMD plus HT analysis (see Fig. 4 and Supplementary Fig 1). Hence it is possible that those previous analysis may contain significant artifacts, what emphasizes the usefulness of this new approach to extract time-frequency information from neural recordings.

In addition, this procedure was also applied to visual cortex simultaneous multiunit recordings. To the best of our knowledge, this is the first attempt of extracting oscillatory information from spiking activity using NA-MEMD analysis. Our T-F analysis of mean population activity evidenced intrawave modulations before, during and after stimulation, with a power peak that started at 35 Hz and increased to 45 Hz lasting approximately 200 ms in the response window (Fig. 6D). This response feature was nonlinear, as it changed in time and frequency simultaneously, therefore spectrogram analysis was not able to accurately depict it (Fig. 6C). Further analysis of neuronal populations oscillatory response to stimulation at different time-scales will be addressed in future studies

5 CONCLUSIONS

We have shown how NA-MEMD analysis, a noise-assisted nonlinear non-stationary template free approach, extracts monocomponent oscillatory information of neurophysiological recordings from deep vibrissal nerve and improves previous discrimination analysis using Bhattacharyya distance with enhanced temporal resolution. Moreover, we used NA-MEMD to extract oscillatory components from population multielectrode spiking recordings of rat visual cortex while visually stimulated and obtained oscillatory components related to cortical response in order to describe it with instantaneous T-F resolution. We compared these results with spectrogram analysis and showed how T-F resolution was strongly increased, and how nonlinear response features were obtained with increased accurancy.

We propose to extend NA-MEMD analysis to oscillatory dynamics of neuronal populations to solve the problem of facing nonlinearity and non-stationarity when studying the data, as it has already been doing on certain high-scale experimental paradigms (EEG/EMG/LFP, Huang et al. 2013; Al-Subari et al. 2015; Naik et al. 2015, Hu and Liang 2014). The instantaneous resolution achieved in both frequency and time

domains, as well as the noise-removal capability demonstrated by this algorithm may open a new field in any kind of neural analysis.

Acknowledgements

We thank Lucas J. Morales Moya for his helpful advice in NA-MEMD implementation.

This work has been supported in part by grant MAT2012-39290-C02-01 from the Spanish Government, by the Bidons Egara Research Chair of the University Miguel Hernández, by a research grant of the Spanish Blind Organization (ONCE) and by grants from Agencia Nacional de Promoción Científica y Tecnológica (ANPCYT) PICT 2012-1210; Consejo Nacional de Investigaciones Científicas y Técnicas (CON-ICET), Consejo de Investigaciones de la Universidad Nacional de Tucumán (CIUNT) E532 and Institutional funds from Instituto Superior de Investigaciones Biológicas (INSIBIO).

FIGURES

Figure 1

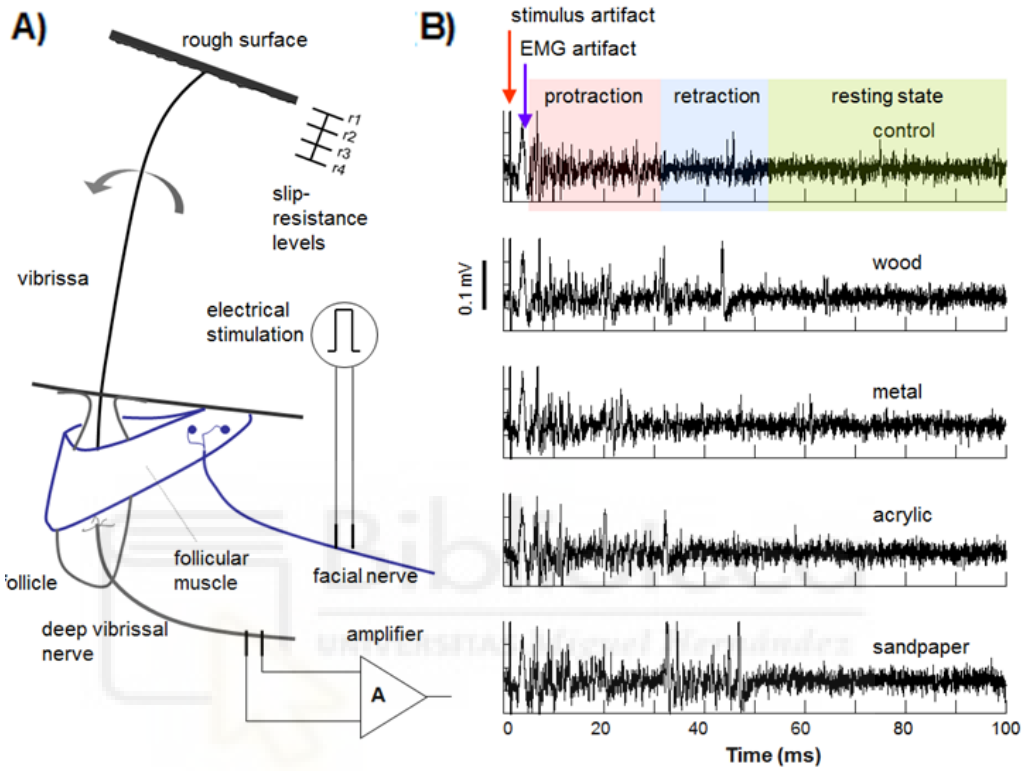

Fig. 1 Schematic representation of the experimental stimulus-recording design. A) The facial nerve is stimulated to induce the artificial movement of the vibrissa. Rough surfaces are faced to vibrissal movement to force contact during movement with controlled pressure while afferent activity is recorded. B) Afferent activity recordings obtained in five sweep situations: air sweep (control), sweep on wood, sweep on metal, sweep on acrylic and sweep on sandpaper P1000. All activity recordings were obtained at slip-resistance 4. Stimulus artifact and an artifact due to EMG volume conduction are observed. Protraction, retraction and resting phases are identified (Albarracín et al, 2006).

Figure 2

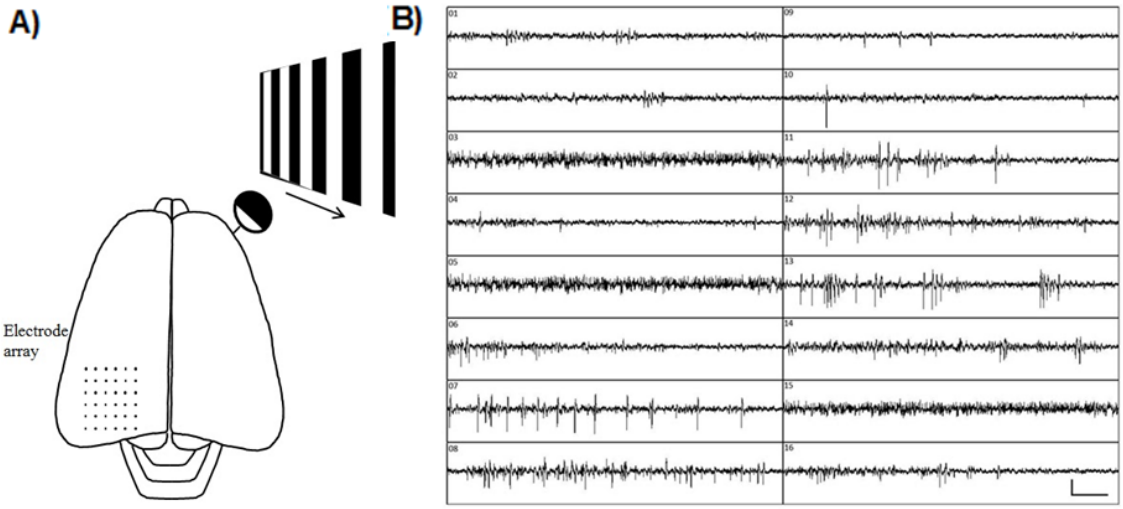

Fig. 2 A) Schematic representation of the experimental stimulus-recording design. B) Screen capture showing the display of the extracellular recording from 16 electrodes simultaneously. Each panel in the image corresponds to an individual electrode of the array. Scale bar in the last bottom panel corresponds to 150 μV in the vertical axis and 50 ms in the horizontal axis.

Figure 3

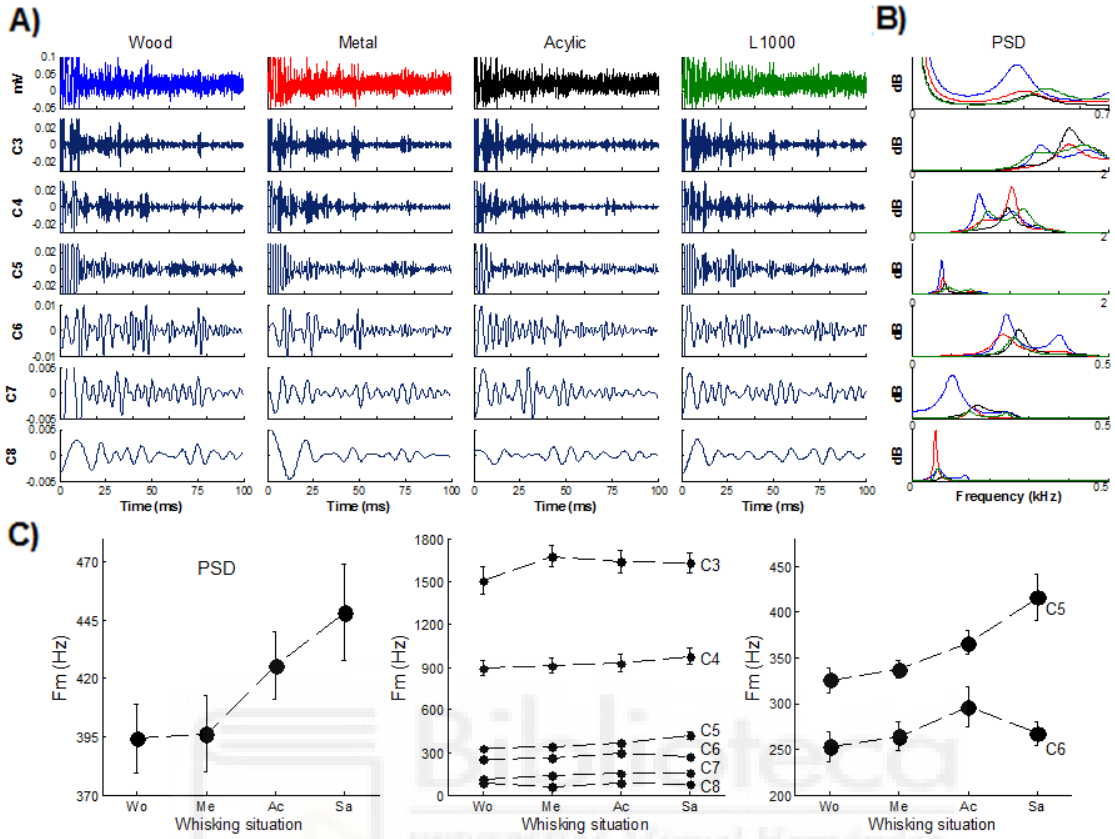

Fig. 3 Spectral analysis using power spectral density (PSD) and noise-assisted empirical mode decomposition (NA-MEMD). (A) NA-MEMD analysis of four afferent activity recordings evoked by sweep on wood (blue), metal (red), acrylic (black) and on sandpaper P1000 (L1000, green). All activity recordings were obtained at slip-resistance. The 3rd to 8th intrinsic mode functions (IMF) from each afferent recording and IMFs for each whisking situation are shown. B) PSDs computed using the Burg parametric estimation method [110] for each whisking situation. C) PSD represented by its mean spectral frequency (Fm). Left, fifty Fm values were obtained for each experimental situation. For raw data, Fm values within the range of 100 to 600 Hz were obtained. Middle, Fm values from IMFs were obtained within its corresponding bandwidth. Right, Fm values from C5 and C6 modes for each whisking situation.

Figure 4

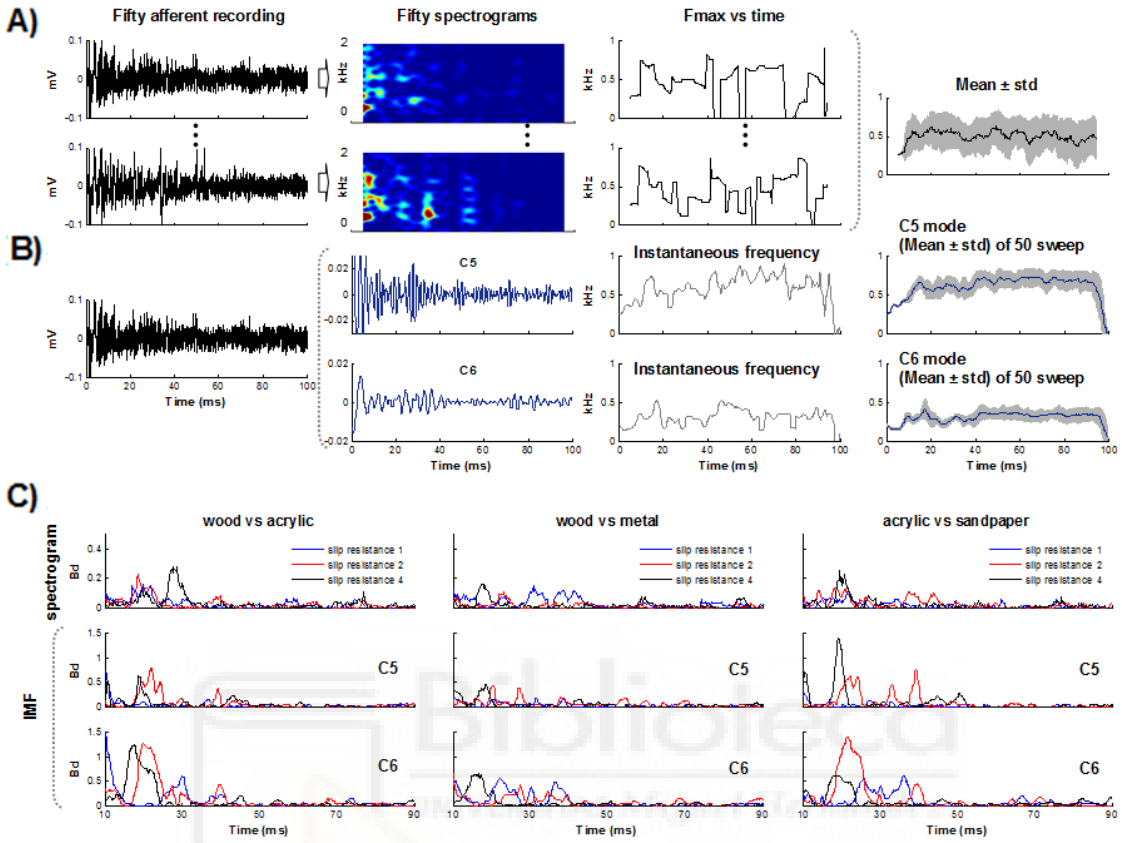

Fig. 4 Time-frequency analysis from spectrogram, NA-MEMD and Hilbert spectral methods. A) Spectrogram method. Fifty spectrograms were obtained from fifty afferent recordings for one experimental situation. Then, maximum energy components (Fmax) into frequency range of 10–1000 Hz were obtained for each spectrogram along time. Thus, a mean ± std of Fmax values along time is obtained. B) NA-MEMD and Hilbert spectral method. Each afferent recording is subjected to the empirical decomposition, and a Hilbert transform is applied to each IMF to obtain de instantaneous frequency along time (time-frequency information). C) Comparisons and discriminability measure. A discriminability measure was obtained by using Bhattacharyya distance (Bd).

Figure 5

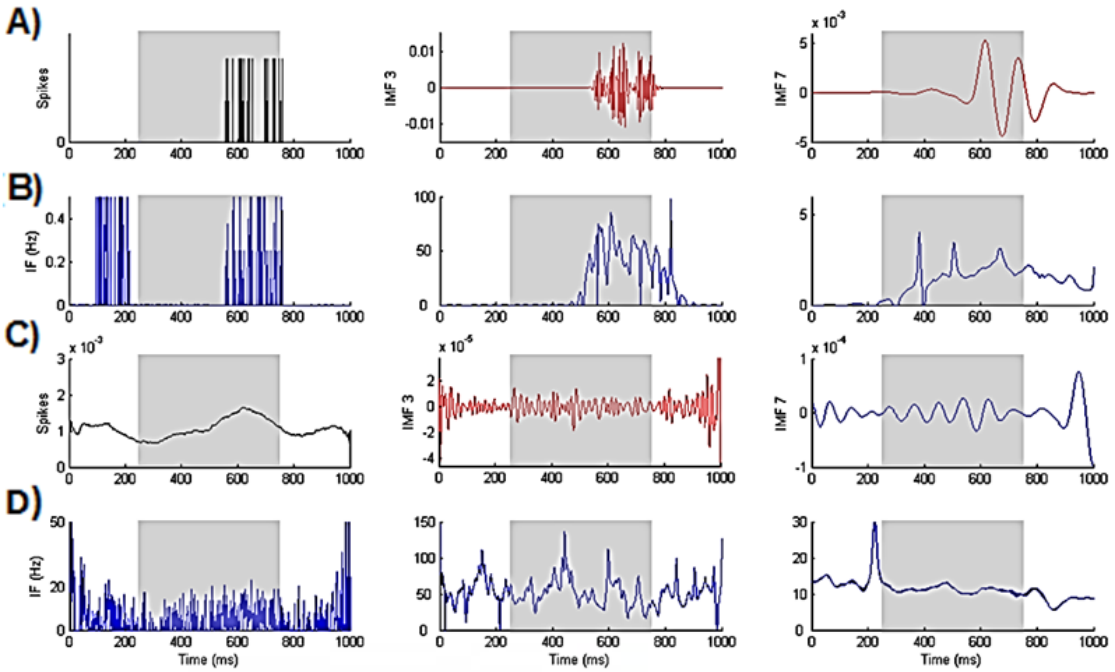

Fig. 5 Time frequency analysis from single trial and mean activity vectors. A) Left, single trial mean population activity; center, IMF 3, containing high frequency (±50 Hz) oscillations; right, IMF7 containing low frequency (±2 Hz) oscillations. B) Instantaneous frequency from graphs in A) calculated with Hilbert transform. C) Left, mean population activity for all electrodes and trials; center, IMF 3, containing high frequency (±50 Hz) oscillations; right, IMF7 containing low frequency (±10 Hz) oscillations. D) Instantaneous frequency from graphs in C) calculated with Hilbert Transform. Stimulus represented as a grey shaded rectangle.

Figure 6

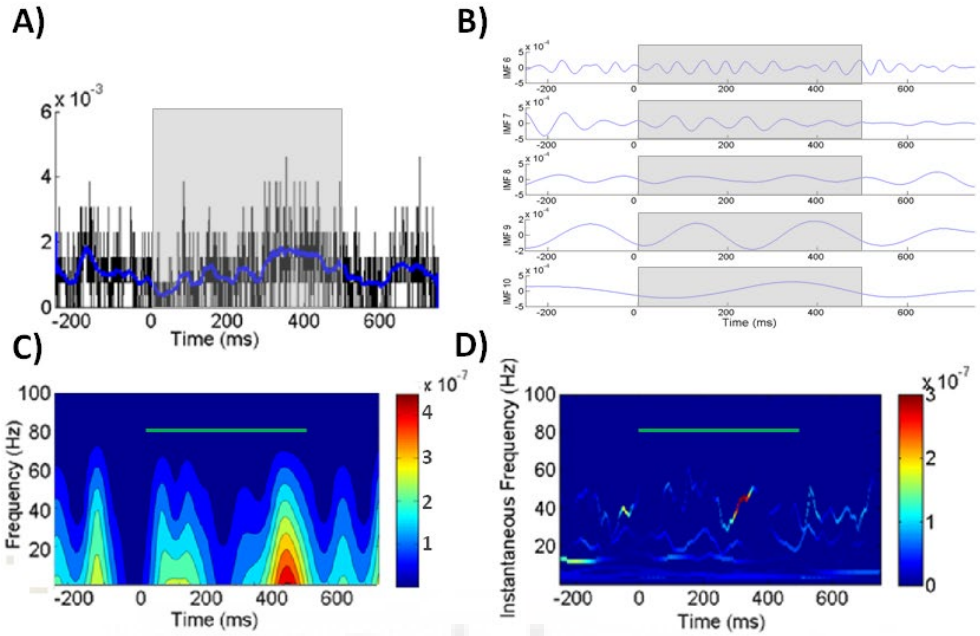

Fig. 6 A) Mean population activity during visual stimulation, mean activity smoothed with a 30 ms window displayed in blue color for easier visualization. B) Resulting IMFs from 6 to 10 after NA-MEMD decomposition. C) Spectrogram of mean population activity data. D) Hilbert Spectrum of IMFs 6 to 10. An increase in temporal resolution and power locking is observed. Stimulus represented as a grey shaded rectangle in A) & B) and a green horizontal bar in C) & D).

6 REFERENCES

Albarracín AL, Farfán FD, Felice CJ, Décima EE. Texture discrimination and multi-unit recording in the rat vibrissal nerve. BMC Neurosci. 2006;7-42. DOI: 10.1186/1471-2202-7-42

Al-Fahoum AS, Al-Fraihat AA. Methods of EEG Signal Features Extraction Using Linear Analysis in Frequency and Time-Frequency Domains. ISRN Neurosci. 2014; 1-7. DOI: 10.1155/2014/730218

Al-Subari K Al-Baddai S, Tomé AM, Goldhacker M, Faltermeier R, Lang EW. EMDLAB : a toolbox for analysis of single-trial EEG dynamics using empirical mode decompostion. J Neurosci Methods. 2015;253:1-14. DOI: 10.1016/j.jneumeth.2015.06.020

Averbeck BB, Latham PE, Pouget A. Neural correlations, population coding and computation. Nat Rev Neurosci 2006;7(5):358–66. DOI: 10.1038/nrn1888

Bathellier B, Buhl DL, Accolla R, Carleton A. Dynamic ensemble odor coding in the mammalian olfactory bulb: sensory information at different timescales. Neuron 2008;57(4):586–98. DOI: 10.1016/j.neuron.2008.02.011

Bhattacharyya A. On a measure of divergence between two multinominal populations. Sankhyā: The Indian Journal of Statistics (1933-1960) 1946; 7(4):401–6

Buonomano D V, Maass W. State-dependent computations: spatiotemporal processing in cortical networks. Nat Rev Neurosci 2009;10(2):113–25. DOI: 10.1038/nrn2558

Buzsáki G, Draguhn A. Neuronal Oscillations in Cortical Networks. Science 2004: 304 (5679), 1926-9. DOI:10.1126/science.1099745

Carandini M. Amplification of trial-to-trial response variability by neurons in visual cortex. PLoS Biol 2004;2(9):E264. DOI: 10.1371/journal.pbio.0020264

Druckmann S, Chklovskii DB. Neuronal circuits underlying persistent representations despite time varying activity. Curr Biol 2012;22:2095–103. DOI: 10.1016/j.cub.2012.08.058

Dürig F, Albarracín AL, Farfán FD, Felice CJ. Design and construction of a photoresistive sensor for monitoring the rat vibrissal displacement. J Neurosci Methods 2009;180(1):71–6.

Durstewitz D, Deco G. Computational significance of transient dynamics in cortical networks. Eur J Neurosci 2008;27(1):217–27. DOI: 10.1111/j.1460-9568.2007.05976.x

Farfán FD, Albarracín AL, Felice CJ. Neural encoding schemes of tactile information in afferent activity of the vibrissal system. J Comput Neurosci. 2013;34(1):89-101. DOI: 10.1007/s10827-012-0408-6.

Flandrin P, Rilling G, Goncalves P. Empirical mode decomposition as a filter bank. IEEE Signal Process Lett. 2004;11(2):112–4. DOI: 10.1109/LSP.2003.821662

Haider B, Duque A, Hasenstaub AR, Yu Y, McCormick DA. Enhancement of visual responsiveness by spontaneous local network activity in vivo. J Neurophysiol. 2007;97(6):4186–202. DOI: 10.1152/jn.01114.2006

Hu M, Liang H. Intrinsic mode entropy based on multivariate empirical mode decomposition and its application to neural data analysis. Cogn Neurodyn. 2011;5(3):277-84. DOI: 0.1007/s11571-011-9159-8

Hu M, Liang H. Noise-assisted instantaneous coherence analysis of brain connectivity. Comput Intell Neurosci. 2012;2012:275073. DOI: 10.1155/2012/275073

Hu M, Liang H. Search for information-bearing components in neural data. PLoS One. 2014;16;9(6):e99793. DOI: 10.1371/journal.pone.0099793

Huang NE, Shen Z, Long SR, Wu MC, Shih HH, Zheng Q, et al. The empirical mode decomposition and the Hilbert spectrum for nonlinear and non-stationary time series analysis. Proc R Soc London Ser A Math Phys Eng Sci 1998;454:903–5. DOI: 10.1098/rspa.1998.0193

Huang JR, Fan SZ, Abbod MF, Jen KK, Wu JF, Shieh JS. Application of multivariate empirical mode decomposition and sample entropy in EEG signals via artificial neural networks for interpreting depth of anesthesia. Entropy. 2013;15(9):3325–39. DOI: 10.3390/e15093325

Klampfl S, David SV, Yin P, Shamma SA, Maass W. A quantitative analysis of information about past and present stimuli encoded by spikes of A1 neurons. J Neurophysiol. 2012;108(5):1366–80. DOI: 10.1152/jn.00935.2011

Laurent G. 1996. Dynamical representation of odors by oscillating and evolving neural assemblies. Trends Neurosci. 1996;19(11):489-96. DOI: 10.1016/S0166-2236(96)10054-0

Liang H, Bressler SL, Desimone R, Fries P. Empirical mode decomposition: a method for analyzing neural data. Neurocomputing. 2005a;65,801-7. DOI:10.1016/j.neucom.2004.10.077

Liang H, Bressler SL, Buffalo EA, Desimone R, Fries P. Empirical mode decomposition of field potentials from macaque V4 in visual spatial attention. Biological cybernetics. 2005b; 92:380-92. DOI 10.1007/s00422-005-0566-y

Luczak A, Barthó P, Marguet SL, Buzsáki G, Harris KD. Sequential structure of neocortical spontaneous activity in vivo. Proc Natl Acad Sci U S A. 2007;104(1):347–52. DOI: 10.1073/pnas.0605643104

Mandic DP, Rehman N, Wu Z, Huang NE. Empirical mode decomposition-based time-frequency analysis of multivariate signals: The power of adaptive data analysis. IEEE Signal Process Mag. 2013;30(6):74–86. DOI: 10.1109/MSP.2013.2267931

Naik G, Selvan S, Nguyen H. Single-Channel EMG Classification With Ensemble-Empirical-Mode-Decomposition-Based ICA for Diagnosing Neuromuscular Disorders. IEEE Trans Neural Syst Rehabil Eng. 2015;4320(c). DOI: 10.1109/TNSRE.2015.2454503

Niederreiter H. Random number generation and Quasi-Monte Carlo methods. Encycl. Actuar. Sci. Philadelphia: Society for Industrial and Applied Mathematic. 1992. DOI: 10.1137/1.9781611970081

Okun M, Yger P, Marguet SL, Gerard-Mercier F, Benucci A, Katzner S, et al. Population rate dynamics and multineuron firing patterns in sensory cortex. J. Neurosci. 2013;32(48):17108–19. DOI:10.1523/JNEUROSCI.1831-12.2012.

Okun M, Steinmetz NA, Cossell L, Iacaruso MF, Ko H, Barthó P, et al. Diverse coupling of neurons to populations in sensory cortex. Nature. 2015; 521(7553):511-5 DOI: 10.1038/nature14273

Pardey J, Roberts S, Tarassenko L. A review of parametric modelling techniques for EEG analysis. Med Eng Phys. 1996;18(1):2–11. DOI: 10.1016/1350-4533(95)00024-0

Petersen CC, Hahn TT, Mehta M, Grinvald A, Sakmann B. Interaction of sensory responses with spontaneous depolarization in layer 2/3 barrel cortex. Proc Natl Acad Sci U S A. 2003;100(23):13638–43. DOI: 10.1073/pnas.2235811100

Phinyomark A, Limsakul C, Phukpattaranont P. A Novel Feature Extraction for Robust EMG Pattern Recognition. J Comput. 2009;1(1):71–80. DOI: 0912.3973

Pizá ÁG, Farfán FD, Albarracín AL, Ruiz GA, Felice CJ. Discriminability measures and time–frequency features: An application to vibrissal tactile discrimination. J Neurosci Methods.; 2014;233:78–88. DOI: 10.1016/j.jneumeth.2014.06.007

Rehman N, Mandic DP. Multivariate empirical mode decomposition. Proc R Soc A Math Phys Eng Sci . 2010;466:1291–302. DOI: 10.1098/rspa.2009.0502

Rehman N, Mandic DP. Filter bank property of multivariate empirical mode decomposition. IEEE Trans Signal Process. 2011;59(5):2421–6. DOI: 10.1109/TSP.2011.2106779

Rilling G, Flandrin P, Goncalves P. on Empirical Mode Decomposition and Its Algorithms. IEEEEURASIP Work Nonlinear Signal Image Process NSIP. 2003;3:8–11. DOI: 10.1140/epjnbp/s40366-014-0014-9

Safaai H, von Heimendahl M, Sorando JM, Diamond ME, Maravall M. Coordinated population activity underlying texture discrimination in rat barrel cortex. J Neurosci. 2013;33(13):5843–55. DOI:10.1523/JNEUROSCI.3486-12.2013

Shamir M, Sompolinsky H. Nonlinear population codes. Neural Comput. 2004;16(6):1105-36. DOI: 10.1162/089976604773717559

Theunissen F, Miller JP. Temporal encoding in nervous systems: A rigorous definition. J Comput Neurosci. 1995;2(2):149–62. DOI: 10.1007/BF00961885

Zhan Y, Halliday D, Jiang P, Liu X, Feng J. Detecting time-dependent coherencebetween non-stationary electrophysiological signals – A combined statisticaland time–frequency approach. J Neurosci Methods 2006;156(1–2):322–32. DOI: 10.1016/j.jneumeth.2006.02.013

ZhaohuaW, Huang NE. Ensemble Empirical Mode Decomposition : A Noise Assisted Data Analysis Method. Adv Adapt Data Anal. 2009;1(1):1–41. DOI: 10.1142/S1793536909000047

Supplementary Figures:

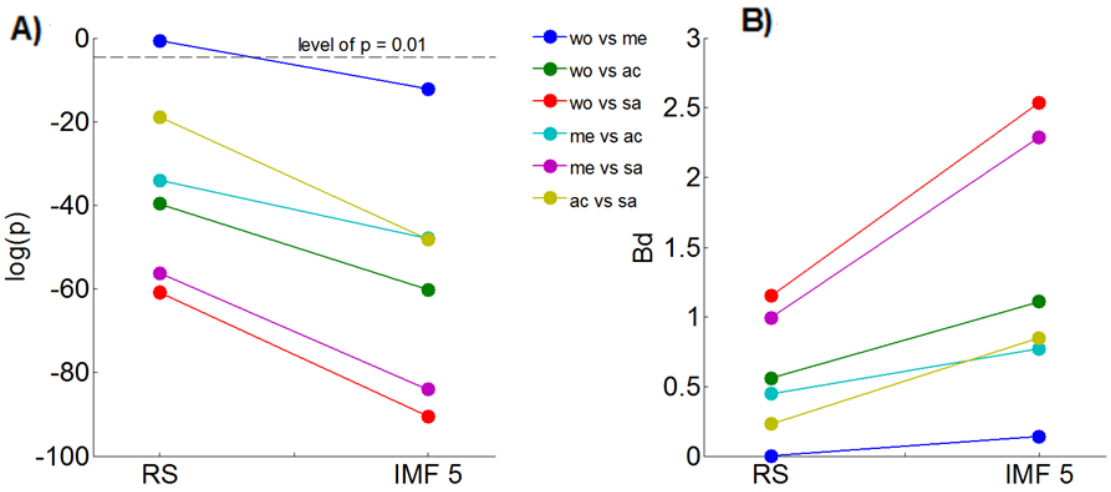

Supp fig. 1 P values (p) obtained from multiple comparisons (Dunn method) and Bhattacharyya distance values (Bd) before and after NA-MEMD. A) P values strongly decreases when compare evoked Fm decomposing the signal with NA-MEMD plus Hilbert Transform over raw signal (RS). B) Bd values are increased when NA-MEMD plus Hilbert Transform is implemented.

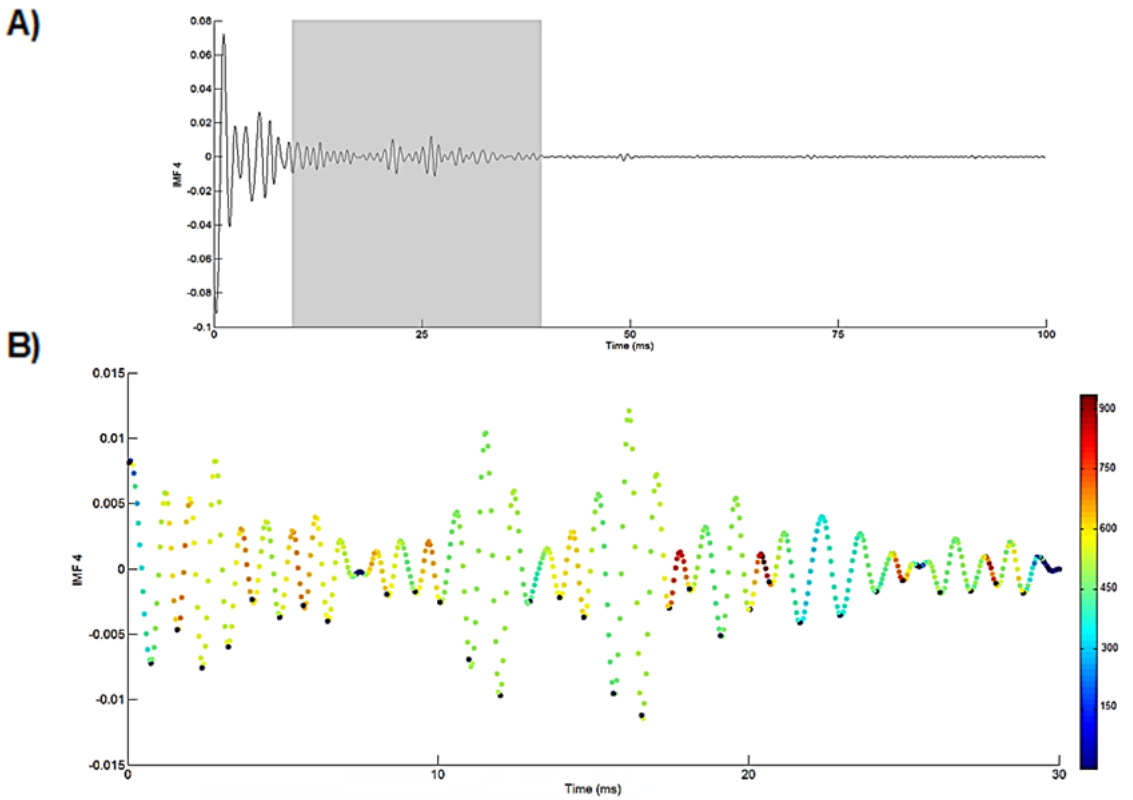

Supp fig. 2 IF example profile of 30 ms of afferent recordings 10ms after stimulation and P1000 texture, slip1. A) IMF 4 B) IF modulation in Hz of shaded region in A). Intrawave modulations (nonlinearity) are seen along the whole recording. IF (Hz) is shown as a color scale (dark red for higher frequencies and dark blue for lower frequencies) over the recording

PAPER II: Multiscale dynamics of interstimulus interval integration in visual cortex

Javier Alegre-Cortés, Cristina Soto-Sánchez, Eduardo Fernandez

PLoS ONE 2018 13(12):e0208822

PLOS ONE

RESEARCH ARTICLE

Multiscale dynamics of interstimulus interval integration in visual cortex

J. Alegre-Cortés[1], C. Soto-Sánchez[1,2,3]*, E. Fernandez[1,2]

1 Bioengineering Institute, Miguel Hernández University (UMH), Alicante, Spain, **2** Biomedical Research Networking center in Bioengineering, Biomaterials and Nanomedicine (CIBER-BBN), Madrid, Spain, **3** Biotechnology Department, University of Alicante (AU), Alicante, Spain

* sotosanc@gmail.com

Citation: Alegre-Cortés J, Soto-Sánchez C, Fernandez E (2018) Multiscale dynamics of interstimulus interval integration in visual cortex. PLoS ONE 13(12): e0208822. https://doi.org/10.1371/journal.pone.0208822

Editor: Gennady Cymbalyuk, Georgia State University, UNITED STATES

Received: May 31, 2018

Accepted: November 24, 2018

Published: December 17, 2018

Data Availability Statement: All relevant data are available at http://nbio.umh.es/visual-cortex-dataset.

Funding: This work was supported in part by the Spanish national research program (MAT2015-69967-C3-1; http://www.mineco.gob.es/portal/site/mineco/), by Research Chair Bidons Egara (http://www.bidonsegara.com/) and by a research grant of the Spanish Blind Organization (ONCE; https://www.once.es/). The funders had no role in study design, data collection and analysis, decision to publish, or preparation of the manuscript.

Abstract

Although the visual cortex receives information at multiple temporal patterns, much of the research in the field has focused only on intervals shorter than 1 second. Consequently, there is almost no information on what happens at longer temporal intervals. We have tried to address this question recording neuronal populations of the primary visual cortex during visual stimulation with repetitive grating stimuli and intervals ranging from 1 to 7 seconds. Our results showed that firing rate and response stability were dependent of interval duration. In addition, there were collective oscillations with different properties in response to changes in intervals duration. These results suggest that visual cortex could encode visual information at several time scales using oscillations at multiple frequencies.

Introduction

Despite the increasing interest in how visual cortex neurons encode visual information [1–4], there are still many open questions concerning the temporal integration at long (seconds) scale. While the encoding of sensory information at sub seconds scale has been extensively studied [5–8], the processing of longer time intervals has traditionally been less studied[9–12], and it has usually been addressed via pharmacological studies [13]. An exception to this is the study of reward timing in visual cortex; during the last years it has been discovered that reward timing [10] and visually cued action timing [12] are represented in visual cortex in experiments on which the delay between the cue and the reward lasted up to 3 s.

How the brain encodes temporal information is indeed an open field of research [14–16]. Thereby, some models propose that time is encoded in populations of pacemaker neurons that are the only responsible of temporal coding in the brain via oscillating at different frequencies [17], while others propose that time is encoded by arrays of neurons with different time constants that respond to different intervals. Furthermore, there is evidence showing that *in-vitro* cortical networks can reflect specific temporal patterns [18].

On the other hand, many theories of perception are based on cortical oscillations [19] which have been well characterized in response to visual stimulation [20,21], attention [22], speech recognition [23], motor function [24] or reward expectation in visual cortex [25,26]. Furthermore, our sensory environment is full of regularities, for example, repetitive stimuli,

Competing interests: The authors have declared that no competing interests exist.

which we use to predict future events. In this framework, the main goal of this study was to get insights about if neuronal populations of deep layers of visual cortex can convey and process interval information at seconds scale using spikes. To answer this question, we recorded neuronal populations from rat visual cortex while visually stimulated with a unique type of stimulus and different interstimulus intervals (ISI), ranging from 1 to 7 seconds.

To obtain a high-resolution picture of population oscillations we decomposed the signals obtained averaging all the electrodes using a Noise Assisted Multivariate Empirical Mode Decomposition (NA-MEMD) [27] and computed the Huang-Hilbert Spectrum (HHS) for nonlinear and non-stationary time series analysis. This procedure was chosen because it allows to analyze the recordings with instantaneous temporal and frequency resolutions [28–30], which is crucial to depict nonlinear properties of the responses [31–33] and moreover it is robust against signal intermittency in the data [27,34][35]. Our results showed that the responses of visual cortex neuronal populations to an unchanged grating stimulus had different Time-Frequency (T-F) dynamical spectra, depending on which ISI was used. Furthermore, these spectral differences were present at different frequencies and times which fully agrees with temporal multiplexing theory [36,37].

Materials and methods

Experimental design

Visual cortex multiunit recordings were obtained from Long Evans adult rats (n = 4, Janvier Labs, France) weighing 450–500 gr. Analgesia was induced by buprenorphine (0.025mg kg-1 s. c), and surgical anesthesia and sedation were induced by ketamine HCl (40 mg kg^{-1} i.p). The anesthesia was continued and maintained with a mix of oxygen and 2.5% of isoflurane during the surgery and afterward reduced to 1.5% during the electrophysiological recordings. The blinking and the toe pinch reflexes were continuously checked along the experiment to guarantee a proper level of anesthesia for the animal. The body temperature was maintained with a thermal pad and the heart rate and O_2 concentration in blood were monitored throughout the experiment. Animals were pre-treated with dexamethasone (1 mg kg^{-1} i.p) 24 hours and 20 minutes prior to surgery in order to avoid brain edema caused by the electrode insertion.

A craniotomy was drilled on top of the visual cortex and a customized 6x6 Utah Electrode Array (UEA) covering a brain surface of 2 mm x 2 was inserted 2 mm lateral to the midline and 0.5 mm anterior to lambda. The UEA was inserted in the deep layers of the visual cortex (>600 μm) through the duramatter with the help of a Blackrock pneumatically-actuated inserter device (Blackrock Microsystems, Salt Lake City, USA). After the insertion, the ipsilateral eyelid to the craniotomy site was closed with cyanoacrylate and atropine sulphate 1% was used to dilate the pupil of the contralateral eye.

In vivo neural activity from visual cortex was recorded simultaneously from 16 individual electrodes. The UEA array was connected to a MPA32I amplifier (Multichannel Systems, MCS) and the extracellular recordings were digitized with an MCS analog-to-digital board. The data were sampled at a frequency of 20 kHz and slow waves were digitally filtered out (100–3000 Hz, 2^{nd} order Butterworth type IIR digital filter) from the raw data. Neural spike events were extracted with a free-tool application for offline spike sorting analysis (Neural Sorter, http://sourceforge.net/projects/neuralsorter/) and the resulting multiunit information obtained from each electrode was stored for further analysis.

Visual stimulation consisted on a vertical drifting square-wave grating (90˚, light and dark bars, 100% contrast, 6 Hz, 0.6 cycles/degree) of 500 ms duration interspersed with a dark (uniform) stimulus of variable duration. The stimulus was displayed on an LCD monitor (refresh rate 60 Hz) and a luminance of ≈100 cd/m^2, placed 25 cm in front of the right eye,

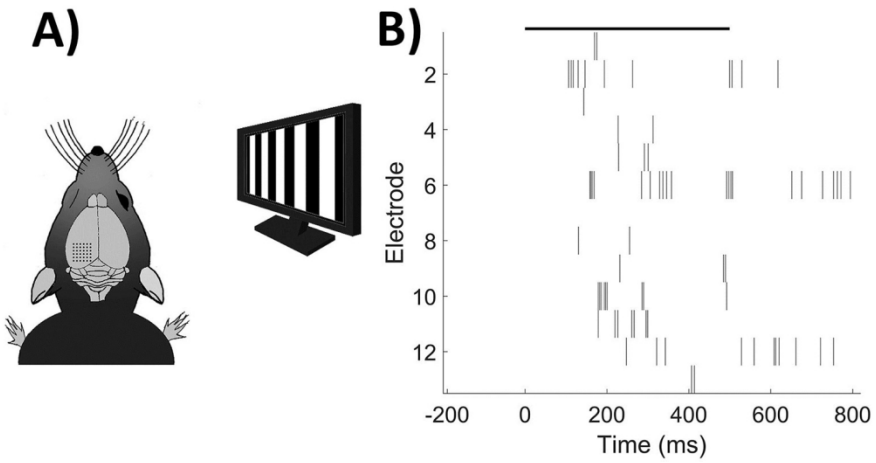

Fig 1. Experimental paradigm and representative trial. A) Schematic representation of the experimental stimulus-recording design. B) Example raster plot of a single trial and all electrodes. Stimulus displayed as black line.

https://doi.org/10.1371/journal.pone.0208822.g001

approximately at 30˚ from the midline covering a visual field spanning of ≈100˚ (Fig 1A) and repeated 15 times for each ISI. We used 1, 3, 5 and 7 seconds ISI protocols in separated experiments. The stimuli were generated using the Vision Egg library and customized python scripts. The room was kept in darkness all along the visual stimulation experiments. Euthanasia of the animals was performed once the recording protocols were ended.

Ethical approval

All the experimental procedures performed in this study conform to the directive 2010/63/EU of the European Parliament and of the Council, and the RD 53/2013 Spanish regulation on the protection of animals use for scientific purposes and were approved by the Miguel Hernandez University Committee for Animal use in Laboratory.

Data analysis

Neural activity analysis was performed in Matlab (MathWorks). Single or multiunit spiking activity was isolated from the background. We observed multiunit activity in the majority of the electrodes through the whole recording sessions, then, only those electrodes with neural activity higher than 0.5 spikes/s were considered in the analysis. (Fig 1B).

We constructed time-dependent population activity vectors by temporally binding the activity of each electrode with 1 ms resolution. We considered one second before and one second after each stimulus presentation for each ISI. The first stimulus of each recording was not considered for the analysis. Possible anticipation dynamics were not subject to analysis, as they exceeded the aim of this paper.

NA-MEMD

We used an extension of the EMD algorithm[38] to study the T-F properties of the neural response. It has recently described [30,39] that the result of using EMD family of algorithms to study the oscillatory properties of spike trains improves the results obtained by means of using other traditional T-F techniques due to the presence of nonlinearities and nonstationarities in the signal [30–32,40].

To overcome the problems associated to univariate EMD analysis, we used the Multivariate Empirical Mode Decomposition (MEMD) [41], which is a multivariate extension of EMD algorithm [38], where analysis of simultaneous dimensions is performed simultaneously to obtain a meaningful decomposition of the whole multidimensional signal in a subset of vectors called Intrinsic Mode Functions (IMFs). Furthermore, we added White Gaussian Noise (WGN) to the MEMD, which increases its performance via reducing mode mixing produced by signal intermittency [34]. This procedure acts as a filter bank that enhances time-frequency resolution [41, 42]. Briefly, WGN is added in additional dimensions:

$$d = n + k,$$

Where d is the final number of dimensions, n the dimensions of the original data (electrodes, trials. . .) and k the number of additional dimensions including WGN [41].

In order to apply this Noise Assisted Multivariate Empirical Mode Decomposition (NA-MEMD) to our data, we adapted the MEMD Matlab package (http://www.commsp.ee.ic.ac.uk/~mandic/research/emd.htm). We used the low-discrepancy Hammersley sequence to generate a set of 300 direction vectors for computing signal projections and 4 WGN channels. Standard stopping criterion was described elsewhere [43].

Since in our study, we seek for depicting features present in the whole recorded population, we averaged the activity of all electrodes for the presentations of the moving grating for each ISI in each animal and then added 4 additional dimensions with WGN.

Hilbert transform

We measured present frequencies in our data as the instantaneous frequency (IF) using Hilbert Transform (HT) (Huang et al. 1998). For a given time series x(t), its Hilbert Transform H(x)(t) is defined as:

$$H(x)(t) = \frac{1}{\pi} C \int_{-\infty}^{\infty} \frac{x(t')}{t - t'} dt',$$

Where C indicates the Cauchy principal value. Hilbert Transform results in a complex sequence with a real part which is the original data and an imaginary part which is a version of the original data with a 90˚ phase shift. This *analytic signal* is useful to calculate instantaneous amplitude and frequency, thereby instantaneous amplitude is the amplitude of H(x)(t), and the instantaneous frequency is the time rate of change of the instantaneous phase angle.

Phase space

We created a low dimensional phase space considering mean population firing rate as well as two IMFs that statistically carried ISI information with different temporal dynamics and were consistent with multiplexed theory, IMF 8 (5.93 +/- 0.37 Hz) and IMF 6 (18.37 ± 1.29) [36,37].

To compare the Euclidean distance of the mean population trajectories in this phase space we normalized all axes to prevent from any biasing and computed the center of all trajectories. A 200 ms duration window of time ranging from 400 ms to 200 ms before stimulus onset was used to localize the fixed point representing the population resting state before stimulation.

Statistical analysis

All experimental comparisons were tested using Wilcoxon rank-sum test. P values for multiple comparisons were corrected ad hoc using Storey method [44].

Results

Our procedures allow studying whether visual cortex neurons synchronized oscillations do carry information about interstimulus intervals (ISIs) at the level of instant frequency (IF). Fig 2A shows the mean firing rate of all electrodes and presentations during and after stimulation for each recorded ISI. We appreciated an overall increase in the normalized mean firing rate when 3 and 5 seconds ISI were used with respect to 1s ISI (Fig 2B, Wilcoxon test, corrected p value <0.03). These differences were persistent during the whole stimulation window when 5 seconds ISI was used, and restricted to a 300 ms window starting 100 ms after stimulus onset when a 3 second ISI was used (Fig 2A). At last, in the case of 7 versus 1 second ISI, a transient peak of discrimination was found 150–200 ms after stimulus onset (Fig 2A).

We next tried to determine if the responses to visual stimulation with longer ISIs were more stable. As it is known that stimulation quenches neural variability[45], we asked whether changes in the ISI could drive to more or less stable responses for different time lengths. Therefore, we computed the Coefficient of variance (C.V.) during the stimulation window across different presentations in each animal independently to analyze the reliability of the population firing rate in the response to stimulation with different ISI (Fig 2C). We found that C.V. was significantly reduced for ISIs longer than 1s (corrected p value <0.05).

Then, we studied whether neurons modulated their oscillatory dynamics at the population levels to process ISI length. To do so, we compared the instantaneous amplitude of each IMF

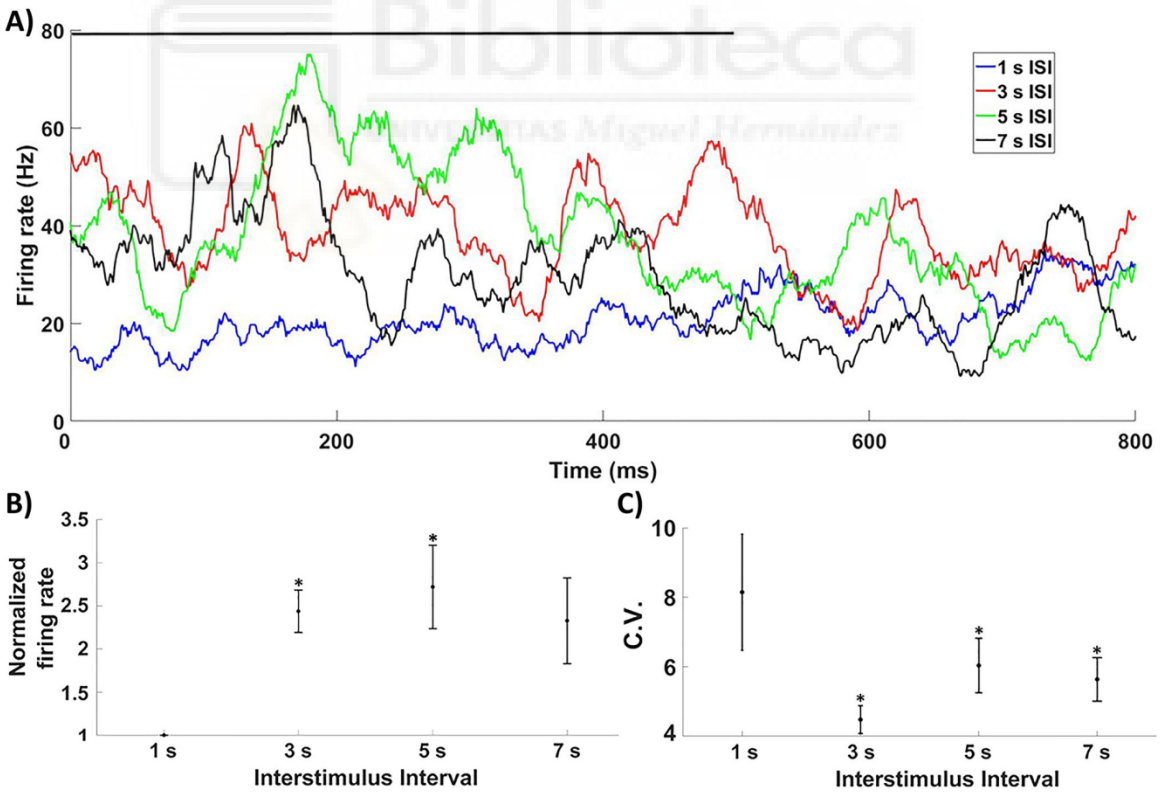

Fig 2. Mean firing rate. A) Mean firing rate dynamics depending on ISI used. Stimulus shown as a black line. B) Normalized mean firing rate during the stimulation window. 3 and 5 s ISIs display significant increases when compared with 1 s ISI. C) C.V. across trials was statistically reduced for longer than 1s ISIs.

https://doi.org/10.1371/journal.pone.0208822.g002

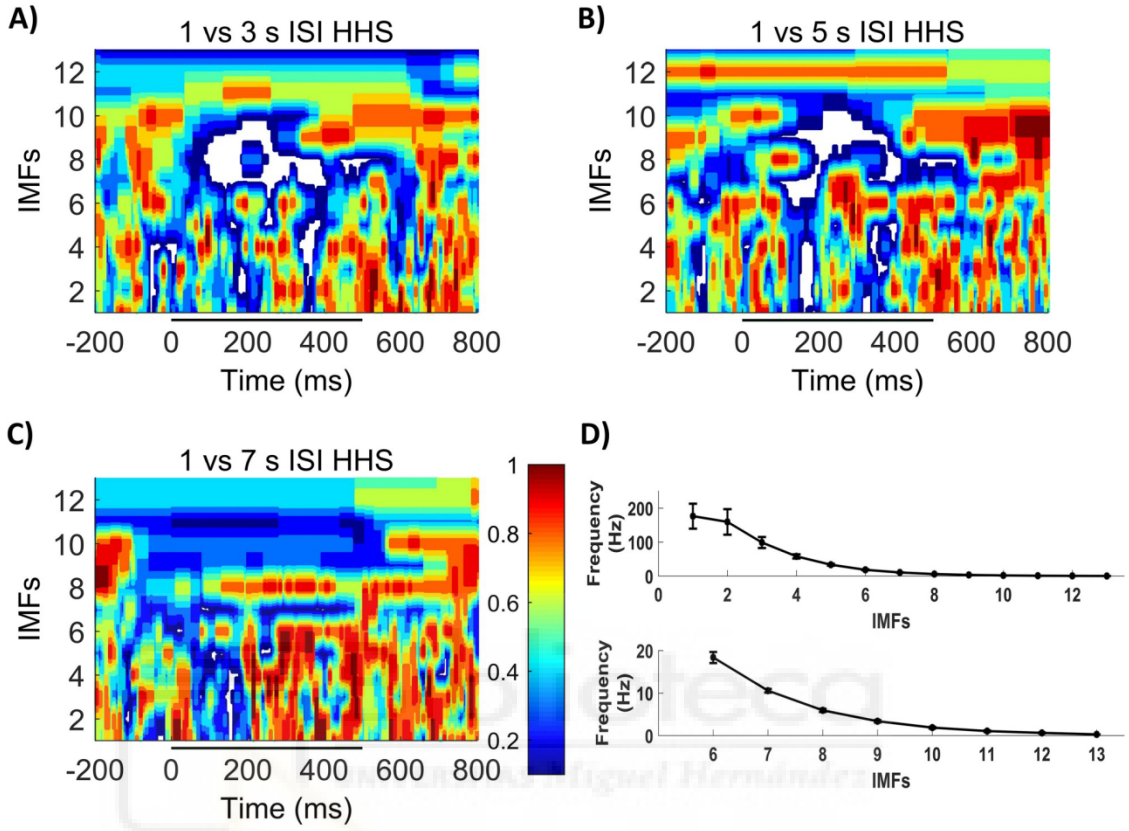

Fig 3. Comparative HHSs IMFs shown in y axis, higher frequencies at the bottom of the HHS. A) P values comparing the obtained HHSs using 1s and 3s ISI. B) P values comparing the obtained HHSs using 1s and 5s ISI. C) P values comparing the obtained HHSs using 1s and 7s ISI. D) Frequency range of each IMF. Wilcoxon P value displayed as color code; unique color bar for the 3 comparisons; significant values displayed in white color. Stimulus displayed as black line.

https://doi.org/10.1371/journal.pone.0208822.g003

across time of 1second ISI with longer intervals (S1 Fig). Thus, we created a "discriminability spectrum" (Fig 3) were the differences in amplitude at each IMF and time point were represented as the p value We appreciated significant differences (white color) in multiple IMFs for 3 and 5 seconds, mainly during and shortly after stimulations (Fig 3A and 3B), but little differences were seen against the 7 seconds ISI (Fig 3C). This suggests that ISI information was encoded simultaneously at different timescales along the response, ranging from [1.87±0.18 to 159.34 ±37.53 Hz], consistent with multiplex theory [36,37].

To further study how ISI can be encoded at different frequencies during stimulation we extended our analysis to particular IMFs. We found that IMFs carrying information about low frequencies (Fig 3D), IMFs 7–9 (3.37±0.28 to 10.56±0.43 Hz), were statistically significant or statistically relevant (corrected p value < 0.1) from those at 1 seconds ISI stimulation during almost the whole stimulation window (i.e. IMF 8, Fig 4). Thus, slow frequencies seem to be able to encode information about longer ISIs only until a certain time interval. IMF 8 was of particular interest, since it carried out the responses in the frequency band of the used gratings. We found that this particular phenomenon was reinforced when 3 or 5 seconds ISI were used and was inexistent when we used a 7 seconds ISI. Moreover, the IMF 7 (10.56±0.43 Hz), was

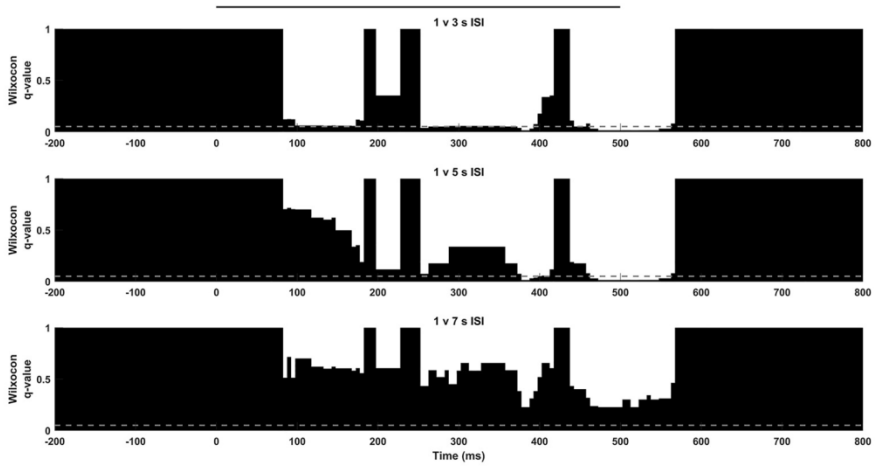

Fig 4. 6 Hz population dynamics. IMF 8 (5.93±0.37 Hz). 1s ISI is compared with 3s (top), 5s (middle) and 7 s (bottom) along stimulation using Wilcoxon test and Storey correction. Significance level shown as grey line, stimulus displayed as a black line.

https://doi.org/10.1371/journal.pone.0208822.g004

also different for each ISI against 1seconds (Fig 5), which suggest that low frequency properties were modified for ISIs longer than 1seconds.

When we extended our analysis to higher frequency components of the response (33.43 ±2.73 to 159.34±37.53 Hz), the discriminability spectrum became more intermittent (Fig 3A–3C). Statistically significant differences remained present with different temporal profile, especially when 1 second ISI was compared with 3 and 5 seconds intervals. A brief discrimination window emerged ± 200 ms after stimulus onset when 3, 5 and 7 seconds ISI were used against 1 second ISI across several high frequency IMFs, indicating a common high frequency peak in population response for longer ISIs. On the other hand, high frequency components were present in the second half of the stimulation when 3 or 5 seconds ISI were used.

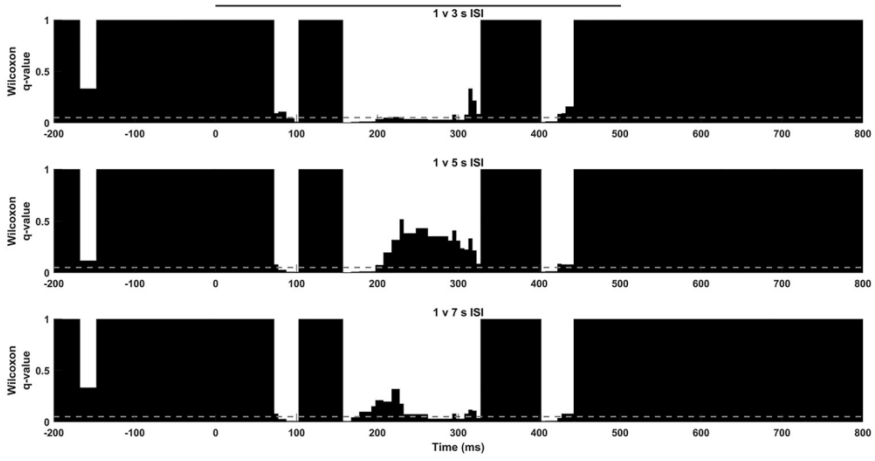

Fig 5. 10 Hz population dynamics. IMF 7 (10.56±0.43 Hz). Different temporal discrimination profiles were obtained when 1 s ISI was compared with 3s (top), 5s (middle) or 7 s (bottom). Significance level shown as grey line, stimulus displayed as a black line.

https://doi.org/10.1371/journal.pone.0208822.g005

In summary, in our work, we show how the response of neuronal populations of the visual cortex to a grating stimulus is sensitive to the length of the ISI at seconds scale. We described how these differences were present at the level of firing rate, the variability of the response, and in the oscillatory properties of the population response.

Discussion

Even though the capability of neurons to discriminate temporal patterns is known since the 60's [46], we are far from understanding how cortical circuits encode time. This statement is particularly true when we refer to times in seconds scale. In this work, we studied how visual cortex neuronal populations of adult rats were responsive to ISI variations in the seconds scale. We found that population firing rate and spiking oscillatory dynamics were sensitive to the ISI we used, suggesting that visual cortex activity encodes temporal information up to several seconds. Furthermore, these range of frequencies were consistent with classical works of neuronal oscillations during visual stimulation [20,21].

The differences were present in the signal amplitude at different frequencies and temporal profiles. Thus we found significant differences at the level of firing rate and low frequency components, including the temporal frequency of the grating. These differences were present throughout the whole stimulating window when 3 or 5 seconds ISI were used and vanished for longer times (7 seconds). Furthermore, there were differences in high frequency components when intervals longer than 1 second were used. These high frequency features appeared 100–120 ms before stimulus offset when 3 or 5 seconds were used, but were not found when 7 seconds ISI were used. In addition, the variability of individual presentations response was reduced when longer than 1-second trails were used, which suggests that longer temporal patterns increase the reliability of the responses. In addition, as it had been previously described [30], the population responses were intermittent and strongly nonlinear, as intrawave modulations were present during the response.

Considering the presented results, we propose a low dimensional phase space for ISI discrimination considering three relevant parameters of the response: firing rate, low frequency (6 Hz) and high frequency (18 Hz) dynamics (Fig 6A), in which visual cortex neuronal populations would be able to discriminate among ISIs depending on the elicited dynamics. In this space, population dynamics are constricted to a fixed point (dotted line, Fig 6A) upon stimulation, when different trajectories are evoked depending on the ISI used during the stimulation. In order to compare the dynamics of the response to different ISIs, we computed the Euclidean distance to the centroid given by the mean point of all trajectories from 400 to 200 ms prior to stimulation (Fig 6B). We can see different temporal dynamics depending on the ISI that we used in this low dimensional space that may lead to ISI discrimination. When 1 second ISI is used, the population trajectory does not move away from the fixed point, as it happens when using longer ISIs. In these series, the evoked trajectories temporal dynamics diverge depending on whether 3/5 seconds ISI or a 7 second ISI was used. In the first case, population dynamics are projected distally to this low-dimensional space during the whole stimulation window. On the other hand, 7 second ISI leads to transient dynamics where the population activity leaves the fixed point for a brief period (±200 ms) and then returns to the previous subspace. Hence, we could easily outline a boundary which would be able to discriminate a certain window of ISIs (3–5 seconds) during stimulation from longer or shorter times. Similar results were seen using IMFs containing oscillations up to 57.98 ± 6.26 Hz in the high frequency axes. These results support the idea of a multiscale response, in which neuronal populations encode ISI information using multiple frequencies and firing rates in their spiking dynamics.

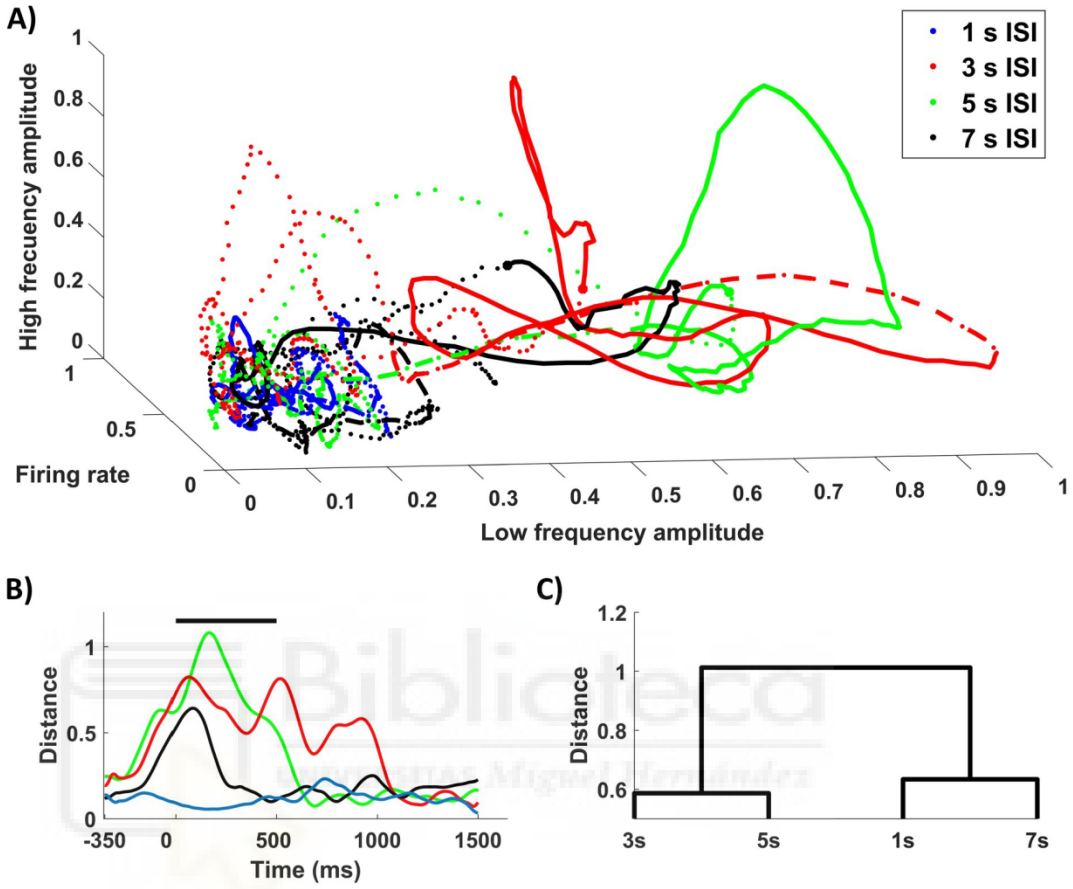

Fig 6. Low dimensional dynamics for ISI discrimination. A) Phase space created using Raw signal mean firing rate, IMF 8 (5.93 ± 0.37 Hz) and IMF 6 (18.37 ± 1.29) as axes where trajectories for all ISIs are plotted ranging from -350 ms to 1500ms after stimulus onset. Trajectories during stimulation shown as whole lines starting as a thick dot during a 300 ms window, starting on stimulus offset as discontinuous line. B) Euclidean distance to the resting state centroid of mean trajectories for the different ISIs. C) Hierarchical tree based on Euclidean distances between trajectories during the stimulation window.

https://doi.org/10.1371/journal.pone.0208822.g006

Recent works address the multiscale response in different sensory cortices [47,48], where slow cortical rhythms were proposed to stabilize sensory representation. A different study [49] suggested that different information was carried in the low frequency components of LFP and spikes. Our results show a similar behavior for spiking oscillatory activity in primary visual cortex and support the point of view of multiplexed dynamics for ISI encoding at seconds scale [36,37].

Previous work in the seconds scale on visual cortex was focused on reward timing [12,26]. In these papers, the authors already described a role for oscillatory activity in visual cortex in a different type of timing behavior. Bearing in mind the differences among our study of the interval between visual stimulation and previous work in reward timing, it results interesting that different experiments which involve timing in the seconds scale evoke oscillatory activity in the visual cortex. Nevertheless, oscillations during reward timing were never present before at least 50 correct trials [26], while we describe the oscillatory activity in the response to visual stimulation that was repeated 15 times. Hence, we cannot discuss that the underlying

mechanism is the same for the oscillations in the activity of visual cortex that are modulated by the interval in visual stimulation and reward timing.

Given that temporal coding at seconds scale has been reported to be crucial for behavior [50,51], the presence of an optimal temporal window of response to stimuli is an important question that should be assessed in future studies (Fig 6A). Our results suggest that neuronal population response dynamics strongly differ when 1 vs 3 seconds and 5 second ISI are used for a vertical grating stimulus (Fig 6C). These differences are softened when a longer ISI (7 seconds) was used. Therefore, we may consider facilitation at certain frequencies for intermediate times in the temporal scale of seconds. No clear differences between 3 and 5 seconds ISIs were seen during stimulation. Thus, it might reflect a window of time in which visual cortex response to stimulation is strengthened.

An important question remaining to answer is the source of these oscillatory dynamics. Although in this work we describe temporal discrimination in visual cortex, this kind of computational studies has been classically studied in prefrontal cortex [52–54] but, at present, it is still unclear how prefrontal and sensory cortices interact during interval timing at seconds scales. Future studies will be required to assess the communication and hierarchical organization of these areas during the estimation of interval time, as well as the probable effect of dopamine via the frontostriatal circuit [13,55].

Supporting information

S1 Fig. Representative examples of individual stimulation. Evoked population response to single stimulation using A) 1s ISI B) 3s ISI C) 5s ISI D) 7s ISI. Top, PSTH summing the activity in all the electrodes in response to stimulation; Bottom, HHS spectrum of the signal above. Stimulus displayed as a black line.
(TIF)

Acknowledgments

We thank Dr. Lawrence Humphreys for his help with the English revision.

Author Contributions

Conceptualization: J. Alegre-Cortés, C. Soto-Sánchez, E. Fernandez.

Data curation: J. Alegre-Cortés, C. Soto-Sánchez.

Formal analysis: J. Alegre-Cortés.

Funding acquisition: E. Fernandez.

Investigation: J. Alegre-Cortés, C. Soto-Sánchez, E. Fernandez.

Methodology: J. Alegre-Cortés, C. Soto-Sánchez.

Project administration: E. Fernandez.

Resources: E. Fernandez.

Software: J. Alegre-Cortés.

Supervision: J. Alegre-Cortés, C. Soto-Sánchez, E. Fernandez.

Visualization: J. Alegre-Cortés, C. Soto-Sánchez.

Writing – original draft: J. Alegre-Cortés, C. Soto-Sánchez, E. Fernandez.

Writing – review & editing: J. Alegre-Cortés, C. Soto-Sánchez, E. Fernandez.

References

1. Okun M, Steinmetz N., Cossell L, Iacaruso MF, Ko H, Barthó P, et al. Diverse coupling of neurons to populations in sensory cortex. Nature. 2015; 521:511–515. https://doi.org/10.1038/nature14273 PMID: 25849776
2. Busse L, Ayaz A, Dhruv NT, Katzner S, Saleem AB, Schölvinck ML, et al. The detection of visual contrast in the behaving mouse. J Neurosci. 2011; 31: 11351–61. https://doi.org/10.1523/JNEUROSCI.6689-10.2011 PMID: 21813694
3. Carandini M. Amplification of trial-to-trial response variability by neurons in visual cortex. PLoS Biol. 2004; 2: E264. https://doi.org/10.1371/journal.pbio.0020264 PMID: 15328535
4. Ko H, Cossell L, Baragli C, Antolik J, Clopath C, Hofer SB, et al. The emergence of functional microcircuits in visual cortex. Nature. 2013; 496: 96–100. https://doi.org/10.1038/nature12015 PMID: 23552948
5. Burr D, Tozzi A, Morrone MC. Neural mechanisms for timing visual events are spatially selective in real-world coordinates. Nat Neurosci. 2007; 10: 423–425. https://doi.org/10.1038/nn1874 PMID: 17369824
6. Ghose GM, Maunsell JHR. Attentional modulation in visual cortex depends on task timing. Nature. 2002; 419: 616–620. https://doi.org/10.1038/nature01057 PMID: 12374979
7. Johnston A, Arnold DH, Nishida S. Spatially localized distortions of event time. Curr Biol. 2006; 16: 472–479. https://doi.org/10.1016/j.cub.2006.01.032 PMID: 16527741
8. Nikolić D, Häusler S, Singer W, Maass W. Distributed fading memory for stimulus properties in the primary visual cortex. PLoS Biol. 2009; 7: e1000260. https://doi.org/10.1371/journal.pbio.1000260 PMID: 20027205
9. Gavornik JP, Bear MF. Learned spatiotemporal sequence recognition and prediction in primary visual cortex. Nature Neurosci. 2014; 17:732–737. https://doi.org/10.1038/nn.3683 PMID: 24657967
10. Shuler MGl; Bear MF. Reward Timing in the Primary Visual Cortex. Science. 2006; 311: 1606–1610. https://doi.org/10.1126/science.1123513 PMID: 16543459
11. Chubykin AA, Roach EB, Bear MF, Shuler MG. A Cholinergic Mechanism for Reward Timing within Primary Visual Cortex. Neuron. 2013; 77: 723–735. https://doi.org/10.1016/j.neuron.2012.12.039 PMID: 23439124
12. Namboodiri VMK, Huertas MA, Monk KJ, Shouval HZ, Shuler MG. Visually cued action timing in the primary visual cortex. Neuron. 2015; 86: 319–330. https://doi.org/10.1016/j.neuron.2015.02.043 PMID: 25819611
13. Meck WH. Neuropharmacology of timing and time perception. Cogn Brain Res. 1996; 3: 227–242. https://doi.org/10.1016/0926-6410(96)00009-2
14. Finnerty GT, Shadlen MN, Jazayeri M, Nobre AC, Buonomano D V. Time in Cortical Circuits. J Neurosci. 2015; 35: 13912–13916. https://doi.org/10.1523/JNEUROSCI.2654-15.2015 PMID: 26468192
15. Mauk MD, Buonomano D V. the Neural Basis of Temporal Processing. Annu Rev Neurosci. 2004; 27: 307–340. https://doi.org/10.1146/annurev.neuro.27.070203.144247 PMID: 15217335
16. Buonomano D V, Laje R. Population clocks: motor timing with neural dynamics. Trends Cogn Sci. 2010; 14: 520–527. https://doi.org/10.1016/j.tics.2010.09.002 PMID: 20889368
17. Miall C. The Storage of Time Intervals Using Oscillating Neurons. Neural Comput. 1989; 1: 359–371. https://doi.org/10.1162/neco.1989.1.3.359
18. Jonhson HA, Goel A, Buonomano D V. Neural Dynamics of invitro cortical networks reflects experienced temporal patterns. Nat Neurosci. 2010; 13: 917–919. https://doi.org/10.1038/nn.2579 PMID: 20543842
19. Buzsáki G, Draguhn A. Neuronal Oscillations in Cortical Networks. 2014; 1926: 1926–1930. https://doi.org/10.1126/science.1099745 PMID: 15218136
20. Gray CM, Singer W. Stimulus-specific neuronal oscillations in orientation columns of cat visual cortex. Proc Natl Acad Sci U S A. 1989; 86: 1698–1702. https://doi.org/10.1073/pnas.86.5.1698 PMID: 2922407
21. Engel AK, König P, Gray CM, Singer W. Stimulus-dependent neuronal oscillations in cat visual cortex: inter-columnar interactions as determined by cross-correlation analysis. Eur J Neurosci. 1990; 2: 588–606. PMID: 12106294
22. Fries P, Schröder J-H, Roelfsema PR, Singer W, Engel AK. Oscillatory neuronal synchronization in primary visual cortex as a correlate of stimulus selection. J Neurosci. 2002; 22: 3739–3754. PMID: 11978850

23. Schroeder CE, Lakatos P, Kajikawa Y, Partan S, Puce A. Neuronal oscillations and visual amplification of speech. Trends Cogn Sci. 2008; 12: 106–113. https://doi.org/10.1016/j.tics.2008.01.002 PMID: 18280772

24. Jenkinson N, Brown P. New insights into the relationship between dopamine, beta oscillations and motor function. Trends Neurosci. 2011; 34: 611–618. https://doi.org/10.1016/j.tins.2011.09.003 PMID: 22018805

25. Levy JM, Zold CL, Namboodiri VMK, Hussain Shuler MG. The Timing of Reward-Seeking Action Tracks Visually-Cued Theta Oscillations in Primary Visual Cortex. J Neurosci. 2017; 37(43): 10408–10420. https://doi.org/10.1523/JNEUROSCI.0923-17.2017 PMID: 28947572

26. Zold CL, Hussain Shuler MG. Theta Oscillations in Visual Cortex Emerge with Experience to Convey Expected Reward Time and Experienced Reward Rate. J Neurosci. 2015; 35: 9603–9614. https://doi.org/10.1523/JNEUROSCI.0296-15.2015 PMID: 26134643

27. Ur Rehman N, Mandic DP. Filter bank property of multivariate empirical mode decomposition. IEEE Trans Signal Process. 2011; 59: 2421–2426. https://doi.org/10.1109/TSP.2011.2106779

28. Mandic DP, Ur Rehman N, Wu Z, Huang NE. Empirical mode decomposition-based time-frequency analysis of multivariate signals: The power of adaptive data analysis. IEEE Signal Process Mag. 2013; 30: 74–86. https://doi.org/10.1109/MSP.2013.2267931

29. Hu M, Liang H. Search for information-bearing components in neural data. PLoS One. 2014; 9: e99793. https://doi.org/10.1371/journal.pone.0099793 PMID: 24932596

30. Alegre-Cortés J, Soto-Sanchez C, Piza AG, Albarracin AL, Farfan FD, Felice CJ, et al. Time-frequency analysis of neuronal populations with instantaneous resolution based on noise-assisted multivariate empirical mode decomposition. J Neurosci Methods. 2016; 267: 35–44. https://doi.org/10.1016/j.jneumeth.2016.03.018 PMID: 27044801

31. Laurent G. Dynamical representation of odors by oscillating and evolving neural assemblies. Trends Neurosci. 1996; 19: 489–496. https://doi.org/10.1016/S0166-2236(96)10054-0 PMID: 8931275

32. Averbeck BB, Latham PE, Pouget A. Neural correlations, population coding and computation. Nat Rev Neurosci. 2006; 7: 358–66. https://doi.org/10.1038/nrn1888 PMID: 16760916

33. Shamir M. Nonlinear Population Codes. Neural Comput. 2004; 16(6): 1105–1136. https://doi.org/10.1162/089976604773717559 PMID: 15130244

34. Zhaohua W and Huang NE. Ensemble Empirical Mode Decomposition : A Noise Assisted Data Analysis Method. Adv Adapt Data Anal. 2009; 1: 1–41. https://doi.org/10.1142/S1793536909000047

35. Luczak A, McNaughton BL, Harris KD. Packet-based communication in the cortex. Nat Rev Neurosci. 2015; 16: 745–755. https://doi.org/10.1038/nrn4026 PMID: 26507295

36. Panzeri S, Brunel N, Logothetis NK, Kayser C. Sensory neural codes using multiplexed temporal scales. Trends Neurosci. 2010; 33: 111–20. https://doi.org/10.1016/j.tins.2009.12.001 PMID: 20045201

37. Victor JD. How the brain uses time to represent and process visual information. Brain Res. 2000; 886: 33–46. https://doi.org/10.1016/S0006-8993(00)02751-7 PMID: 11119685

38. Huang N. E., Shen Z., Long S., Wu M., Shih H., Zheng Q., et al. The empirical mode decomposition and the Hilbert spectrum for nonlinear and non-stationary time series analysis. Proc R Soc London Ser A Math Phys Eng Sci. 1998; 454: 903–995. PMID: 26953177

39. Alegre-Cortés J, Soto-Sánchez C, Albarracín AL, Farfán FD, Val-Calvo M, Ferrandez JM, et al. Toward an Improvement of the Analysis of Neural Coding. Front Neuroinform. 2018; 11: 1–6. https://doi.org/10.3389/fninf.2017.00077 PMID: 29375359

40. Bathellier B, Buhl DL, Accolla R, Carleton A. Dynamic ensemble odor coding in the mammalian olfactory bulb: sensory information at different timescales. Neuron. 2008; 57: 586–98. https://doi.org/10.1016/j.neuron.2008.02.011 PMID: 18304487

41. Rehman N, Mandic DP. Multivariate empirical mode decomposition. Proc R Soc A Math Phys Eng Sci. 2010; 466: 1291–1302. https://doi.org/10.1098/rspa.2009.0502

42. Flandrin P, Rilling G, Goncalves P. Empirical mode decomposition as a filter bank. IEEE Signal Process Lett. 2004; 11: 112–114. https://doi.org/10.1109/LSP.2003.821662

43. Rilling G, Flandrin P, Gon P, Lyon D. On Empirical Mode Decomposition and Its Algorithms. IEEEEURASIP Work Nonlinear Signal Image Process NSIP. 2003; 3: 8–11.

44. Storey JD. The postive fase discovery rate: a bayesian interpretation and the q-value. Ann. Stat 2003; 31:2013–2035.

45. Churchland MM, Yu BM, Cunningham JP, Sugrue LP, Cohen MR, Corrado GS, et al. Stimulus onset quenches neural variability: a widespread cortical phenomenon. Nat Neurosci. 2010; 13: 369–78. https://doi.org/10.1038/nn.2501 PMID: 20173745

46. Segundo JP, Moore GP, Stensaas LJ, Bullock TH. Sensitivity of neurons in Aplysia to temporal patterns of arriving impulses. J Exp Biol. 1963; 40: 643–667. PMID: 14086809

47. Montemurro MA, Rasch MJ, Murayama Y, Logothetis NK, Panzeri S. Phase-of-Firing Coding of Natural Visual Stimuli in Primary Visual Cortex. Curr Biol. 2008; 18: 375–380. https://doi.org/10.1016/j.cub.2008.02.023 PMID: 18328702

48. Kayser C, Montemurro MA, Logothetis NK, Panzeri S. Spike-Phase Coding Boosts and Stabilizes Information Carried by Spatial and Temporal Spike Patterns. Neuron. 2009; 61: 597–608. https://doi.org/10.1016/j.neuron.2009.01.008 PMID: 19249279

49. Belitski A, Gretton A, Magri C, Murayama Y, Montemurro M, Logothetis N, et al. Local Field Potentials and Spiking Activity in Primary Visual Cortex Convey Independent Information about Natural Stimuli. J Neurosci. 2008; 28: 5696–5709.

50. Buhusi C V., Meck WH. What makes us tick? Functional and neural mechanisms of interval timing. Nat Rev Neurosci. 2005; 6: 755–765. https://doi.org/10.1038/nrn1764 PMID: 16163383

51. Ivry R. The neural representation of time. Curr Opin Neurobiol. 2004; 14: 225–232. https://doi.org/10.1016/j.conb.2004.03.013 PMID: 15082329

52. Duncan J. An adaptive coding model of neural function in prefrontal cortex. Nat Rev Neurosci. 2001; 2: 820–829. https://doi.org/10.1038/35097575 PMID: 11715058

53. Xu M, Zhang S-Y, Dan Y, Poo M. Representation of interval timing by temporally scalable firing patterns in rat prefrontal cortex. Proc Natl Acad Sci. 2014; 111: 480–485. https://doi.org/10.1073/pnas.1321314111 PMID: 24367075

54. Kim J, Jung AH, Byun J, Jo S, Jung MW. Inactivation of medial prefrontal cortex impairs time interval discrimination in rats. Front Behav Neurosci. 2009; 3: 1–9.

55. Meck WH. Frontal cortex lesions eliminate the clock speed effect of dopaminergic drugs on interval timing. Brain Res. 2006; 1108: 157–167. https://doi.org/10.1016/j.brainres.2006.06.046 PMID: 16844101

PAPER III: Toward an Improvement of the analysis of neural coding

Javier Alegre-Cortés, Cristina Soto-Sánchez, Ana L Albarracín, Fernando D Farfán, Mikel Val-Calvo, José M Ferrandez, Eduardo Fernandez

Frontiers in neuroinformatics 2018 11(77)

doi: 10.3389/fninf.2017.00077

frontiers in Neuroinformatics

PERSPECTIVE
published: 10 January 2018
doi: 10.3389/fninf.2017.00077

Toward an Improvement of the Analysis of Neural Coding

Javier Alegre-Cortés[1], Cristina Soto-Sánchez[1,2,3], Ana L. Albarracín[4,5], Fernando D. Farfán[4,5], Mikel Val-Calvo[6], José M. Ferrandez[6] and Eduardo Fernandez[1,2]*

[1] *Neuroprosthetics and Visual Rehabilitation Research Unit, Bioengineering Institute, Miguel Hernández University, Alicante, Spain,* [2] *Biomedical Research Networking Center in Bioengineering, Biomaterials and Nanomedicine, Madrid, Spain,* [3] *Biotechnology Department, University of Alicante, Alicante, Spain,* [4] *Laboratorio de Medios e Interfases, Departamento de Bioingeniería, Facultad de Ciencias Exactas y Tecnología, Universidad Nacional de Tucumán, Tucumán, Argentina,* [5] *Departamento de Bioingeniería, Instituto Superior de Investigaciones Biológicas, Consejo Nacional de Investigaciones Científicas y Técnicas, Tucumán, Argentina,* [6] *Departamento de Electrónica, Tecnología de Computadoras, Universidad Politécnica de Cartagena, Cartagena, Spain*

Machine learning and artificial intelligence have strong roots on principles of neural computation. Some examples are the structure of the first perceptron, inspired in the retina, neuroprosthetics based on ganglion cell recordings or Hopfield networks. In addition, machine learning provides a powerful set of tools to analyze neural data, which has already proved its efficacy in so distant fields of research as speech recognition, behavioral states classification, or LFP recordings. However, despite the huge technological advances in neural data reduction of dimensionality, pattern selection, and clustering during the last years, there has not been a proportional development of the analytical tools used for Time–Frequency (T–F) analysis in neuroscience. Bearing this in mind, we introduce the convenience of using non-linear, non-stationary tools, EMD algorithms in particular, for the transformation of the oscillatory neural data (EEG, EMG, spike oscillations…) into the T–F domain prior to its analysis with machine learning tools. We support that to achieve meaningful conclusions, the transformed data we analyze has to be as faithful as possible to the original recording, so that the transformations forced into the data due to restrictions in the T–F computation are not extended to the results of the machine learning analysis. Moreover, bioinspired computation such as brain–machine interface may be enriched from a more precise definition of neuronal coding where non-linearities of the neuronal dynamics are considered.

Keywords: neuronal coding, non-linear signals, NA-MEMD, machine learning classification, single trial classification

OPEN ACCESS

Edited by:
Qingming Luo, Huazhong University of Science and Technology, China

Reviewed by:
Amar R. Marathe, U.S. Army Research Laboratory, United States
Saad Al-Baddai, University of Regensburg, Germany

***Correspondence:**
Javier Alegre-Cortés
javier.alegre@hotmail.es

Received: *25 April 2017*
Accepted: *22 December 2017*
Published: *10 January 2018*

Citation:
Alegre-Cortés J, Soto-Sánchez C, Albarracín AL, Farfán FD, Val-Calvo M, Ferrandez JM and Fernandez E (2018) Toward an Improvement of the Analysis of Neural Coding. Front. Neuroinform. 11:77. doi: 10.3389/fninf.2017.00077

INTRODUCTION

The mutual benefits of the interplay between natural and artificial computation are well-known. Moreover, the increasing volume and complexity of the generated data in neuroscience exceeds the capacity of classical analysis, and they are becoming more and more difficult to analyze. In this scenario, the emergence of artificial computation and machine learning (ML) techniques is becoming crucial for the interpretation and analysis of these complex data. Some examples are the interaction between networks and behavior (Bathellier et al., 2012), stimulus coding (Nikolić et al., 2009; Klampfl et al., 2012), population dynamics in neural networks (Buonomano and Merzenich, 1995), classification of behavioral states (Kabra et al., 2012), and spike sorting procedures

(Bongard et al., 2014; Carlson et al., 2014; Dimitriadis et al., 2016). On the other hand artificial computation has received inspiration from neuroscience since the first artificial neuron developed in the 40's (McCulloch and Pitts, 1943), continuing to the first perceptron, inspired in the circuitry of the retina (Rosenblatt, 1957), Hopfield networks (Hopfield, 1982), or Self-Organizing maps (Kohonen, 1982) and is still widely present nowadays.

The scope of this perspectives paper is to highlight the reliability and usefulness of ML techniques for the analysis of electrophysiological recordings. In particular, we will address the manipulation of the data prior to its analysis and classification, specifically regarding to Time–Frequency (T–F) features. In this framework we think that T–F analysis tools have not been as extensively implemented as other ML algorithms in neuroscience research. To facilitate the analysis of relevant T–F information using ML analysis, we propose to use Empirical Mode Decomposition data-driven algorithms (Huang et al., 1998, EMD) to extract the relevant T–F features to be studied. This procedure is widely used in signal analysis and has been proved successfully in the analysis of electrophysiological data (Li, 2006; Huang et al., 2013; Hu and Liang, 2014; Al-Subari et al., 2015; Alegre-Cortés et al., 2016); nevertheless, they have not yet become of common use and are sparsely found in neuroscience publications. As a result, we still use linear and stationary techniques that are unavoidably biasing and blurring relevant information, since they are not able to accurately depict the intermittency and non-linearity of the data. This approach usually leads to the underperformance of classification or pattern extraction using ML algorithms, hence limits the strength of the posterior analysis (Mandic et al., 2013). The general idea behind this suggestion is that a more precise transformation into the T–F domains of the data will improve the result of the classification and/or search for patterns in the data performed by the ML algorithms.

SYNERGY BETWEEN EMDS, MACHINE LEARNING, AND BRAIN PROCESSES

Most of the brain processes are non-linear and non-stationary. Hence, the selected analytical tools require the capability to deal with these properties of the data. EMDs (Huang et al., 1998) are data driven algorithms designed to extract oscillatory information without its projection onto any predefined function, converting the original signal into a sum of oscillatory components called Intrinsic Mode Functions (IMFs). In this way they facilitate the extraction of meaningful information from the data without temporal or waveform restrictions, usually using the Hilbert transform (Huang et al., 1998). In addition, there exist multivariate variations of these algorithms (Rehman and Mandic, 2010; Ur Rehman and Mandic, 2011) that allow a simultaneous decomposition of multiple recorded neuronal signals. This is possible thanks to the simultaneous decomposition of all dimensions of the data, which ensures the same number of IMFs containing the information in the same frequency ranges (Rehman and Mandic, 2010). Thus, thanks to the advantages of EMD algorithms over classic linear analysis, they are being increasingly used in neuronal analysis (Liang et al., 2005; Huang et al., 2013; Al-Subari et al., 2015; Alegre-Cortés et al., 2016), and they are helping us to achieve a better understanding of the oscillatory properties of neuronal activity (Buzsáki and Draguhn, 2004).

Despite the advantages of this approach, we should take into account that EMD algorithms increase the dimensionality of the data, since they convert the original signal in a set of IMFs. Hence these procedures increase the difficulties in the management of the data to extract useful results or perform any desired classification.

In this context, ML techniques are the perfect tools to analyze and classify the decomposed neuronal activity. ML is a subfield of statistics and computer science, which takes advantage of the power of computers to perform iterative computations to identify the existing patterns on the data to make future models and predictions. Furthermore, the projection of the data into a higher dimensional space provides an additional advantage, since it helps to improve discrimination (Cover, 1965).

To support these ideas and the advantages of the proposed approach, we will briefly introduce a couple of real examples based on different experimental approaches and electrophysiological techniques.

TEXTURE DISCRIMINATION FROM VIBRISSAL NERVE RECORDINGS

The first example are electrophysiological recordings from rat vibrissal nerve during a texture discrimination task (see Albarracín et al., 2006 for details). Previous work with this data (Lucianna et al., 2016) using linear techniques for T–F features extraction (Root Mean Square value to estimate signal energy and Burg parametric estimation method to compute the Power Spectrum Density) and a simple perceptron (Hertz et al., 1991) concluded that five sweeps were required for an adequate texture classification. To probe our thoughts, we performed a similar analysis on the discrimination of the pair of materials of hardest discrimination, wood vs. L1000 sandpaper (**Figure 1A**), using information from single sweeps on the surface. Previous results on these pair of textures had described that a single swept provided just 70% correct texture classification and had great variability.

We decomposed the data using Noise Assisted Multivariate Empirical Mode Decomposition (NA-MEMD, Ur Rehman and Mandic, 2011) to obtain the T–F spectrum of the response to each texture (see Alegre-Cortés et al., 2016 for details). Standard stopping criterion is described in Rilling et al. (2003). The obtained mean amplitude and mean IF of the different IMFs between 115 and 384 Hz were used to train a multilayer perceptron (MLP) to perform the classification (Cybenko, 1989). We used a single hidden layer of 14 neurons and scaled conjugated gradient as supervised training algorithm (Powell, 1977). We repeated this analysis on a sliding window to compute the temporal profile of discrimination between these textures during 100 ms after stimulus offset. To prevent from biased results due to the finite number of experiments, we shuffled

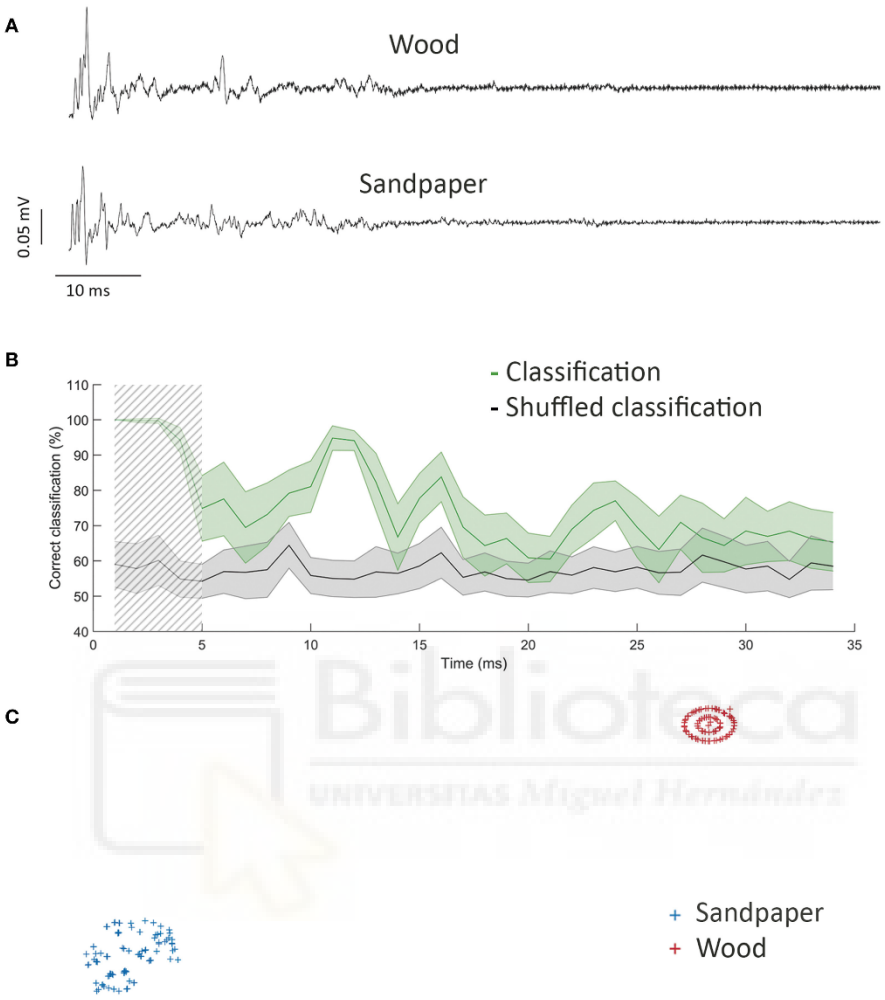

FIGURE 1 | Texture discrimination using NA-MEMD plus MLP. **(A)** Mean vibrissal nerve response to sweeping wood (top) and sandpaper (bottom). **(B)** Percentage of correct classification (green) and classification after shuffling (gray). Shadow square represents maximum discrimination window, used in **(C)**. Error displayed as s.e.m. **(C)** t-SNE representation of vibrissal nerve activity during the first 5 ms of the response.

texture across our data to determine the average error in classification. This process was repeated 100 times in each window.

Figure 1 shows the main results. Discrimination was maximal (99.5 ± 0.5%, shadow square, **Figure 1B**) during a 5 ms window starting 5 ms after stimulus offset. Discrimination performance decreased during time, but a second peak of discrimination was seen 15–20 ms after stimulation, coinciding in time with the second contact with the surface during the withdrawal of the whisker. When we compared this maximum value of discrimination (**Figure 1B**) with the previous results obtained on the discrimination on these dataset (≈70% on average, Lucianna et al., 2016) we confirmed an evident increase in texture discrimination thanks to the combined use of NA-MEMD followed by ML classification. Moreover, the classification was based on single-trial recordings and was shown to had almost no variability in the peak of discrimination (**Figure 1B**), providing an additional improvement over previous results.

We used the t-distributed stochastic neighbor embedding algorithm (t-SNE) (van der Maaten and Hinton, 2008) as an additional ML technique to differentiate the vibrissal nerve response to the different stimulating textures (wood and sandpaper), starting from the same parameters we used to train the MLP in a time window of 5 ms length starting 5 ms after stimulation, coinciding with maximum discrimination in **Figure 1B**. This technique is useful to reduce the dimensionality of the data and allowed us to classify our complex data into two different and well-separated clusters, each one corresponding to one of the stimulating textures: wood and sandpaper (**Figure 1C**).

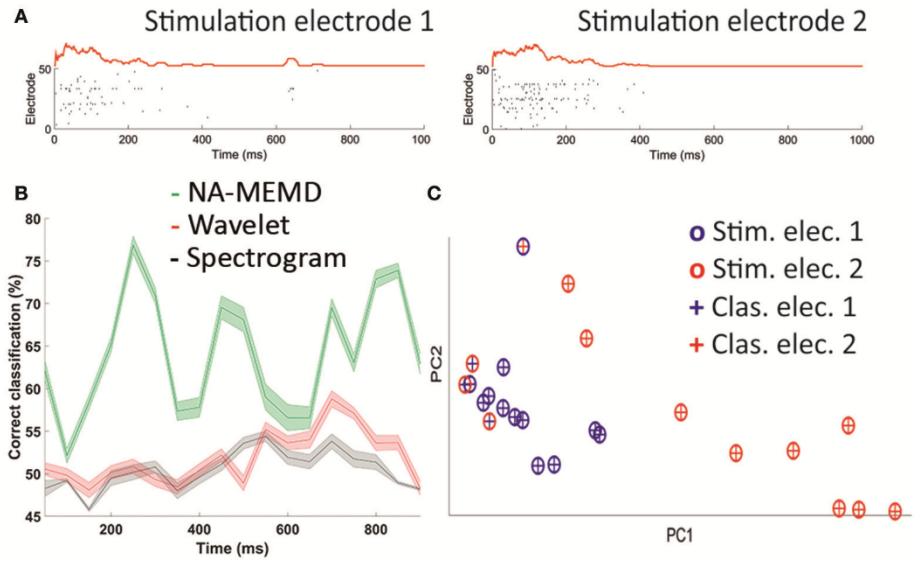

FIGURE 2 | Stimulation electrode discrimination. **(A)** Example of a single stimulation in each stimulation electrode. Raster plot of the whole electrode and mean activity vector. **(B)** Percentage of correct classification using NA-MEMD (green), Morlet wavelet (red), and spectrogram (gray). Error displayed as s.e.m. **(C)** Distribution of individual trials after using PCA (crosses) and clusterization using DBSCAN algorithm (circles).

STIMULATION ELECTRODE DISCRIMINATION FROM MULTIELECTRODE PRIMARY CORTICAL NEURONS CULTURE RECORDINGS

To further illustrate the power and potential of this approach, we carried out an additional analysis of simultaneous recordings in primary cortical neurons cultures (see Calvo et al., 2016 for details). Briefly, embryonic primary cortical neurons were cultured on a multielectrode array; then, population activity was recorded simultaneously at 60 points of the culture while electrically stimulated in two different electrodes of the array (**Figure 2A**). We decomposed the averaged activity present in the electrode to obtain the mean oscillatory activity during 100 stimulations in each of the stimulation electrodes independently using NA-MEMD. Then, we extracted different values of mean amplitude and mean IF at different T–F windows (IMFs ranging from 30 to 90 Hz) to train a MLP to discriminate the stimulation electrode, from the recorded activity when a minimum number of spikes were evoked in the whole response window. We used a single hidden layer of 15 neurons and scaled conjugated gradient as supervised training algorithm. An equivalent shuffling procedure was done to subtract chance-level classification. This process was repeated 100 times.

Once we subtracted chance-level classification, stimulation electrode had its maximum discrimination peak 200–300 ms after stimulation, exceeding 75% successful classification when we used NA-MEMD as the feature extraction tool (**Figure 2B**). Therefore, we were able to discriminate the electrode on which the unique stimulation had occurred analyzing the oscillatory properties of the generated response. This was not possible when we extracted the T–F features to train the MLP using either spectrogram or wavelet (Morlet) analysis. When we used these linear techniques, stimulation electrode classification was similar to chance-level classification (**Figure 2B**).

We performed an additional analysis applying a density-based algorithm for discovering clusters in large spatial databases with noise named DBSCAN that is designed to discover clusters of arbitrary shape (Ester et al., 1996). This algorithm was applied to the extracted parameters during the window of maximum discrimination using NA-MEMD in **Figure 2B** (200–300 ms after stimulus onset). We found two clusters (**Figure 2C**), corresponding to the two stimulation electrodes. A total of 83% of the trials were in the correct clusters, in clear coincidence with the mean percentage of correct classification of the MLP in that window of time before the subtraction of the chance-level classification.

CONCLUDING REMARKS

Over the last decade, many technical and conceptual issues related with the analysis of neuronal recordings have been addressed, but there are still some problems related with the analysis of T–F data. We suggest that a combination of T–F signal decomposition via EMD algorithms (NA-MEMD, in our case) plus a posterior classification of the obtained parameters using ML techniques are powerful tools in this framework. Therefore, the implementation of this combination of analytical tools in the daily neuroscience research would improve the information extracted from the recorded single or

multiple neuronal activities and, in ultimate extent, increase our understanding of the nervous system. Furthermore, although more studies are still needed, these tools could be also useful for a better understanding of some pathological processes of the brain.

ETHICS STATEMENT

All the procedures carried out at the Institute for Biological Research (INSIBIO)/Instituto Superior de Investigaciones Biológicas, were in accordance with the recommendations of the Guide for the Care and Use of Laboratory Animals (National Research Council, NRC). All the experimental procedures carried out at the Miguel Hernandez University were conformed to the directive 2010/63/EU of the European Parliament and of the Council, and the RD 53/2013 Spanish regulation on the protection of animals use for scientific purposes and approved by the Miguel Hernandez University Committee for Animal use in Laboratory.

AUTHOR CONTRIBUTIONS

Data have been provided by AA, FF, and MV-C. Data have been analyzed by JA-C. Paper was written by JA-C, CS-S, JF, and EF.

ACKNOWLEDGMENTS

This work has been supported in part by the Spanish national research program (MAT2015-69967-C3-1), by Research Chair Bidons Egara and by a research grant of the Spanish Blind Organization (ONCE).

REFERENCES

Albarracín, A. L., Farfán, F. D., Felice, C. J., and Décima, E. E. (2006). Texture discrimination and multi-unit recording in the rat vibrissal nerve. *BMC Neurosci.* 7:42. doi: 10.1186/1471-2202-7-42

Alegre-Cortés, J., Soto-Sánchez, C., Pizá, A. G., Albarracín, A. L., Farfán, F. D., Felice, C. J., et al. (2016). Time-frequency analysis of neuronal populations with instantaneous resolution based on noise-assisted multivariate empirical mode decomposition. *J. Neurosci. Methods* 267, 35–44. doi: 10.1016/j.jneumeth.2016.03.018

Al-Subari, K. S. A., Al-Baddai, S. M. H., Tomé, A. M., Goldhacker, M., Faltermeier, R., and Lang, E. W. (2015). EMDLAB : a toolbox for analysis of single-trial EEG dynamics using empirical mode decompostion. *J. Neurosci. Methods* 253, 1–14. doi: 10.1016/j.jneumeth.2015.06.020

Bathellier, B., Ushakova, L., and Rumpel, S. (2012). Discrete neocortical dynamics predict behavioral categorization of sounds. *Neuron* 76, 435–449. doi: 10.1016/j.neuron.2012.07.008

Bongard, M., Micol, D., and Fernández, E. (2014). NEV2lkit: a new open source tool for handling neuronal event files from multi-electrode recordings. *Int. J. Neural Syst.* 24:1450009. doi: 10.1142/S0129065714500099

Buonomano, D. V., and Merzenich, M. M. (1995). Temporal information transformed into a spatial code by a neural network with realistic properties. *Science* 267, 1028–1030. doi: 10.1126/science.7863330

Buzsáki, G., and Draguhn, A. (2004). Neuronal oscillations in cortical networks. *Science* 304, 1926–1929. doi: 10.1126/science.1099745

Calvo, M., Ferrández, J., De la Paz López, F., Álvarez Sánchez, J., Troncoso, J., and Eduardo, F. (2016). Functional connectivity graphs in hippocampal cultures using tetanic stimulation for real time robotic control. *Front. Neurosci.* 10:104. doi: 10.3389/conf.fnins.2016.93.00104

Carlson, D. E., Vogelstein, J. T., Wu, Q., Lian, W., Zhou, M., Stoetzner, C. R., et al. (2014). Multichannel electrophysiological spike sorting via joint dictionary learning and mixture modeling. *IEEE Trans. Biomed. Eng.* 61, 41–54. doi: 10.1109/TBME.2013.2275751

Cover, T. M. (1965). Geometric and statistical properties of systems of linear in-equalities with applications in pattern recognition. *IEEE Trans. Electron. Comput.* 14, 326–334. doi: 10.1109/PGEC.1965.264137

Cybenko, G. (1989). Approximation by superpositions of a sigmoidal function. *Math. Control Signals Syst.* 2, 303–314. doi: 10.1007/BF02551274

Dimitriadis, G., Neto, J., and Kampff, A. (2016). T-SNE visualization of large-scale neural recordings. *bioRxiv* 1–22. doi: 10.1101/087395

Ester, M., Kriegel, H. P., Sander, J., and Xu, X. (1996). "A density-based algorithm for discovering clusters in large spatial databases with noise," in *Proceedings of 2nd International Conference on Knowledge Discovery and Data Mining.* (Munich), 226–231.

Hertz, J. A., Krogh, A. S., and Palmer, R. G. (1991). *Introduction to the Theory of Neural Computation, New Edn.* Redwood City, CA: Westview Press.

Hopfield, J. J. (1982). Neural networks and physical systems with emergent collective computational abilities. *Proc. Natl. Acad. Sci. U.S.A.* 79, 2554–2558. doi: 10.1073/pnas.79.8.2554

Hu, M., and Liang, H. (2014). Search for information-bearing components in neural data. *PLoS ONE* 9:e99793. doi: 10.1371/journal.pone.0099793

Huang, J. R., Fan, S. Z., Abbod, M. F., Jen, K. K., Wu, J. F., and Shieh, J. S. (2013). Application of multivariate empirical mode decomposition and sample entropy in EEG signals via artificial neural networks for interpreting depth of anesthesia. *Entropy* 15, 3325–3339. doi: 10.3390/e15093325

Huang, N. E., Shen, Z., Long, S., Wu, M., Shih, H., Zheng, Q., et al. (1998). The empirical mode decomposition and the Hilbert spectrum for nonlinear and non-stationary time series analysis. *Proc. R. Soc. Lond. A* 454, 903–995. doi: 10.1098/rspa.1998.0193

Kabra, M., Robie, A. A., Rivera-Alba, M., Branson, S., and Branson, K. (2012). JAABA: interactive machine learning for automatic annotation of animal behavior. *Nat. Methods* 10, 64–67. doi: 10.1038/nmeth.2281

Klampfl, S., David, S. V., Yin, P., Shamma, S. A., and Maass, W. (2012). A quantitative analysis of information about past and present stimuli encoded by spikes of A1 neurons. *J. Neurophysiol.* 108, 1366–1380. doi: 10.1152/jn.00935.2011

Kohonen, T. (1982). Self-organized formation of topologically correct feature maps. *Biol. Cybern.* 43, 59–69. doi: 10.1007/BF00337288

Li, X. (2006). Temporal structure of neuronal population oscillations with empirical model decomposition. *Phys. Lett. A* 356, 237–241. doi: 10.1016/j.physleta.2006.03.045

Liang, H., Bressler, S. L., Desimone, R., and Fries, P. (2005). Empirical mode decomposition: a method for analyzing neural data. *Neurocomputing* 65–66, 801–807. doi: 10.1016/j.neucom.2004.10.077

Lucianna, F. A., Farfán, F. D., Piz, G. A., Albarracín, A. L., and Felice, C. J. (2016). Functional specificity of rat vibrissal primary afferents. *Physiol. Rep.* 4, 1–6. doi: 10.14814/phy2.12810

Mandic, D. P., Ur Rehman, N., Wu, Z., and Huang, N. E. (2013). Empirical mode decomposition-based time-frequency analysis of multivariate signals: the power of adaptive data analysis. *IEEE Signal Process. Mag.* 30, 74–86. doi: 10.1109/MSP.2013.2267931

McCulloch, W. S., and Pitts, W. A. (1943). A logical calculus of the ideas immanent in nervous activity. *Bull. Math. Biophys.* 5, 115–133. doi: 10.1007/BF02478259

Nikolić, D., Häusler, S., Singer, W., and Maass, W. (2009). Distributed fading memory for stimulus properties in the primary visual cortex. *PLoS Biol.* 7:e1000260. doi: 10.1371/journal.pbio.1000260

Powell, M. J. D. (1977). Restart procedures for the conjugate gradient method. *Math. Program.* 12, 241–254. doi: 10.1007/BF01593790

Rehman, N., and Mandic, D. P. (2010). Multivariate empirical mode decomposition. *Proc. R. Soc. A* 466, 1291–1302. doi: 10.1098/rspa.2009.0502

Rilling, G., Flandrin, P., and Goncalves, P. (2003). "On empirical mode decomposition and its algorithms," in *IEEE EURASIP Work Nonlinear Signal Image Process NSIP* 3 (Grado), 8–11.

Rosenblatt, F. (1957). *The Perceptron: A Perceiving and Recognising Automaton.* Report 85-460-1, Project PARA.

Ur Rehman, N., and Mandic, D. P. (2011). Filter bank property of multivariate empirical mode decomposition. *IEEE Trans. Signal Process.* 59, 2421–2426. doi: 10.1109/TSP.2011.2106779

van der Maaten, L., and Hinton, G. (2008). Visualizing data using t-SNE. *J. Mach. Learn. Res.* 9, 2579–2605.

Conflict of Interest Statement: The authors declare that the research was conducted in the absence of any commercial or financial relationships that could be construed as a potential conflict of interest.